

Heat Transfer Study of the In-situ Automated Fiber Placement (AFP) for
Thermoplastic Composites

Omid Aghababaei Tafreshi

A Thesis

In the Department of
Mechanical, Industrial and Aerospace Engineering

Presented in Partial Fulfillment of the Requirements
For the Degree of Master of Applied Science (Mechanical Engineering) at
Concordia University
Montreal, Quebec, Canada

December 2019

© Omid Aghababaei Tafreshi, 2019

CONCORDIA UNIVERSITY
School of Graduate Studies

This is to certify that the thesis prepared

By: Omid Aghababaei Tafreshi

Entitled: Heat Transfer Study of the In-situ Automated Fiber Placement (AFP) for Thermoplastic Composites

and submitted in partial fulfilment of the requirements for the degree of

Master of Applied Science (Mechanical Engineering)

complies with the regulations of the university and meets the accepted standards with respect to originality and quality.

Signed by the final Examining Committee:

_____	Chair
<i>Dr. Javad Dargahi</i>	
_____	Examiner
<i>Dr. Mehdi Hojjati</i>	
_____	Examiner
<i>Dr. Ahmed Soliman</i>	
_____	Supervisor
<i>Dr. Suong Van Hoa</i>	
_____	Supervisor
<i>Dr. Farjad Shadmehri</i>	

Approved by _____

Dr. Martin Pugh

Chair, Department of Mechanical, Industrial & Aerospace Engineering

November 18, 2019

Dr. Amir Asif, Dean

Dean, Gina Cody School of Engineering and Computer Science

ABSTRACT

Heat Transfer Study of the In-situ Automated Fiber Placement (AFP) for Thermoplastic Composites

Omid Aghababaei Tafreshi

With more and more use of composites in engineering applications, the need for automated composites manufacturing is evident. The use of automated fiber placement (AFP) machine for the manufacturing of thermoplastic composites is under rapid development. In this technique, a moving heat source (hot gas torch, laser, or heat lamp) is melting the thermoplastic composite tape and consolidation occurs in situ. Due to the rapid heating and cooling of the material, there are many issues to be addressed. First is the development of the temperature distribution in different directions which gives rise to temperature gradients. Second is the quality of the bond between different layers, and third is the rate of material deposition to satisfy industrial demand. This thesis addresses the first issue. The temperature distribution affects the variation in crystallinity, and residual stresses throughout the structure as it is being built. The end result is the distortion of the composite laminate even during the process. In order to address this problem, first the temperature distribution due to a moving heat source needs to be determined. From the temperature distribution, the development and distribution of crystallinity, residual stresses and deformation of the structure can then be determined.

As the first phase of the work, this thesis investigates the temperature distribution due to a moving heat source for thermoplastic composites, without considering the material deposition. A finite difference (FD) code based on the energy balance approach is developed to predict the temperature distribution during the process. Unidirectional composite strips are manufactured using AFP and fast-response K-type thermocouples are used to determine the thermal profiles in various locations through the thickness of the composite laminate subjected to a moving heat source. It is shown that temperature variations measured experimentally during the heating pass, using thermocouples embedded into the composite substrate, underneath layers of the composite

material, are consistent with the generated thermal profiles from the numerical model. The temperature distribution, both in the direction of the tape and through-thickness direction can be predicted numerically.

It should be noted that the convective heat transfer coefficient employed in the thermal analysis of the process plays an important role in the heat transfer mechanism. Information from the literature shows values of h that vary from $80 \text{ W/m}^2 \cdot \text{K}$ to $2500 \text{ W/m}^2 \cdot \text{K}$. This large range can provide a great degree of uncertainty in the determination of important quantities such as temperature distributions and residual stresses. The reason for these large differences can be due to the differences in the process parameters in each of the studies. The process parameters can include the flow rate of the hot gas, the gas temperature, the distance between the nozzle exit and the surface of the composite substrate, the angle of the torch with respect to the surface of the substrate etc. The purpose of the final part of this thesis is to investigate the effect of different AFP process parameters on the convective heat transfer coefficient and to propose a procedure for the determination of the h value according to the particular experimental setup.

KEYWORDS

Thermoplastic composites, automated fiber placement, hot gas torch, thermal analysis

ACKNOWLEDGEMENTS

I would like first to express my sincerest appreciation to my supervisors, Dr. Suong Van Hoa and Dr. Farjad Shadmehri, for their unconditional support and invaluable advice throughout this program. The present work would not be possible without them.

I would like to thank all my colleagues at Concordia Center for Composites for their support and friendship. I would like to thank Dr.Daniel Rosca and Mr.Minh Duc Hoang for their considerable help in performing my experimental work. I am also thankful of Mr.Nima Bakhshi, Mr.Parham Taherkhani and Mr.Sobhan Goudarzi for their support and friendship.

I would also like to thank the examining committee, Dr.Mehdi Hojjati and Dr.Ahmed Soliman for reading this thesis and providing comments.

Last but not least, my deepest appreciation is expressed to my parents and my dear brother for their endless love, support and continuous encouragement throughout my entire life. I would like to dedicate this work to them.

Table of Content

List of Figures	viii
List of Tables	xi
Chapter 1: INTRODUCTION	1
Chapter 2: LITERATURE REVIEW AND RESEARCH OBJECTIVES	5
2.1 In-Situ Thermoplastic Fiber Placement.....	5
2.1.1 Importance of Thermoplastic Fiber Placement Technique.....	5
2.1.2 Description of Fiber Placement Technique	8
2.2 Definition of The Problem	11
2.3 Thermal Model of The Process	15
2.4 Research Objectives	20
Chapter 3: THERMAL ANALYSIS MODEL	23
3.1 Heat Transfer Mechanism in AFP Thermoplastic Composites Process.....	23
3.2 Transient Heat Transfer Model of AFP Process Based on Finite Difference Formulation.....	25
3.2.1 Assumptions	26
3.2.2 Discretization of The Finite Difference Model	28
3.2.3 Energy Balance Approach.....	31
3.2.4 Stability Criterion.....	37
3.3 Solution Algorithm for Moving Heat Source Problem In MATLAB	38
3.3.1 Input Values Directory	41
3.3.2 Procedure for The Analysis of Heat Transfer by A Moving Heat Source.....	44
3.4 Mesh Size Study (Mesh Convergence)	46
Chapter 4: EXPERIMENTAL SETUP	50
4.1 Automated Fiber Placement Setup	50
4.2 Prepreg Material	54
4.3 Thermal Measurement Apparatus	55
4.3.1 Selection Criteria of Thermocouple	55
4.3.2 Selection of Fast-Response K-Type Thermocouple.....	59
4.3.3 Comparison of Response Time of Thermocouples	61
4.3.4 Other Measurement Instruments	62
4.4 Manufacturing Procedure	63
Chapter 5: RESULTS AND DISCUSSION	66
5.1 Numerical and Experimental Temperature Variations for Different Through-Thickness Locations of The Composite Substrate.....	67
5.2 Temperature Distribution in the Vicinity of the Heat Source Along the Lay-Up Direction at Different Through-Thickness Locations	70

5.3 Temperature Variations Through the Thickness of the Composite Substrate at Different Locations Along the Layup Direction.....	72
Chapter 6: EFFECT OF AFP PROCESS PARAMETERS ON CONVECTIVE HEAT TRANSFER COEFFICIENT	75
6.1 Overview of The Chapter	75
6.2 Literature Review	76
6.3 Introduction to Impinging Flow	79
6.4 Theoretical Formulations	80
6.4.1 Assumption.....	81
6.4.2 Reynolds And Prandtl Numbers.....	81
6.4.3 Nusselt Number.....	83
6.4.4 Angle of Impact.....	86
6.5 Theoretical Results	90
6.5.1 Effect of Nozzle Geometry.....	91
6.5.2 Effect of Nozzle Temperature	93
6.5.3 Effect of Gas Flow Rate	95
6.5.4 Effect of Nozzle to Plate Spacing.....	98
6.6 Discussion	99
6.7 Experimental Methodology	100
6.7.1 Experimental Setup	100
6.7.2 Design of Experiment.....	101
6.7.3 Manufacturing Procedure	105
6.7.4 Methodology for Determination of Convective Heat Transfer Coefficient	108
6.8 Results and Discussion.....	112
6.8.1 Experimental Temperature Results	113
6.8.2 Experimental Convective Heat Transfer Coefficient Results.....	117
6.9 Conclusion.....	121
Chapter 7: CONCLUSIONS, CONTRIBUTIONS AND FUTURE WORK	123
7.1 Concluding Remarks	123
7.2 Contributions.....	125
7.3 Future Work	127
REFERENCES	128
APPENDIX	136

List of Figures

Figure 1. Use of advanced composite materials in Boeing 787 Dreamliner [4]	2
Figure 2. Formation of gaps and overlaps during the manufacturing process [23].....	7
Figure 3. Accudyne thermoplastic tape placement head [26]	8
Figure 4. Automated fiber placement machine in Concordia Centre for Composites	10
Figure 5. Thermoplastic fiber placement head [18]	11
Figure 6. Stages in processing thermoplastic composites using AFP [6,13]	13
Figure 7. Distortion of the composite laminate during and after the process	14
Figure 8. Potential solutions to make flat thermoplastic parts with AFP; (Left) Accudyne thermoplastic head design [37] (Right) Flat laminates made in Concordia Centre for Composites (CONCOM) [6]	15
Figure 9. Heat transfer mechanism between the hot gas flow and the composite substrate	24
Figure 10. The finite difference model to predict the transient temperature field of the composite substrate – aluminum mandrel assembly during the lay-up process	26
Figure 11. Finite difference mesh for 2D conduction in rectangular coordinates (Left); volume element of a node and the change in the energy content during a time interval Δt (Right) [64] ...	29
Figure 12. Space and time discretization of a 2D transient heat conduction problem	30
Figure 13. The volume element of a general interior node (m,n) for 2D transient heat conduction problem in rectangular coordinates [64]	34
Figure 14. Upper side boundary condition consisting of two zones; Zone 1 (ambient air) and Zone 2 (hot gas flow)	36
Figure 15. The energy balance on a volume element for a boundary node [64].....	37
Figure 16. Flow chart of the FD program code in MATLAB.....	40
Figure 17. Procedure for the analysis of heat transfer by a moving heat source implemented in FD code in MATLAB	45
Figure 18. Temperature variation at underneath 9 th layer for different number of divisions for the heating length at $x = 254$ mm (10 inch)	48
Figure 19. Mesh size study (mesh convergence); (Left) maximum temperature (Right) time to reach maximum temperature in the laminate in three different layers for different number of divisions for the heating length	49
Figure 20. Thermoplastic Fiber Placement Head.....	52
Figure 21. Consolidation roller of AFP setup	52
Figure 22. Nitrogen supply line (Left); HGT nitrogen regulator (Right).....	53
Figure 23. AFP Operator interface	53
Figure 24. Micrograph of CYTEC prepreg (Left); Heat flow curve of APC-2/AS4 prepreg (Right) [6].....	55
Figure 25. Common thermocouple temperature ranges [82]	56
Figure 26. Different junction types of thermocouples [82].....	58

Figure 27. Thermocouple response time for different wire diameters [82] (the vertical axis is subdivided into two parts, from 0 to 1.1 in the left and from 1.1 to 2.1 in the right).....	58
Figure 28. Schematic of unsheathed fine gauge thermocouple [82]	60
Figure 29. Fast-response K-type thermocouple assembly.....	60
Figure 30. Oil bath for response time measurement (Left), temperature versus time for typical and developed thermocouples (Right).....	61
Figure 31. Temperature measurement apparatus	62
Figure 32. Connector assembly to the thermocouple wires [82].....	63
Figure 33. Experimental setup; location of AFP head (Left) at the beginning of the pass (Right) over the embedded thermocouples.....	65
Figure 34. Schematic illustration of 20-layer composite laminate with embedded TCs	65
Figure 35. Schematic illustration of 20-layer composite laminate with embedded TCs	69
Figure 36. Temperature variations; numerical simulation versus experimental results at $x = 10$ inch	69
Figure 37. Temperature distribution in the vicinity of the heat source along the lay-up direction at different through-thickness locations at $t = 10$ seconds	71
Figure 38. Temperature variations through the thickness (z direction) of the composite substrate at five different x locations at $t = 10$ seconds.....	73
Figure 39. Experimental setup for the determination of the convective heat transfer coefficient [38]	78
Figure 40. Schematic of the impinging flow by a torch nozzle (a: free jet region, b: stagnation flow region, c: wall jet region)	80
Figure 41. Schematic of Inclined Impinging Jet	86
Figure 42. Displacement of stagnation point from impact point for different angle of impacts (Left); Asymmetry distribution of Nu number in acute angles of impact (Right) [87]	88
Figure 43. Different nozzle shapes in impingement studies (Left); Effect of different nozzle shapes on Nusselt at stagnation point (Right) [109]	92
Figure 44. Effect of nozzle temperature on gas velocity at nozzle exit (left) and Reynolds number (right) at different gas flow rates.....	94
Figure 45. Effect of nozzle temperature on convective heat transfer coefficient at stagnation point h_{stag} at different gas flow rates	95
Figure 46. Effect of Nitrogen gas flow rate on gas velocity at nozzle exit (left) and Reynolds number (right) at different nozzle temperatures.....	96
Figure 47. Effect of Nitrogen gas flow rate on convective heat transfer coefficient at stagnation point h_{stag} at different nozzle temperatures.....	97
Figure 48. Effect of non-dimensionalized nozzle to plate spacing (H/D) on the h coefficient at stagnation point for nozzle temperatures at a constant gas flow rate of 70 SLPM.....	98
Figure 49. Automated Fiber Placement at Concordia Center for Composites (Left); Thermoplastic Fiber Placement Head (Right).....	101
Figure 50. Positioning of the torch nozzle with respect to the consolidation roller and the composite substrate	104

Figure 51. Positioning of the embedded thermocouple inside the composite substrate (Left); AFP head over the embedded thermocouple (Right)	107
Figure 52. Schematic of the layup of the composite, the tool, location of the embedded thermocouple, data acquisition system and data analysis apparatus	107
Figure 53. Flow chart of the strategy to determine the convective heat transfer coefficient	109
Figure 54. Error percentage versus different h coefficients in scanning algorithm	111
Figure 55. Temperature variations at the location of the thermocouple for iterations of different assumed values of the h coefficient.....	112
Figure 56. Effect of gas flow rate (left) and the nozzle temperature (right) on the maximum temperature results for the nozzle to substrate spacing of 2.5 mm	114
Figure 57. Effect of gas flow rate (left) and the nozzle temperature (right) on the maximum temperature results for the nozzle to substrate spacing of 5 mm	115
Figure 58. Effect of gas flow rate (left) and the nozzle temperature (right) on the maximum temperature results for the nozzle to substrate spacing of 10 mm	116
Figure 59. Effect of gas flow rate (top) and the nozzle temperature (bottom) on the average h coefficient for the nozzle to substrate spacing of 2.5 mm.....	118
Figure 60. Effect of gas flow rate (top) and the nozzle temperature (bottom) on the average h coefficient for the nozzle to substrate spacing of 5 mm.....	119
Figure 61. Effect of gas flow rate (top) and the nozzle temperature (bottom) on the average h coefficient for the nozzle to substrate spacing of 10 mm.....	120

List of Tables

Table 1. Summary of relevant publications in literature	21
Table 2. Stability criteria for interior nodes and boundary nodes	38
Table 3. Nodal temperatures for interior and boundary nodes based on energy balance approach	39
Table 4. Temperature dependent physical properties of AS4/APC-2 [5].....	42
Table 5. Temperature dependent physical properties of AS4/APC-2 [5].....	42
Table 6. Input parameters for the FD code	43
Table 7. Description of different mesh sizes	46
Table 8. Parameters of the hot gas torch for three different set of process parameters (Thermophysical properties of Nitrogen gas in different temperatures can be found in Appendix C)	82
Table 9. List of relevant publications in literature for Nusselt calculation [88].....	85
Table 10. Maximum Nusselt number in different angle of impingements, the effect of nozzle to plate spacing (H/D) at a constant Re=5000 (Left), the effect of Reynolds number for constant nozzle to plate spacing (H/D = 10) [107].....	90
Table 11. Parameters values used in this study	91
Table 12. List of AFP parameters.....	102
Table 13. Design of experiments.....	104

Chapter 1: INTRODUCTION

In recent years, fiber reinforced polymer composites have been widely used in high performance structural applications in different industries including automotive, aerospace, civil structures, electrical and marine applications [1–3]. For instance, in Boeing 787, advanced composite materials consist 50% of the total weight of the aircraft (Figure 1) [4]. There are many reasons why advanced composite materials have been used in fabricating many important industrial applications [1,3]: the first reason is the low weight, but high strength of these materials compared to metals and plastics. The second reason is the wide range of mechanical properties that can be achieved by using composites. This in turn, broaden the application of these advanced materials in a variety of markets. The third reason is their numerous attractive characteristics including good corrosion resistance, temperature stability, excellent adhesion, energy absorption, good fatigue resistance, etc. And eventually processing versatility that exists for composite materials. There are numerous manufacturing techniques that can be used to fabricate composite structures. These include hand laminating, filament winding, pultrusion, liquid composite molding, fiber placement techniques etc. Each manufacturing process has its own characteristics which make them an ideal candidate in processing composite structures [1].

With increasing use of composites in many engineering applications, the need for manufacturing techniques with higher production rates for large scale production in low cost is evident [5,6]. Traditional processing techniques such as hand laminating, is slow and cannot provide a fast rate of production for new demanding applications [1]. Furthermore, it is based on the skill of technicians and thereby the issue of repeatability in terms of quality and performance of the final composite parts may arise [7]. In order to overcome the limitations in traditional manufacturing techniques, the trend is towards the robotic processing of composite structures [7]. Automated Fiber Placement (AFP) is one of the solutions to traditional techniques by automating the layup process. Owing to its unique features such as using narrow tapes and having control over steering the fibers, it holds many potential benefits which satisfies the demands for high performance structural components [8].

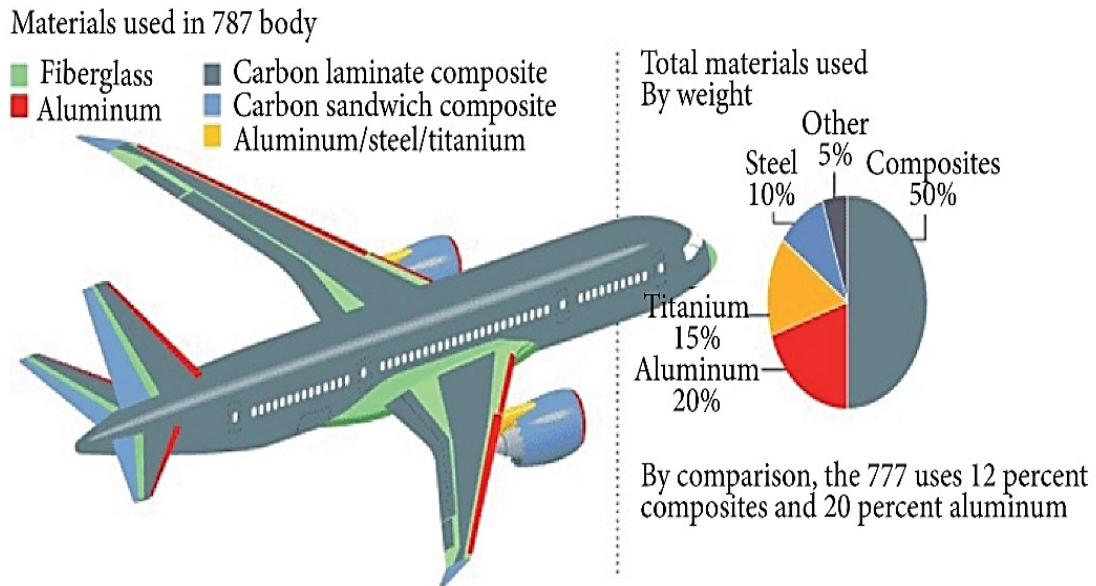


Figure 1. Use of advanced composite materials in Boeing 787 Dreamliner [4]

AFP can be used for processing both thermoset and thermoplastic composites [5]. In the last decade, automated manufacturing of thermoplastic composite parts has garnered the attention of different industries due to their advantages over thermosets [1,9–11]: (i) thermoplastic composites can be processed in-situ without the necessity to perform post processing such as curing in the oven or an autoclave. Consequently, despite the processing time of thermosets which is in the order of hours, thermoplastic composites can be processed within the order of minutes. This can significantly decrease the manufacturing costs and increase the production rate, (ii) thermoplastics have infinite shelf life because no chemical reaction occurs in the process and it is based on solidification which is a physical phenomenon, (iii) they are recyclable and can be reshaped into a new product. This feature can be useful in healing the existing defects in structures, (iv) for structures subjecting to high impact loads, thermoplastics can perform much better compared to thermosets. This is because of the fact that thermoplastics have larger fracture toughness and thereby can endure larger plastic deformations compared to thermosets.

For the above reasons, AFP can be potentially used to fabricate good quality thermoplastic composite parts. However, processing thermoplastic composites using AFP is lagging behind because of technical challenges and difficulties in the process [12]. Previous studies pointed out that in making structures with free edges such as flat plates, flat panels and shells, the warpage emerges during and after the process [6,13]. One of the consequences is in testing and evaluation of composite structures made by this process. It is necessary to determine the mechanical properties of composite laminates fabricated using the fiber placement process for performance and design objectives [13]. However, existing challenges in making a flat unidirectional composite plate to make a test coupon needs to be rectified first by understanding the fundamental issues that underlie the distortion of the laminates. Due to the rapid heating and cooling of the thermoplastic composite material during the process, there are many issues to be addressed. First is the development of the temperature distribution in different directions which gives rise to temperature gradients. Second is the quality of the bond between different layers, and third is the rate of material deposition to satisfy industrial demand. This thesis addresses the first issue. The temperature distribution affects the variation in crystallinity, and residual stresses throughout the structure as it is being built. In fact, residual stresses are developed as a result of temperature gradients because of different cooling rates in different layers along the thickness of the laminate. Consequently, the distortion of the composite laminate takes place even during the process.

With the aim of improving the manufacturing of thermoplastic composites using AFP and filling the existing gaps in literature, the thesis objective is: *“To develop a thermal analysis of in-situ AFP of thermoplastic composites using finite difference approach with experimental validation of numerical results.”*

In order to fulfil the thesis objective, the organization of this study is as follows: in Chapter 2, fundamentals of the in-situ thermoplastic fiber placement are presented. The problem of distortion is clearly defined by notifying the key factors contributing to the problem during the process. An extensive literature review on thermal model of the AFP process is presented and eventually the research objectives in this thesis are discussed. In Chapter 3, the methodology adopted to model the process is presented. This includes the strategy employed to convert the continuous movement of the heat source into discretized steps along with the finite difference formulation of the problem. In Chapter 4, the experimental setup which is used for validation of numerical results will be

discussed in detail. In Chapter 5, the results of the thermal analysis are presented along with experimental results. In Chapter 6, determination of the convective heat transfer coefficient is presented under different operational conditions. This includes the design of experiments and scanning scheme in obtaining the coefficient values. Finally, in Chapter 7, conclusions are drawn for this thesis and recommendations for future studies are stated.

Chapter 2:

LITERATURE REVIEW AND RESEARCH OBJECTIVES

2.1 In-Situ Thermoplastic Fiber Placement

2.1.1 Importance of Thermoplastic Fiber Placement Technique

With more and more use of composites in many important engineering applications like airplane fuselage, automotive components, pressure vessels etc., the need for automated composites manufacturing is evident. Thermoplastic composites offer many attractive characteristics such as high fracture toughness, good temperature resistance, and better recyclability as compared to thermoset matrix composites [1,14,15]. The use of automated fiber placement (AFP) machine for the manufacturing of thermoplastic composites is under rapid development. Compared to traditional manufacturing methods, AFP of thermoplastic composites holds many potential benefits as following:

- It provides high speed and large volume of production in a cost efficient way which is crucial for new demanding applications. This is because of two reasons: first, the processing of thermoplastic parts is performed in-situ without necessity to perform post processing such as curing in the oven or an autoclave [13]. The second reason is that the AFP is able to manufacture large parts without the necessity to assemble many small parts [7].
- It provides more repeatability in terms of quality and performance of the final component. The reason is it is less labour intensive [1,6].
- AFP can have control over steering the fibers. This is possible by utilizing narrow tapes in the process. Steering the fibers provides the ability to transit more seamlessly from design to manufacturing which is useful in fabricating variable stiffness laminates [13,16,17].

- Because of fiber steering, there is less waste in the material compared to other techniques. This in turn reduces manufacturing costs.
- It can be used for wide range of materials such as polyetheretherketone (PEEK), polyetherketoneketone (PEKK), polyphenylene sulfide (PPS) or polyetherimide (PEI) reinforced with either carbon or glass fibers. As such, the range of properties of composites made by this method can vary greatly. This in turn, broaden the application of this method in a variety of markets from automotive to aerospace and military applications [1,3,13].
- The traditional techniques can be used for fabricating specific shape of structures; for example, the filament winding process is only applicable to make structures in the form of cylinders or spheres (mainly convex surfaces). However, AFP can be used for fabricating composite structures with variety of geometries including both convex and concave surfaces [18].

Despite numerous benefits of the process, there are some limitations:

- Because of the characteristics of the AFP process, defects can emerge within the final composite parts. These can be in the form of gaps and/or overlaps (Figure 2). Occurrence of these defects in the composite laminate can affect the structural performance by reducing certain mechanical properties such as strength and stiffness of the laminate [19–23].
- Thermoplastic composites have relatively high viscosity (1000 Pa.s at 400 °C for PEEK compared to 1 Pa.s at room temperature for polyester) [1]. This makes the process and design of the heating system challenging to provide enough heat energy to melt the resin.
- The rate of deposition is relatively slow which is not desirable for industrial demands. If the rate of deposition increases, it may result in improper bonding between layers. This can affect the quality of the composite part in terms of degree of crystallinity, void fraction and interlaminar shear strength [1,2,6].
- For complex mold geometries, consolidation roller and the fiber placement head may require modification. The reason is using a single roller with fixed geometry cannot provide adequate and uniform pressure to consolidate the towpreg onto the surface of the part. It is therefore necessary to adjust the head assembly (for example by employing a conformable roller) to fit the geometry of the part at different locations [24,25].

- In complicated head assemblies like the one developed by Accudyne [26] (Figure 3) several issues may arise. First of all, the price of the head alone is in the order of million dollars. Secondly, the setup has the capability to place 12 prepreg tapes. Although it sounds like an advantage to the process as it provides faster rate of deposition, it may create mismatch between the designed and real fiber paths. The reason is by increasing the number of tows in the setup to perform the layup, the fiber orientation becomes nonuniform and irregularity of the thickness distribution can occur [27].

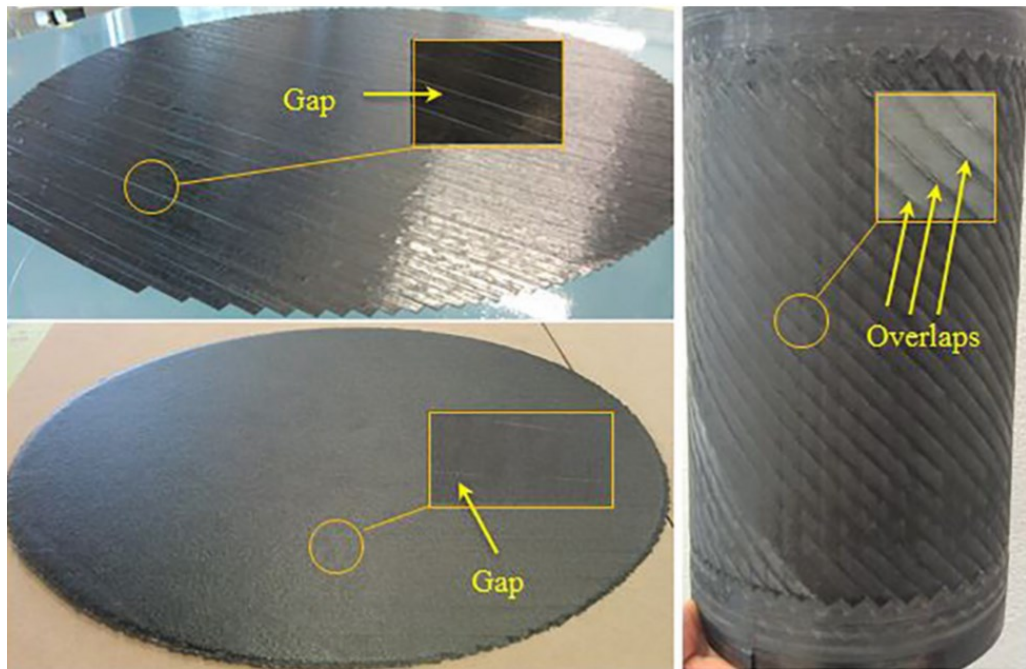


Figure 2. Formation of gaps and overlaps during the manufacturing process [23]

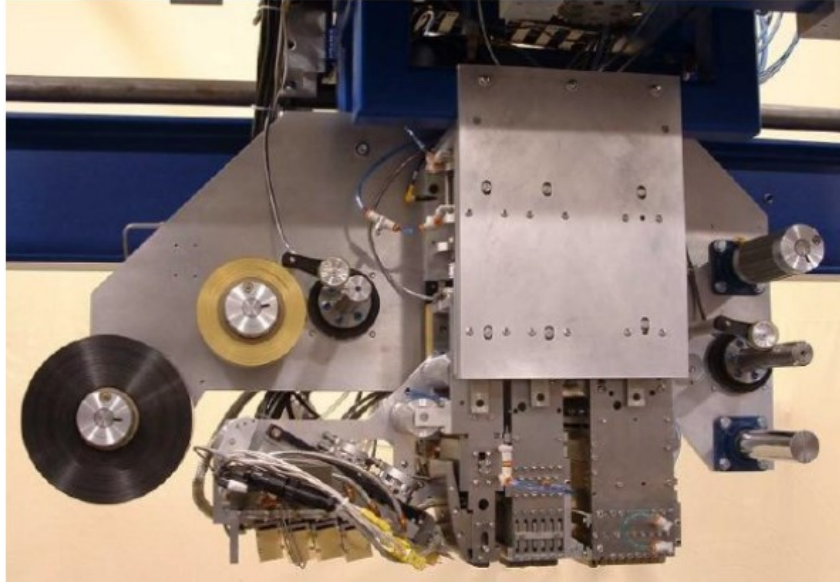


Figure 3. Accudyne thermoplastic tape placement head [26]

2.1.2 Description of Fiber Placement Technique

The AFP machines are designed for different applications. Depending on type of the material being used (thermoset or thermoplastic), type of the heat source (laser, heat lamp, infrared or hot gas torch) and configuration of the placement head (single or multi tow heads), there are different AFP systems. However, typical components are in common between each of those systems. These include: (a) robotic arm, (b) control panel, (c) fiber feeding system and (d) fiber placement head which are illustrated in Figure 4. The design of the desired part is converted into the movement of the robotic arm in the control panel using a dedicated software developed by the AFP manufacturers. Along with the control of the robot motion, processing parameters such as layup speed (rate of deposition) is also set by the control panel. The use of robot manipulator increases the precision of the process, repeatability of the final part and flexibility of the process in fabricating complex geometries [25,28]. In bigger sizes where the AFP is used for fabricating larger structures like wings or fuselage of the aircrafts, gantry style is employed [25,29]. Fiber feeding system is shown in Figure 4. The system is equipped with a creel cabinet in which the material is stored. The AFP machines use the pre-impregnated tow tape which is called towpreg [27]. Towpregs which act as an incoming tape in the setup is generally based on thermoset or thermoplastic resins

reinforced with either carbon or glass fibers. Towpregs that are stored in a creel system are fed into the fiber placement head with a controlled amount of tension [2,28]. Before entering the towpregs into the placement head, a series of guide eyelets and tensioners are mounted to guide and position the towpregs. This is important in order to avoid misalignment and entanglement of tows prior to the placement of tows onto the part [28]. Fiber placement head is the main component of the AFP machines. In order to address the details of this part and its subcomponents, the thermoplastic fiber placement head is shown in detail in Figure 5.

In thermoplastic fiber placement head as shown in Figure 5, there is a heat source (either laser, infrared, heat lamp or hot gas torch) which is used to heat up the incoming tape (towpreg) and a certain area of the substrate. Thermoplastics have relatively high viscosity and it is important to provide enough heat to melt the matrix to be able to penetrate through the fiber networks to wet the fibers. On the other hand, the temperature should be kept at a certain level to avoid thermal degradation. In the setup shown in Figure 4, Nitrogen gas is used in the heating system to heat up the incoming tape. Nitrogen as an inert gas helps to protect the towpregs from oxidation [2,6]. After the incoming tape is melted by the hot gas, the tape is driven towards a compaction roller. In this stage, the compaction force is applied by a consolidation roller at the Nip point. Nip point refers to the contact point of the consolidation roller with the incoming tape [30]. The compaction force is employed because of two major reasons: first, to consolidate the material i.e., the incoming tape onto the substrate. This is known as solidification phase. In this phase, the sustained pressure prevents the fiber network from springing back which plays an active role in the development of intimate contact at the interface of layers [24]. Second, the compaction force minimizes voids that are emerged between individual layers during the process by compressing them [2,6]. Proper compaction is required to remove voids in the final microstructure of composite parts. Eventually, the head assembly consisting of feeding, heating and compaction systems moves at a constant speed (layup speed) to provide heat while the compaction roller consolidates the incoming tape onto the substrate. As the head assembly completes one pass for depositing the first layer, it initiates the next pass to place the subsequent layer. Through a cyclic process, laying up is performed to achieve the required thickness and the desired layup sequence [18,30].

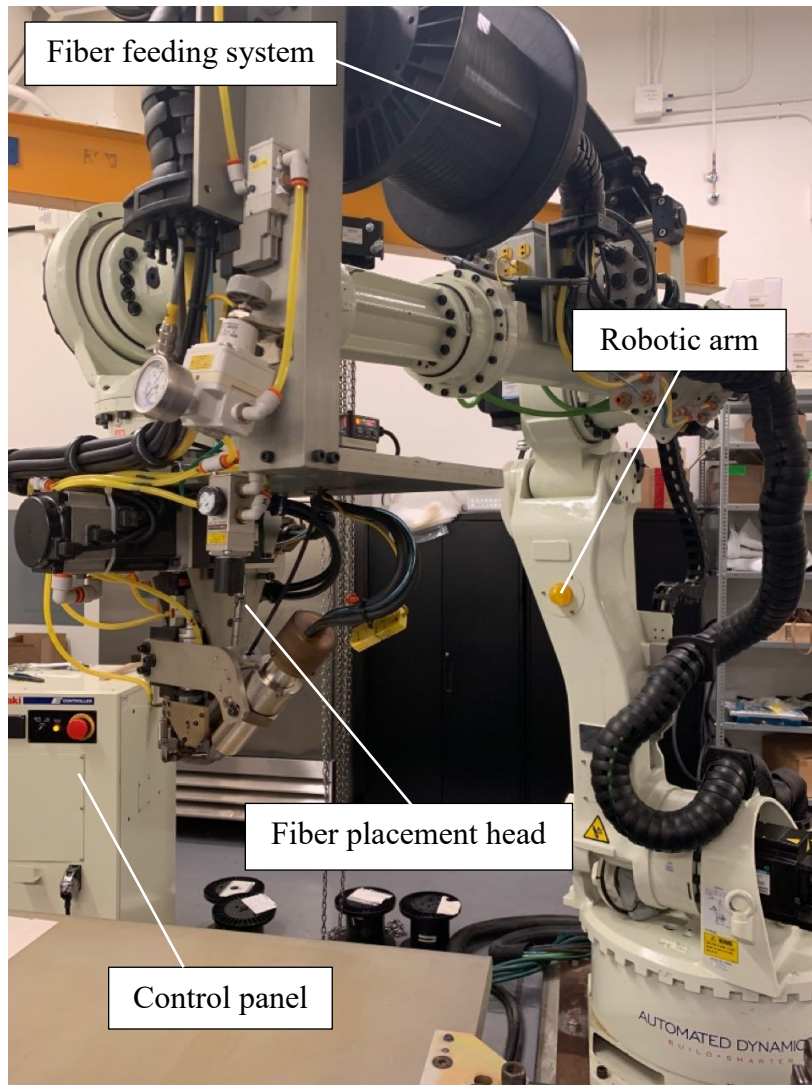


Figure 4. Automated fiber placement machine in Concordia Centre for Composites

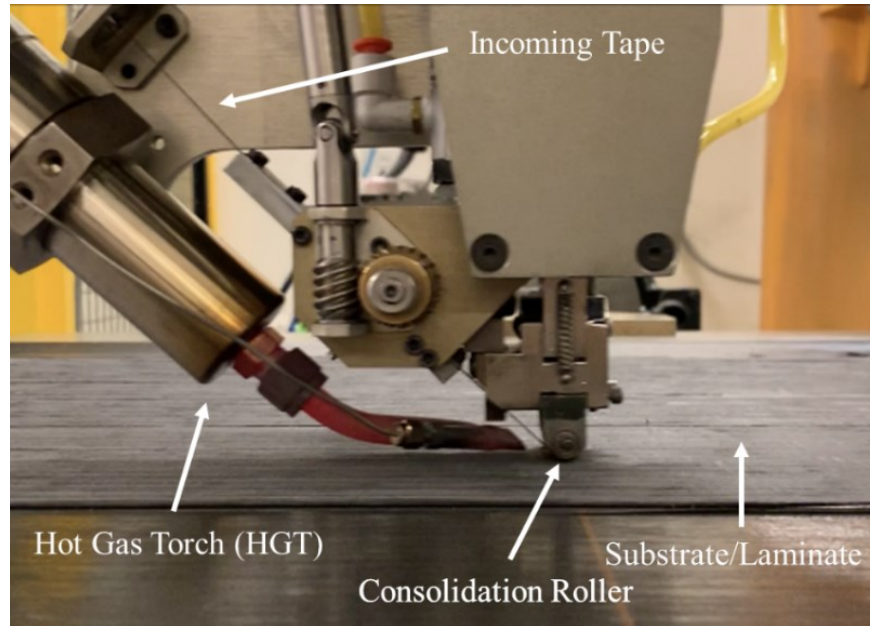


Figure 5. Thermoplastic fiber placement head [18]

2.2 Definition of The Problem

The development of the fiber placement process offers possibilities to manufacture composite structures in variety of geometries and complexities. The structures that can be made using this technique can be classified into two categories: (1) Structures with no free edges such as surfaces of revolution like cylinders or rings, conical structures, and some complex geometries with narrow radius. (2) Structures with free edges such as flat plates, flat panels, shells and concave or convex panels with mild and/or double curvatures. In making structures with free edges (second category), the issue of distortion is important which leads to the warpage of the final composite part.

In order to understand the fundamental issues that underlie the distortion of the laminates, first we need to understand the processing of flat thermoplastic parts using AFP with more focus on development of temperature distribution in different stages during the process. The process consists of four major stages as illustrated schematically in Figure 6. In the first stage (stage A), the incoming towpreg is fed into the nip point while it is subjected to the hot gas torch as an external heat source. The application of high heat energy is required especially for the case of thermoplastics due to their high viscosity. However, the heat energy should be controlled to avoid thermal

degradation. In the second stage (stage B), compaction force is applied via a consolidation roller. Due to compression of the tape onto the substrate, the resin flows through the fiber network both in the layup direction and through the thickness of the substrate. As a result of molecular reptation across the interface of the incoming towpreg and previously deposited layers, bonding occurs [1,13,30,31]. Along with the flow of the resin and development of the bonding at the interface, the temperature is transferred from the melted tape segment into different media. A portion of the heat is transferred into the substrate below while the rest of the heat can be dissipated into the surrounding. Other phenomena to be noticed in this stage, is reduction of the substrate thickness [13]. Stage C refers to the cooling stage. The tape segment which is already laid up, is subjected to the ambient air and it is cooled down. The residual stresses emerge in this stage due to some reasons [13]: (i) shrinkage of the tape segment (ii) formation of crystals in the structure (iii) development of temperature gradients (iv) mismatch in thermal expansion coefficients along different directions in the tape (v) coupling between normal and shear behaviour. Eventually, stage D refers to the case where more than one layer is required to form the laminate. In this case, the tape segments which were deposited in previous pass, are again subjected to high temperature and compaction force but at lower intensities compared to the layer on top. The residual stresses emerge in this stage because of several reasons [13]: (i) development of temperature gradients in different directions. This is one of the pivotal factors in occurrence of residual stresses. The reason is different layers can be deposited at different times during the process and thus temperature variation is a function of both location and time which makes the process more complicated. (ii) variation of modulus of different layers. The reason is modulus of each layer is dependent on the crystallization level of that individual layer. Different layers can be in different state of crystallization. For example, upon cooling, the temperature of a certain layer can drop below glass transition temperature (T_g) and in this case, that layer becomes stiff and there can be no more improvement in crystallization level. (iii) shrinkage can differ from layer to layer i.e., the top layer shrinks more (due to its higher temperature) while the layer underneath shrinks less (due to its lower temperature). This can result in bending which leads to distortion of the laminate.

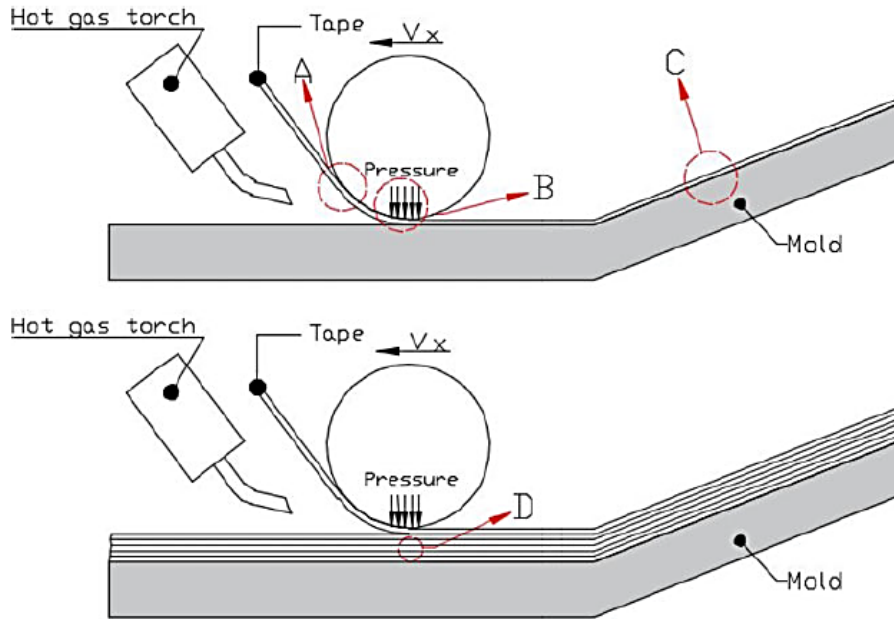


Figure 6. Stages in processing thermoplastic composites using AFP [6,13]

In summary, due to the rapid heating and cooling of the thermoplastic composite material during the process, there are many issues to be addressed. First is the development of the temperature distribution in different directions which gives rise to temperature gradients. Second is the quality of the bond between different layers, and third is the rate of material deposition to satisfy industrial demand. This study addresses the first issue. The temperature distribution affects the variation in crystallinity, and residual stresses throughout the structure as it is being built. In fact, residual stresses are developed as a result of temperature gradients because of different cooling rates in different layers along the thickness of the laminate. Consequently, the distortion of the composite laminate takes place even during the process (Figure 7). There are other reasons as well which give rise to the development of residual stresses. These include deviations from the desired positions of the tape during the lay-up process [18]. The end result is that it may not even be possible to manufacture a flat unidirectional composite plate to make a test coupon. This is the inherent problem associated with thermoplastic laminates made by AFP discussed by several authors in literature [5,6,13,18,32–35]. Lamontia *et al.* [36,37] showed that the problem of making thermoplastic parts using AFP can be rectified by using a more complex thermoplastic head design

as it is shown in Figure 8 (left). The idea was employing multiple rollers (one principal roller and one secondary roller) which could consolidate the part at and after the nip point instead of using a single roller. However, the design of the head can be very expensive and complicated which may not be desirable for industrial applications. In 2016, Hoa *et al.* [13] showed that by using a heated mandrel instead of a cold mandrel, it was possible to make flat thermoplastic parts with AFP (Figure 8 right). The idea was heating up a mandrel above the glass transition temperature and laying up composite layers on top of that. In this way, the difference in thermal expansion between composite layers and the mandrel could be eliminated which could successfully address the distortion problem. However, this idea can face some limitations and drawbacks. In one hand, heating up the mandrel can be expensive, and it may not be feasible to keep the mandrel's temperature uniform everywhere. On the other hand, some defects may arise when the final part is lifted off the mandrel because of the difference between thermal expansion coefficients of the composite part and the mandrel. This can be due to the high temperature of the mandrel which can make some layers very soft during the process [13]. Overall, the challenge of making flat thermoplastic composite parts using AFP still exists and structures with free edges exhibit distortion not only after the process, but also during the process. In order to address this problem, to make laminates with free edges with no or minimum distortion, one needs to understand the effect of different parameters on the process. As such, the first thing to look at would be to determine the temperature distribution history during the process. The focus of this study, specifically, is to gain more understanding of the way temperature gradients develop during the AFP process of thermoplastic composites.



Figure 7. Distortion of the composite laminate during and after the process

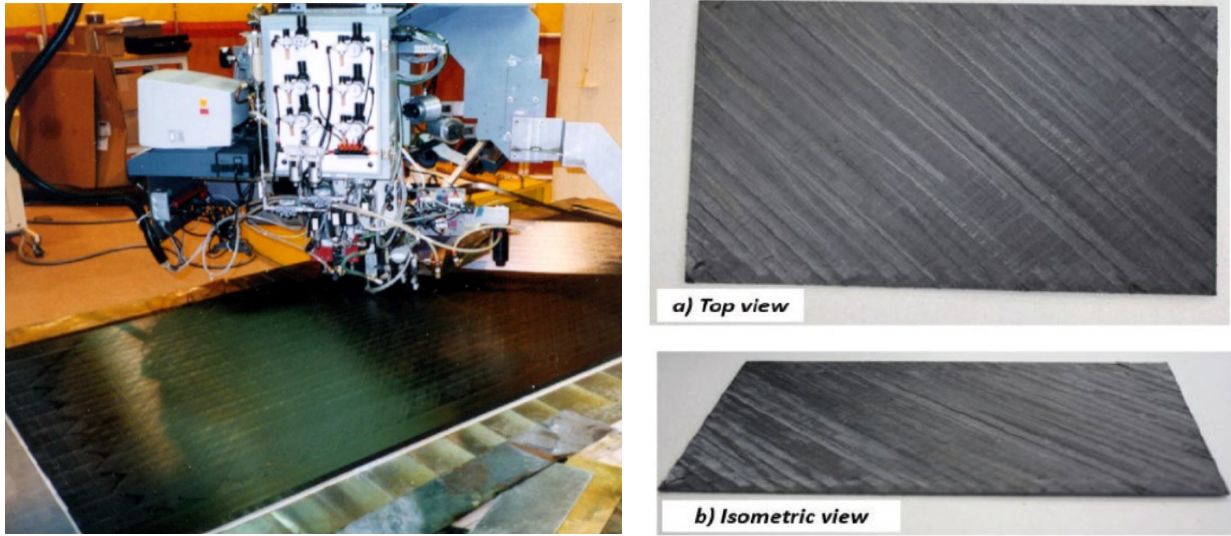


Figure 8. Potential solutions to make flat thermoplastic parts with AFP; (Left) Accudyne thermoplastic head design [37] (Right) Flat laminates made in Concordia Centre for Composites (CONCOM) [6]

2.3 Thermal Model of The Process

The governing heat transfer equation for orthotropic materials (e.g. composites) is presented as following [18]:

$$K_x \frac{\partial^2 T}{\partial x^2} + K_y \frac{\partial^2 T}{\partial y^2} + K_z \frac{\partial^2 T}{\partial z^2} + \rho U = \rho C_p \frac{\partial T}{\partial t} \quad (1)$$

In this equation, ρ is the mass density (Kg/m^3), C_p is the specific heat ($\text{J}/\text{kg } ^\circ\text{C}$), T is the temperature at a material point ($^\circ\text{C}$), U ($\text{J}/\text{kg.S}$) is the heat generation term and K_x, K_y, K_z ($\text{W}/\text{m } ^\circ\text{C}$) are thermal conductivities in longitudinal, transversal and through-thickness directions respectively.

In recent years, several studies have been devoted to develop heat transfer models for AFP process. Some of these have been focused on the development of temperature across the thickness

of the laminate (z direction) at one particular location. The transient and steady state one-dimensional (1D) problems were solved either analytically or numerically by various authors [38–43]. In these studies, the governing heat transfer equation (1) is approximated by a parabolic differential equation as $\frac{\partial T}{\partial t} = \alpha \frac{\partial^2 T}{\partial z^2}$ where the temperature (T) varies along the thickness direction (z) and time (t), and α is thermal diffusivity ($\alpha = \frac{K_z}{\rho C_p}$) which is dependent on the material's thermal properties in through-thickness (z) direction. The transient one-dimensional problem is solved either-analytically or numerically by various authors to predict the temperature distribution results. Among these, Dai and Ye [41] proposed analytical solution of the problem in order to obtain temperature distribution through the tape thickness in the tape winding process. They indicated that the temperature distribution is dependent on tape geometry, thermal properties of the composite substrate and the winding speed. Convective boundary condition for the heated region was assumed along with insulated surface for the bottom of the composite substrate and the exact solution was proposed. Following their method, Weiler *et al.* [39] investigated the transient thermal problem for laser-assisted AFP. Heat flux boundary condition was prescribed for the surface. The focus of their study was on heat accumulation, especially in thin tapes and thin substrates. The method of variation of parameters was used as an alternative mathematical method to solve the problem analytically. With the derived exact solution, the temperature within a body as a function of time and location through the thickness direction was obtained. Lee [40] used the same technique i.e., variation of parameters, to solve the 1D transient model analytically. The solution was later used in development of the functional block diagram of AFP process with new heating alternatives. Tierney *et al.* [42] used even a more simplified thermal model in which the variation of temperature versus time was neglected and a one-dimensional steady state model was used to predict the temperature distribution in the vicinity of the tow-placement head. The temperature data for the surface layer was then applied to void dynamics model and consolidation model to establish void content gradients through the thickness of the laminate. In an attempt to predict the variation of void contents in the laminate, Khan *et al.* [38,43] improved the thermal model proposed by Tierney *et al.* [42] by considering the variation of temperature versus time. As such, they discretized the laminate using one-dimensional transient heat transfer model. In a similar manner to previous study [42], the temperature data was used to obtain the void contents variation during the lay-up process. Furthermore, the effects of compaction force, lay-up speed and hot gas flow

rate were investigated. Although these studies can predict the overall temperature gradient through the thickness using a one-dimensional thermal model, due to several simplifications and approximations applied on the model, they cannot reflect the actual process. As such, several studies focused on extending the 1D model to a more sophisticated two-dimensional thermal model by considering the temperature distribution along the lay-up direction (x-direction) along with temperature gradient through the thickness (z-direction) as shown below.

Earlier studies by Beyeler *et al.* [44] and Nejhad *et al.* [45] in 1980s and 1990s addressed the 2D heat transfer analysis of the tape laying process. In these studies, a mapping technique was used to transform the orthotropic domain into an isotropic domain to obtain a set of differential equations. Using finite difference (FD) techniques, the expressions are discretized and temperature profiles along both lengthwise and through-thickness directions were predicted under the steady state condition. Finite element (FE) techniques as an alternative numerical method were also implemented by Grove [46], Mantell and Springer [47] as well as Sonmez and Hahn [48] to investigate the principal thermal phenomenon taking place in both tape winding and tape placement processes. The model was later used for investigating the effect of process variables on the quality of thermoplastic composites to establish a processing window [34,49]. The previous studies were limited to steady state condition by simplifying the transient problem. The identical FE approach was later extended to include the time dependency of the temperature (transient condition) in a 2D model. In 2011, Zhao *et al.* [50] constructed an ANSYS simulation model to perform a transient heat transfer analysis in AFP process. A novel strategy based on the birth and death of elements technique was used to model the moving heat source and step by step growth of composite substrate (material deposition) in the lay-up process. The predicted thermal history was used in a thermoelastic FE model to compute thermal stresses induced during the process. The manufacturing technique they aimed at modeling, was processing composite rings using AFP in which structures do not have free edges and thus the problem of distortion does not arise. The identical birth and death of elements technique was later utilized by Li *et al.* [51] to obtain the temperature field during the processing of flat thermoplastic composite parts. The effect of heater temperature and roller speed on the bonding temperature was investigated. The numerical results were compared with analytical solution of 1D heat conduction differential equation. Further investigations were performed by Han *et al.* [52] to study the effect of preheating on heat distribution inside the laminate. They stated that preheating, as an influential process parameter,

can expand the melting area in both longitudinal and through thickness directions. They introduced boundary conditions; however, FE methodology implemented for the problem was not presented. Thermal conductivity values for the orthotropic domain were assumed to be constant and independent of the processing temperature. This might lead to erroneous results, since for the case of thermoplastic composites, the processing temperature is extremely high and there are dramatic changes in thermal properties at elevated temperatures which needs to be taken into account. Moreover, verification of their model was not performed and thus the accuracy of results was debatable. More recently in 2018, Kollmannsberger *et al.* [53] performed a 2D transient simulation of laser-assisted AFP. In previous studies, perfect thermal contact between the plies of composite laminate was assumed; however, they took into account thermal contact resistance in the model. They compared temperature results for two cases of with/without presence of thermal contact resistance and they highlighted that in the process modeling for an accurate analysis, it needs to be considered. The focus of their study was on investigating the effect of thermal contact resistance between layers.

In an attempt to provide a more precise prediction tool for composites produced by AFP, a small group of researchers, developed multi-dimensional thermal models to study spatial distribution of temperature in all x, y and z directions. In 1996, James and Black [54] developed a three-dimensional (3D) thermal model to predict temperature profile in filament winding process using an infrared energy source. The generated differential equations were solved numerically using a FD technique and results were compared with experimental temperature measurements using an infrared camera in conjunction with the winding apparatus. Unlike the previous model, Toso *et al.* [55] considered transient 3D effects of the tape winding process. The numerical simulation of the process was constructed based on FE in ANSYS. The predicted temperature results during the lay-up process were compared with experimental measurements using infrared pyrometry to provide validation. The tape winding process was the focus of their study in which structures are made in the form of cylinders or spheres having no free edges. As such, the issue of distortion does not arise, and further studies are required to make structures in the form of strips with free edges where distortion plays an active role. Hassan *et al.* [56] considered the same analysis strategy as [55], yet for thermoset materials. They discretized the model into 8-node brick elements to obtain coupled ordinary differential equations. A 3D FE code was written to obtain nodal temperatures during the lay-up process of a composite ring. In order to verify the FE code,

carbon/epoxy composite rings were fabricated using a filament winding machine and K-type thermocouples were used to measure the temperature during the process. Although the 3D transient analysis of the problem was introduced, the model was limited to manufacturing of thermoset composites using filament winding technique. A few years later in 2016, Jeyakodi [5] performed a FE simulation of in-situ AFP process for manufacturing flat thermoplastic composites. The coupled temperature displacement analysis was performed in ABAQUS to be able to apply the transient laser heat and roller pressure in simulation. The main focus of his study was on predicting the residual stresses developed during the in-situ process. To do so, thermal profiles induced in the laminate for different process configurations were determined and induced stresses in the laminate were calculated accordingly. His study provides a detailed numerical model of laser-assisted AFP process. Although the simulation tool could be used for studying different process parameters and identifying the interactions numerically, experiments have not been performed to provide validation. This necessitates more experimental research on in-situ processing of thermoplastic composites with free edges to gain more understanding of the process and to fill the gaps in existing literature. More recently, Tafreshi *et al.* [30] constructed a FE model based on ANSYS to determine the spatial temperature distribution in thermoplastic composites made by AFP using hot gas torch. In their study, a few different approaches were taken, including closed form (analytical) and FE, in order to obtain understanding of the heat transfer problem. The FE model was developed for isotropic case and then extended to the orthotropic case in which experiments were performed to provide validation of the results.

A summary of relevant publications in literature is provided in Table 1.

Each heat transfer model associated with the process in literature has its own particular application, and thus, thermal models and corresponding process parameters change for different composite materials (thermoset or thermoplastic), specifications (composite rings or flat strips), and heating mechanism (laser, infrared, heat lamp or hot gas torch). Looking at existing literature, it is evident that there are number of works addressing processing of thermoplastic composites along with experimental validation of the results. Nevertheless, they are limited to either-filament/tape winding process or laser-assisted AFP. The focus of this study is on processing thermoplastic composite parts with free edges using hot gas assisted-AFP. There are differences between the previous manufacturing processes: both filament winding process and fiber placement

process are considered additive in nature because the material (thermoset/thermoplastic) is deposited layer by layer. Nevertheless, there are some features that distinguish the fiber placement process. Firstly, filament winding is applicable to make structures in the form of cylinders or spheres (mainly convex surfaces) while fiber placement technique can be used for structures with both convex and concave surfaces. Secondly, filament winding can only be used to make structures having no free edges, where the problem of distortion does not arise. Fiber placement can be used to make structures with free edges, where the issue of distortion is important. Thirdly, in filament winding it is required to apply tension on the tows, while in fiber placement process, tows are placed on the surface of the tool using a consolidation roller [1,29,35]. Hot gas torch, on the other hand, has been implemented since 1986 as the primary heat source for processing thermoplastic composites using AFP due to its low cost and wide process window [57]. More recently, laser heating has garnered attention among manufacturers as it provides high energy density, faster processing rates and better surface finish [57]. Even though this approach may be appropriate for certain applications and people tend to think that laser is better than hot gas torch (due to the fact that it is more focused, and heating can be more efficient), there are benefits from the hot gas torch that laser does not have. One thing is that laser cannot be used for glass fiber composites. This is because laser heats the carbon fibers and the heat from the carbon fiber heats the resin. Glass fibers do not absorb the laser energy and as such it cannot be heated by laser. Secondly, laser imposes safety hazard. Thirdly, hot gas torch spreads out the heat and this can help to preheat the tape. This is more effective for heating for joints. It could be shown that hot gas torch can process much faster than laser due to the better heat creation within the joining area. Laser introduces the heat almost only into the carbon fiber and indirectly heats the polymer, while hot gas melts the polymer directly in the joining area. And fourthly, laser needs to be precisely controlled for the end of the beam to be at the NIP point while the hot gas torch has less of a problem.

2.4 Research Objectives

Although the models proposed in literature provide insight into the transient heat transfer problem of AFP process, they are either limited to the local region in the vicinity of the nip point and did not take into account the temperature distribution in the entire structure; or owing to several simplifications in the model and lack of experimental data, the predicted temperature history did

not reflect the actual AFP process where the problem of distortion arises in manufacturing of composite parts with free edges. The focus of this thesis is to develop a two-dimensional transient heat transfer model for moving heat source problem associated with AFP thermoplastic composites manufacturing with experimental validation of results to gain more understanding of the way temperature gradients develop during the process.

The thesis is organized in such a way that first, finite difference (FD) formulation of the transient heat transfer problem is presented based on energy balance approach. The explicit methodology is then introduced as a solving method for predicting the temperature distribution numerically. A computer code is written in MATLAB (MathWorks Inc.) to generate the temperature distribution along the layup direction and through the thickness of the composite substrate. The methodology implemented for modeling the moving heat source problem is discussed in detail. The temperature distribution history results are presented, and experimental trials are conducted to provide verification of the results. This study can open the way for understanding the development and distribution of crystallinity as a function of space and time. Residual stresses and deformation of the structure can then be determined.

Table 1. Summary of relevant publications in literature

Reference	Model Type	Dimension	Technique	Experiment
Tierney <i>et al.</i> 2003 [42]	Steady state	1D	FD	(AS4/PEEK ATP HGT)
Khan <i>et al.</i> 2010 [38,43]	Transient	1D	FD	(AS4/PEEK AFP HGT)
Dai and Ye 2002 [41]	Transient	1D	Analytical	(GF/PP tape winding)
Weiler <i>et al.</i> 2018 [39]	Transient	1D	Analytical	–
Lee 2004 [40]	Transient	1D	Analytical	–
Beyeler <i>et al.</i> 1988 [44]	Steady state	2D	FD	–

Nejhad <i>et al.</i> 1991 [45]	Steady state	2D	FD, Analytical	–
Agarwal <i>et al.</i> 1992 [58]	Steady state	2D	FD	(APC-2 laser tape winding)
Grove 1988 [46]	Steady state	2D	FE	–
Mantell and Springer 1992 [47]	Steady state	2D	FE	–
Sonmez and Hahn 1997 [48]	Steady state	2D	FE	–
Shih and Loos 1999 [59]	Transient	2D	FE	(AS4/PEEK filament winding)
Tumkor <i>et al.</i> 2001 [60]	Transient	2D	FD	–
Zhao <i>et al.</i> [50] 2011	Transient	2D	FE	–
Li <i>et al.</i> [51] 2015	Transient	2D	FE	–
Han <i>et al.</i> 2014 [52]	Transient	2D	FE	–
Stokes-Griffin <i>et al.</i> 2014 [61,62]	Transient	2D	FE	(AS4/PEEK AFP Laser)
Kollmannsberger <i>et al.</i> 2018 [53]	Transient	2D	FD	(CF/PES AFP Laser)
James and Black 1996 [54]	Steady state	3D	FD	(APC-2 filament winding)
Toso and Ermanni 2003 [55]	Transient	3D	FE	(GF/PP tape winding) (C/Epoxy filament winding)
Hassan <i>et al.</i> 2005 [56]	Transient	3D	FE	–
Jeyakodi 2016 [5]	Transient	3D	FE	–
Tafreshi <i>et al.</i> 2019 [30]	Transient	3D	FE	(AS4/PEEK composite strip using AFP)

Chapter 3: THERMAL ANALYSIS MODEL

3.1 Heat Transfer Mechanism in AFP Thermoplastic Composites Process

As the first step in heat transfer analysis of AFP process using a hot gas torch, it is necessary to understand the heat transfer mechanism between the hot gas torch and the composite substrate. In fact, the heat transfer mechanism is quite complex not only because of the turbulent nature of the thermal fluid flow, but also due to the simultaneous heat transfer that occurs in both the thermal fluid and the composite substrate. The hot gas flow coming out of the torch nozzle, has very high temperature in the range of 800 – 1000 °C for the case of AFP of thermoplastics. As such, noticeable temperature difference exists between the hot gas flow and the composite surface. This results in convective heat transfer between the aforementioned media as shown in Figure 9. A local heat flux equation is utilized to model the convective heat transfer as $q'' = h_{HGT} (\Delta T)$ where h_{HGT} is the convective heat transfer coefficient between the hot gas torch and the composite surface, and for the conversion of a portion of the kinetic energy of the gas upon impact with the surface of the composite material. ΔT accounts for the temperature difference between the two media [63,64]. The localized heat flux diffuses through the composite substrate (Figure 9) and the speed of diffusion depends upon the value of thermal diffusivity α ; the larger the value of α , the faster heat will diffuse through the material. In fact, a temperature gradient exists in the laminate which results in an energy transfer from the upper surface subjected to the hot gas flow (high-temperature region) to the underneath layer (low-temperature region) [63].

In this study, a moving heat source is considered in the transient heat transfer problem. Along with the heat transfer through the thermal fluid (heat convection) and through the composite substrate (heat diffusion), the unheated regions are exposed to the surrounding ambient which plays an important role in the cooling stage. The convection heat transfer follows the Newton cooling law as shown below [63–65]:

$$q'' = h_c (\Delta T) \quad (2)$$

Where q'' is the heat flux (W/m^2), h_c is the convective heat transfer coefficient between the composite substrate and the surrounding ambient ($W/m^2 \cdot K$), and ΔT is the temperature difference between the aforementioned media (K).

The composite substrate surface is subdivided into two separate zones as shown in Figure 9. *Zone 1* represents the region of the substrate exposed to the surrounding ambient and cooled by ambient air while *zone 2* demonstrates the region of the composite substrate which is exposed to the hot gas flow. Therefore, at any moment during the process, the convective heat transfer coefficients can be expressed as following:

$$h = \begin{cases} h_{HGT} & ; \text{zone 2} \\ h_c & ; \text{zone 1} \end{cases} \quad (3)$$

The convective heat transfer coefficient h_{HGT} may vary along the length of the zone 2. As a preliminary analysis, it is taken to be a constant in this study.

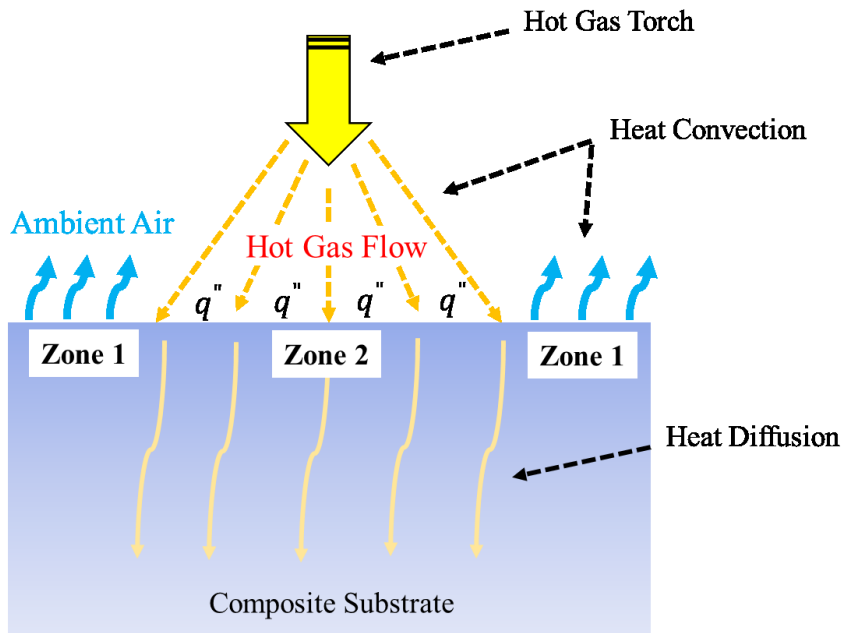


Figure 9. Heat transfer mechanism between the hot gas flow and the composite substrate [18]

3.2 Transient Heat Transfer Model of AFP Process Based on Finite Difference Formulation

In this study, the AFP process is simulated based on Finite Difference (FD) method. The 2D rectangular domain and the coordinate system considered in this study are illustrated in Figure 10. There is a moving heat source which travels with a specified speed from the left edge to the right along the upper side of the rectangular domain. The heat energy provided by the heat source, is transferred to the composite substrate which results in nodal temperature increase. At the same time, the upper side is subjected to the surrounding ambient (room temperature), which accounts for the cooling stage. In this section, we aim at developing the FD formulation of the transient heat transfer problem in a 2D rectangular domain (the composite substrate - aluminum mandrel assembly) subjected to a moving heat source using the energy balance approach. First, the domain is subdivided into a sufficient number of volume elements and the energy balance is applied on each element. An appropriate formulation is derived for the interior nodes. The formulation can be used for all the interior nodes regardless of the boundary conditions, since the boundary conditions have no effect on the FD formulation of these nodes. Second, for nodes on the boundaries, depending on type of the boundary condition, an appropriate formulation is derived for each case. The explicit methodology is introduced as a solving method for the transient heat transfer problem. The stability criteria are defined to confine the variation and oscillation of the nodal temperatures. Eventually, the formulations are coded to be able to generate the nodal temperatures after each time step and plot the temperature distribution.

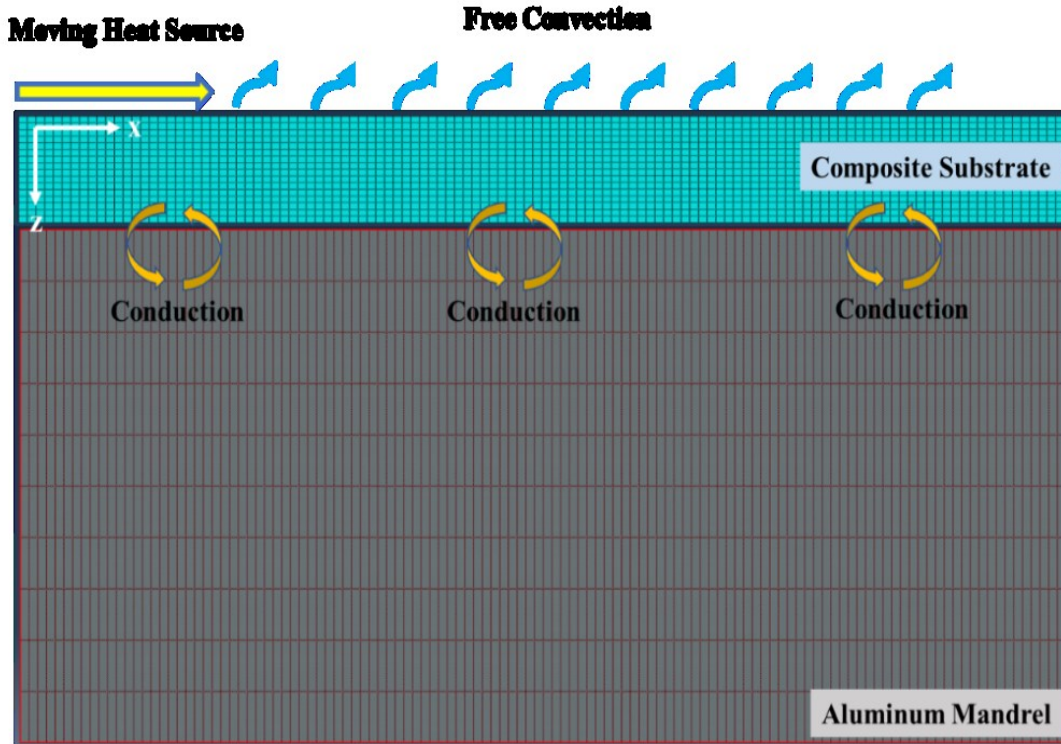


Figure 10. The finite difference model to predict the transient temperature field of the composite substrate – aluminum mandrel assembly during the lay-up process [18]

3.2.1 Assumptions

Prerequisite for a valid FD model is a feasible simplification of the problem, in order to be able to perform the analysis with short computational time with mathematical tools available. The FD model proposed in this study is developed based on the following assumptions [18]:

- (a) In the actual AFP process, the material deposition is part of the model. In other words, it is necessary to address the placement of the incoming tape after passing through the AFP guided assembly on the substrate with the help of the consolidation roller. However, in this study, it is assumed that there is no material deposition and the model is developed for the case of the moving heat source on a composite substrate being in contact with an aluminum mandrel.

- (b) The two-dimensional heat transfer problem is considered in this study. There are some reasons highlighting this assumption: the composite substrate is relatively long with respect to the width and one can neglect the temperature variation through the width. Second, the heat input is almost constant over the tape width and the material is uniformly heated in that direction. As such, one can reasonably ignore the temperature variation in the width direction (y-direction) and the assumption is rated tolerable [45,47,48,59].
- (c) The process is regarded as a transient heat transfer problem which is necessary in order to investigate the temperature profiles in different regions of the composite substrate as time progresses.
- (d) The aluminum mandrel is considered in the model as it cannot be ignored in the actual manufacturing process.
- (e) The composite substrate is modeled as an orthotropic domain and the thermal conductivity depends on the direction (longitudinal and transversal). However, for the aluminum mandrel, only one value is assigned as it is isotropic.
- (f) The thermal conductivity values for the composite domain are temperature dependent. Because in higher temperatures, the molecules move faster, and energy will be transported faster. As such, the value of thermal conductivity, as an indicator of how fast heat flows in a material, needs to be temperature dependent [63].
- (g) The hot gas flow exposing on the composite substrate surface is modeled as a convective boundary condition with a constant heat convection coefficient.
- (h) A convective boundary condition is prescribed to the composite substrate surfaces (exposed to hot gas flow) and left, right and bottom boundaries (exposed to ambient air).
- (i) The heat absorption and generation resulting from melting and crystallization respectively is assumed to be negligible.

3.2.2 Discretization of The Finite Difference Model

3.2.2.1 Space Discretization

In the energy balance approach, the medium is subdivided into a sufficient number of volume elements as shown in Figure 11. This needs to be done separately for both the composite substrate and the aluminum mandrel. Consider a transient two-dimensional heat conduction problem in a rectangular domain. The length of the domain (L) is subdivided into M sections of equal distance ($\Delta x = L/M$) in the x direction. As a result, there are $M + 1$ nodal points $0, 1, 2, \dots, m - 1, m, m + 1, \dots, M$ in the longitudinal direction. The x -coordinate of any point m can be obtained simply by multiplying the m number by the distance Δx , i.e., $x_m = m \Delta x$. For both the composite substrate and the aluminum mandrel, similar number of divisions in x direction is considered. The same procedure is performed for the transversal direction. The thickness of the composite substrate domain (W_c) is subdivided into N_c sections of equal distance ($\Delta z_c = W_c / N_c$) in the z direction. In the same manner, the thickness of the aluminum mandrel domain (W_m) is subdivided into N_m sections of equal distance ($\Delta z_m = W_m / N_m$) in the z direction. As such, there are $N_c + 1$ nodal points $(0, 1, 2, \dots, n_c - 1, n_c, n_c + 1, \dots, N_c)$ in the transversal direction for the composite substrate and $N_m + 1$ nodal points $(0, 1, 2, \dots, n_m - 1, n_m, n_m + 1, \dots, N_m)$ in the same direction for the aluminum mandrel. The z coordinate of any point n_c or n_m can be obtained simply by multiplying the n_c or n_m numbers by the corresponding distance Δz_c or Δz_m respectively i.e., $z_c = n_c \Delta z_c$ for the composite substrate and $z_m = n_m \Delta z_m$ for the aluminum mandrel. In general, each nodal point is denoted by a specific (m, n) coordinate. The corresponding nodal temperature at a coordinate (m, n) can be denoted as $T_{m,n}$ which means the temperature at a node with x coordinate of x_m and z coordinate of z_n . A FD mesh sample for two-dimensional conduction in rectangular coordinates for interior nodes are illustrated in Figure 11 (Left). It is assumed that properties at each node such as temperature and heat generation is representative of the whole element [64].

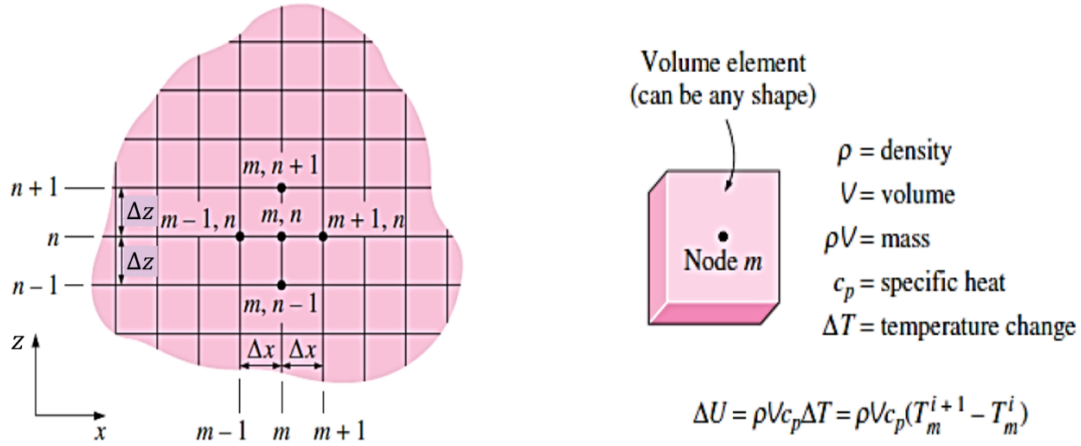


Figure 11. Finite difference mesh for 2D conduction in rectangular coordinates (Left); volume element of a node and the change in the energy content during a time interval Δt (Right) [64]

3.2.2.2 Time Discretization

The FD method can be applied to steady heat transfer problems by discretizing the problem in the space variables. If the steady condition is prevailed, the temperature do not change with time. As a result, the solution obtained for this condition is valid for any time [64]. As for the case of this study, a moving heat source travels across the upper side of the composite substrate. The temperature changes with time as well as position. As such, the heat transfer problem is not steady and a formulation for a transient heat transfer problem is required to be proposed. In the case of the transient condition, in addition to the discretization in space, one needs to consider the discretization in time as well (Figure 12). A suitable step time needs to be selected first. At time $t = 0$, initial condition is applied i.e., it is assumed that before starting the movement of the heat source, the temperature is maintained constant throughout the entire domain and it is the same as room temperature. After one step time Δt , the nodal temperatures need to be updated based on the previous step. Solving for the unknown nodal temperatures repeatedly for each Δt , the final nodal temperatures at desirable time can be calculated. The selection of step time Δt is very important in explicit method since it determines the stability of the iteration method. A smaller Δt is desirable as it increases the accuracy of the solution, but the computation time increases correspondingly [64]. The selection of Δt and the stability criteria will be explained in the following sections.

As demonstrated in Figure 12, the nodal temperatures are denoted using double subscript notation (m, n) as $T_{m,n}$ which means the temperature at a node with x coordinate of x_m and z coordinate of z_n . For the transient problems, we need to define a superscript i , as the counter of time steps. In this definition, $i = 0$ corresponds to the initial condition specified by the problem at $t = 0$. The next step time is denoted by $i = 1$ which accounts for $t = 1 \times \Delta t$. Depending on the required number of steps, the nodal temperatures are obtained at each time step. A general time step i corresponds to $t_i = i\Delta t$. Based on this notation, the temperature at node (m, n) at time step i is denoted by $T_{m,n}^i$. Looking at Figure 12, it can be noticed that at each step, we need to find the nodal temperatures in the 2D rectangular domain. This is performed by solving the formulations for all interior nodes and boundary nodes. Once the solution is obtained for step i , the time is shifted forward for one step time Δt and the counter i is shifted to $i + 1$ accordingly. For the new step, all the nodal temperatures are modified, and the set of formulations need to be solved for the new iteration. This process is repeated for the specified number of steps. Using this method, we are able to obtain temperature at each point and at each time step. The target node location can be determined using two coordinates of x, z and the step in which the temperature is aimed to obtain is notified by the index i [64].

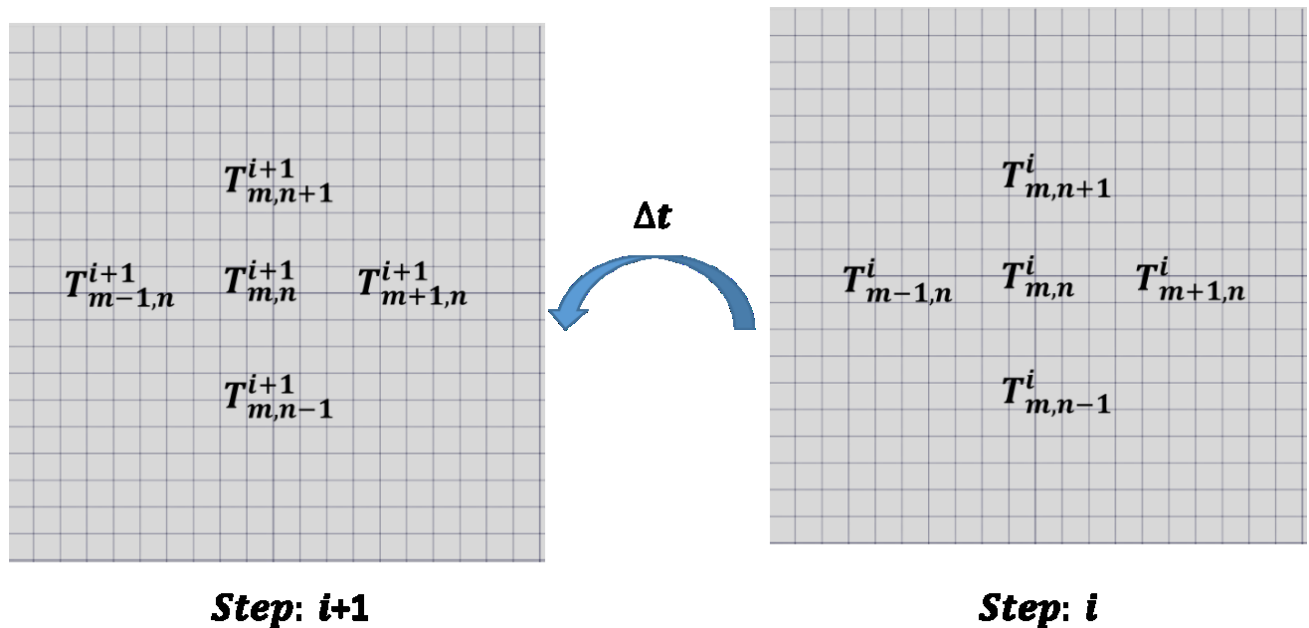


Figure 12. Space and time discretization of a 2D transient heat conduction problem

3.2.3 Energy Balance Approach

In this approach, a volume element for each node is assumed and the energy balance is written for this element. If one assumes that all heat transfer is into the element, the energy balance for a volume element during a time interval Δt can be expressed as [64]:

$$\left(\begin{array}{c} \text{Heat transferred into} \\ \text{the volume element} \\ \text{from all of its surfaces} \\ \text{during } \Delta t \end{array} \right) + \left(\begin{array}{c} \text{Heat generated} \\ \text{within the} \\ \text{volume element} \\ \text{during } \Delta t \end{array} \right) = \left(\begin{array}{c} \text{The change in the} \\ \text{energy content of} \\ \text{the volume element} \\ \text{during } \Delta t \end{array} \right)$$

Or

$$\Delta t \times \sum_{\text{All sides}} \dot{Q} + \Delta t \times \dot{E}_{gen,element} = \Delta E_{element} \quad (4)$$

Where \dot{Q} is the rate of heat transfer. Depending on the boundary conditions, it can account for conduction terms, convection, heat flux or radiation. As shown in Figure 11 (Left), $\Delta E_{element}$ depends on density, volume, specific heat and temperature change of the element. For any node (m, n) in the 2D domain, the equation can be written as [64]:

$$\sum_{\text{All sides}} \dot{Q} + \dot{E}_{gen,element} = \rho V_{element} C_p \frac{T_{m,n}^{i+1} - T_{m,n}^i}{\Delta t} \quad (5)$$

Where $T_{m,n}^{i+1} - T_{m,n}^i$ represents the temperature change of the node (m, n) during the time interval Δt . We should note that the only difference between the transient and steady conditions formulation is the term on the right side of the equal sign. When the steady condition is prevailed in the heat transfer problem, the temperature does not vary with time and the formulation is reduced to the steady condition [64].

There are two general methods to obtain the nodal temperatures after each time step; explicit method and implicit method. In the former, temperatures at previous time step i is used while in the latter temperatures at new time step $i + 1$ is used to obtain temperatures at time step $i + 1$. These two general forms are expressed as following [64]:

$$\text{Explicit method} \quad \sum_{\text{All sides}} \dot{Q}^i + \dot{E}_{gen,element}^i = \rho V_{element} C_p \frac{T_{m,n}^{i+1} - T_{m,n}^i}{\Delta t} \quad (6)$$

$$\text{Implicit method} \quad \sum_{\text{All sides}} \dot{Q}^{i+1} + \dot{E}_{gen,element}^{i+1} = \rho V_{element} C_p \frac{T_{m,n}^{i+1} - T_{m,n}^i}{\Delta t} \quad (7)$$

The objective of this study is calculating the nodal temperatures at new time step i.e., $T_{m,n}^{i+1}$. As can be easily noticed, the explicit method is quite straightforward. The nodal temperatures at previous time step i.e., $T_{m,n}^i$ is known and it is only required to calculate the unknown $T_{m,n}^{i+1}$ using the explicit formulation. However, in implicit method, the only given term is $T_{m,n}^i$ and the rest of the equation is unknown. Hence, in this method, nodal temperatures need to be solved simultaneously for each time step and requires additional computational method to solve the resulting set of equations. Although the explicit method is straightforward, but we should keep in mind that this method may result in instabilities while solving for each iteration. As such, special care is needed to monitor stability while using this method. On the other hand, implicit method is unconditionally stable and for the problems which satisfying the stability criteria is rather difficult, it would be a better choice to implement this method to avoid instabilities [64].

3.2.3.1 Interior Nodes

A schematic illustration of the heat transfer for an interior node inside the domain is shown in Figure 13 in which the heat conduction occurs in both x (longitudinal) and z (transversal) directions. In the y direction, a unit depth of $\Delta y = 1$ is considered. For a general case, the heat generation may exist inside the domain. $\dot{e}_{m,n}$ accounts for the heat generation for each volume element. For the case of this study, the heat generation is negligible, and we can ignore the heat generation term. As stated earlier, for a 2D composite substrate with the length of L and thickness of W_c , there are $M + 1$ nodal points in longitudinal direction (x -direction) and $N_c + 1$ nodal points in transversal direction (z -direction). In the same manner, for the aluminum mandrel with the length of L and width of W_m , there are $M + 1$ nodal points in longitudinal direction (x -direction) and $N_m + 1$ nodal points in transversal direction (z -direction). In general, the entire domain including both the composite substrate and the aluminum mandrel consists of $(M + 1)(N_m + N_c + 1)$ nodes

in which $(M - 1)(N_c - 1)$ nodes are representative of the composite substrate interior nodes and $(M - 1)(N_m - 1)$ nodes are representative of the aluminum mandrel interior nodes. Each nodal point is denoted by specific (m, n) coordinate and the corresponding nodal temperature at a coordinate (m, n) is denoted as $T_{m,n}$.

The energy balance based on equation (4), can be written for all interior nodes as following in which the general interior node (m, n) involves heat conduction from four sides (right, left, top, and bottom) [64]:

$$k_x \Delta z \frac{T_{m-1,n} - T_{m,n}}{\Delta x} + k_x \Delta z \frac{T_{m+1,n} - T_{m,n}}{\Delta x} + k_z \Delta x \frac{T_{m,n+1} - T_{m,n}}{\Delta z} + k_z \Delta x \frac{T_{m,n-1} - T_{m,n}}{\Delta z} = \rho \Delta x \Delta z C_p \frac{T_{m,n}^{i+1} - T_{m,n}^i}{\Delta t} \quad (8)$$

Where k_x and k_z are longitudinal and transverse thermal conductivities respectively. This formulation is valid for all interior nodes inside the composite substrate and the aluminum mandrel domains regardless of the boundary conditions. It should be noted that for the case of the aluminum mandrel (isotropic domain), the thermal conductivities in both longitudinal and transversal directions all identical and equal to k_m .

From equation (8), by dividing the two sides of the equation by the volume of the element $(\Delta x \Delta y \Delta z)$ and using the Taylor series expansion to derive the finite difference approximation of the second derivative of a temperature function (equation 9), the 2D general heat transfer equation (heat diffusion equation) can be derived as equation (10) [64]. It is assumed that heat generation is negligible and there is no heat transfer in y direction.

$$\frac{\partial^2 T}{\partial x^2} = \frac{T_{m+1,n} - 2T_{m,n} + T_{m-1,n}}{(\Delta x)^2}, \quad \frac{\partial^2 T}{\partial z^2} = \frac{T_{m,n+1} - 2T_{m,n} + T_{m,n-1}}{(\Delta z)^2} \quad (9)$$

$$K_x \frac{\partial^2 T}{\partial x^2} + K_z \frac{\partial^2 T}{\partial z^2} = \rho C_p \frac{\partial T}{\partial t} \quad (10)$$

The next step in deriving the nodal temperature, is indicating the time step on the left side of the equation (8). In this study, explicit method is selected to solve the transient heat transfer formulation. Based on the definition, the explicit FD formulation of the heat transfer problem can be expressed by [64]:

$$\begin{aligned}
 k_x \Delta z \frac{T_{m-1,n}^i - T_{m,n}^i}{\Delta x} + k_x \Delta z \frac{T_{m+1,n}^i - T_{m,n}^i}{\Delta x} + k_z \Delta x \frac{T_{m,n+1}^i - T_{m,n}^i}{\Delta z} \\
 + k_z \Delta x \frac{T_{m,n-1}^i - T_{m,n}^i}{\Delta z} = \rho \Delta x \Delta z C_p \frac{T_{m,n}^{i+1} - T_{m,n}^i}{\Delta t}
 \end{aligned} \quad (11)$$

Expressing the left side of the equation (8) at time step $i + 1$, would give the implicit formulation. If one assumes a uniform mesh structure in which $\Delta x = \Delta z = l$, equation (11) can be solved explicitly for the new temperature $T_{m,n}^{i+1}$ to give:

$$T_{m,n}^{i+1} = c [k_x (T_{m-1,n}^i + T_{m+1,n}^i) + k_z (T_{m,n+1}^i + T_{m,n-1}^i)] + [1 - 2c (k_x + k_z)] T_{m,n}^i \quad (12)$$

Where $c = \frac{\Delta t}{\rho \Delta x \Delta z C_p}$ is considered as a coefficient to simplify the formulation above.

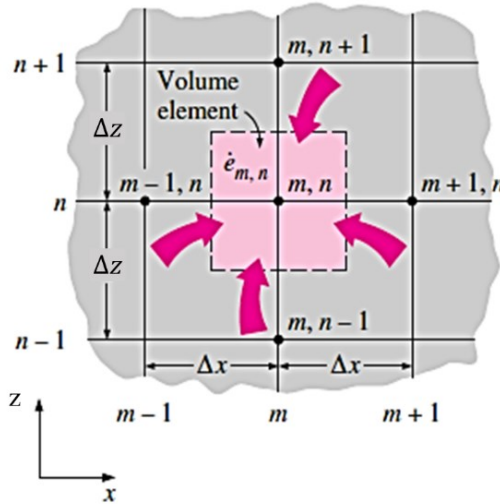


Figure 13. The volume element of a general interior node (m,n) for 2D transient heat conduction problem in rectangular coordinates [64]

3.2.3.2 Boundary Nodes

The formulation presented for interior nodes is not applicable for boundary nodes. The boundary nodes do not have neighboring nodes on at least one side and a separate formulation is required to be obtained for these nodes. There are four common boundary conditions used in problems. These include constant temperature, constant heat flux, convection and radiation [64]. The convective boundary condition (subjected to ambient air) is prescribed as the boundary condition for the left and right boundaries along with the bottom boundary of the aluminum mandrel. For the top boundary in which a moving heat source travels across the upper side of the composite substrate, an appropriate energy balance needs to be applied. The entire heat transfer problem is controlled significantly by the definition of boundary conditions at the upper side edge and special care is required for assigning this boundary condition.

In this study, a moving heat source is encountered in the heat transfer problem. As mentioned earlier, along with the heat transfer through the thermal fluid (heat convection) and through the composite substrate (heat diffusion), the unheated regions are exposed to the surrounding ambient which plays an active role in the cooling stage. As such, the convection heat transfer occurs at the unheated regions in which the heat transfer follows the Newton cooling law as presented in equation (2). In order to take both of the heat convection mechanism by the thermal fluid (heating stage) and the surrounding ambient (cooling stage) into account, the composite substrate surface boundary needs to be subdivided into two separate zones; Zone 1 (the region of the substrate exposed to the surrounding ambient and cooled by ambient air) and Zone 2 (the region of the composite substrate which is exposed to the hot gas flow) as illustrated in Figure 14. We should note that the heat source is moving, thus the location of each zone is varying with time. In other words, if a specific node on the upper side boundary is selected, the boundary condition and consequently the formulation describing the temperature variation of this node varies with time. Regardless of the value of the heat convection coefficient, we are able to write the energy balance for boundary nodes on the upper side boundary to obtain the corresponding formulation. The general energy balance equation presented in equation (5) is used for this purpose.

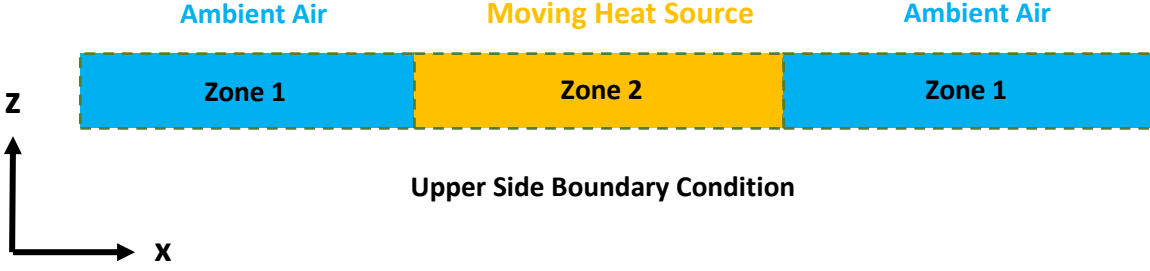


Figure 14. Upper side boundary condition consisting of two zones; Zone 1 (ambient air) and Zone 2 (hot gas flow)

An illustration of a boundary node in the upper side edge is shown in Figure 15. As can be seen, the heat conduction occurs at the left, right and bottom boundaries. The top edge is exposed to a thermal fluid with temperature of T_∞ and the heat convection coefficient of h . Depending on the zone as elaborated earlier, the h and T_∞ values vary for ambient air and the hot gas torch. The energy balance on the volume element can be written as [64]:

$$\begin{aligned}
 h \Delta x (T_\infty - T_{m,n}^i) + k_x \left(\frac{\Delta z}{2} \right) \frac{T_{m+1,n}^i - T_{m,n}^i}{\Delta x} + k_x \left(\frac{\Delta z}{2} \right) \frac{T_{m-1,n}^i - T_{m,n}^i}{\Delta x} \\
 + k_z (\Delta x) \frac{T_{m,n-1}^i - T_{m,n}^i}{\Delta z} = \rho \Delta x \frac{\Delta z}{2} C_p \frac{T_{m,n}^{i+1} - T_{m,n}^i}{\Delta t}
 \end{aligned} \quad (13)$$

One of the main differences between equation (11) for interior nodes and equation (13) for boundary nodes is the volume of the element. For a unit depth $\Delta y = 1$, for all interior nodes, the volume element is full-size ($Volume = \Delta x \cdot \Delta z \cdot 1$) while for the nodes at boundaries is half-size ($Volume = \Delta x \cdot \Delta z \cdot 1/2$) [64].

If one assumes a uniform mesh structure in which $\Delta x = \Delta z = l$, equation (13) can be solved explicitly for the new temperature $T_{m,n}^{i+1}$ to give [64]:

$$T_{m,n}^{i+1} = 2c \left[\frac{k_x}{2} (T_{m-1,n}^i + T_{m+1,n}^i) + k_z (T_{m,n-1}^i) + hlT_\infty \right] + [1 - 2c (k_x + k_z + hl)] T_{m,n}^i \quad (14)$$

Where $c = \frac{\Delta t}{\rho \Delta x \Delta z c_p}$ is considered as a coefficient to simplify the formulation above.

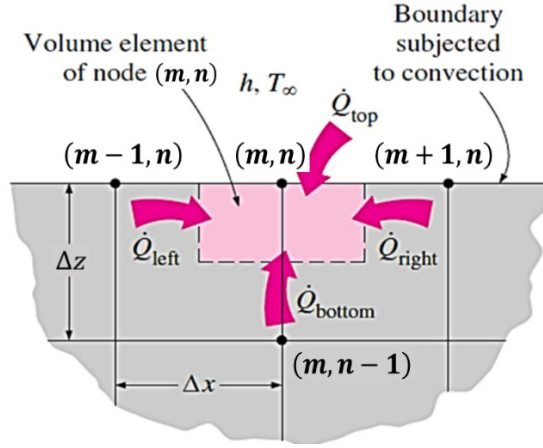


Figure 15. The energy balance on a volume element for a boundary node [64]

3.2.4 Stability Criterion

As stated in previous sections, the explicit method is not unconditionally stable, and the results may fluctuate and become unstable if some conditions are not met. In this study, the explicit method is utilized to formulate FD method for the transient heat transfer problem involving a moving heat source. Therefore, it is important to study the stability criterion for the explicit method. Stability criterion indicates that the explicit solution is stable if the time step Δt is sufficiently small. The value of Δt must be maintained below a certain value throughout the solution to avoid instability in nodal temperatures. On a basis of thermodynamics, the stability criterion is satisfied if the coefficients of all $T_{m,n}^i$ in the explicit representation of $T_{m,n}^{i+1}$ are greater than or equal to zero for all nodes. Based on this definition, one can obtain the required step time to have a stable solution [64].

Equations (12) and (14) were obtained for this study which needs to be solved explicitly for the new temperature $T_{m,n}^{i+1}$. Based on the stability criterion, we have different restrictions for interior nodes and boundary nodes because the coefficients of $T_{m,n}^i$ are different in these two formulations.

The most conservative criteria, i.e., the one with smallest coefficients of $T_{m,n}^i$ is selected for the entire solution. The stability criteria for interior nodes and boundary nodes for the case of this study is summarized in Table 2.

Table 2. Stability criteria for interior nodes and boundary nodes

	Interior nodes	Boundary nodes
Coefficient of $T_{m,n}^i$	$1 - 2c (k_x + k_z)$	$1 - 2c (k_x + k_z + hl)$
Stability Criteria	$\Delta t < \frac{\rho C_p l^2}{2(k_x + k_z)}$	$\Delta t < \frac{\rho C_p l^2}{2(k_x + k_z + hl)}$

* $c = \frac{\Delta t}{\rho \Delta x \Delta z C_p}$ is a coefficient to simplify the formulation above.

3.3 Solution Algorithm for Moving Heat Source Problem In MATLAB

The FD formulation of the transient heat transfer problem in a 2D rectangular domain (a composite substrate - an aluminum mandrel assembly) subjected to a moving heat source was proposed in the previous sections. The energy balance approach was utilized to derive the FD formulation for the interior nodes along with the boundary nodes. The explicit methodology was introduced as a solving method for the transient heat transfer problem. A summary of equations is presented in Table 3. In this section, we aim at developing a computer code in MATLAB (MathWorks Inc.) to be able to solve the system of FD equations numerically for the entire domain. Considering the complexity of the computational works, using a mathematical tool is necessary. Once the computer code was developed, the nodal temperatures can be obtained during the process.

Flow chart of the program is illustrated in Figure 16. The process consists of four principal stages, the input values directory, the mesh generation and the step time selection, the initial condition, and the application of the moving heat source into the problem. At the first stage, the input values are entered by the user. These include physical and thermal properties of the material,

dimensions of domain, number of divisions in x and z directions and the attributes of the boundary conditions. Then, the medium is subdivided into a sufficient number of volume elements based on the input values directory. This is conducted separately for both the composite substrate and the aluminum mandrel. As the explicit methodology is utilized for solving the transient heat transfer problem, the step time needs to be determined in the next step. Based on the stability criteria, an appropriate step time is found to confine the variation and oscillation to provide a stable solution. The initial condition is prescribed, and the continuous movement of the heat source in the actual AFP process is discretized into specified steps in the next step. Eventually, the nodal temperatures are computed for the entire domain. In order to apply the movement of the heat source into the problem, an accurate solution algorithm is devised which will be explained in detail in the following section.

Table 3. Nodal temperatures for interior and boundary nodes based on energy balance approach [18]

<i>Interior nodes</i>	$T_{m,n}^{i+1} = \frac{\Delta t}{\rho \Delta x \Delta z C_p} [k_x (T_{m-1,n}^i + T_{m+1,n}^i) + k_z (T_{m,n+1}^i + T_{m,n-1}^i)] + [1 - \frac{2\Delta t}{\rho \Delta x \Delta z C_p} (k_x + k_z)] T_{m,n}^i$
<i>Boundary nodes (zone 1)</i>	$T_{m,n}^{i+1} = \frac{2\Delta t}{\rho \Delta x \Delta z C_p} \left[\frac{k_x}{2} (T_{m-1,n}^i + T_{m+1,n}^i) + k_z (T_{m,n-1}^i) + h_c \Delta x T_\infty \right] + [1 - \frac{2\Delta t}{\rho \Delta x \Delta z C_p} (k_x + k_z + h_c \Delta x)] T_{m,n}^i$
<i>Boundary nodes (zone 2)</i>	$T_{m,n}^{i+1} = \frac{2\Delta t}{\rho \Delta x \Delta z C_p} \left[\frac{k_x}{2} (T_{m-1,n}^i + T_{m+1,n}^i) + k_z (T_{m,n-1}^i) + h_{HGT} \Delta x T_{HGT} \right] + [1 - \frac{2\Delta t}{\rho \Delta x \Delta z C_p} (k_x + k_z + h_{HGT} \Delta x)] T_{m,n}^i$

Δx : mesh size in x direction, Δz : mesh size in z direction, h_c : convective coefficient of zone 1, T_∞ : surrounding temperature, h_{HGT} : convective coefficient of zone 2, T_{HGT} : HGT temperature

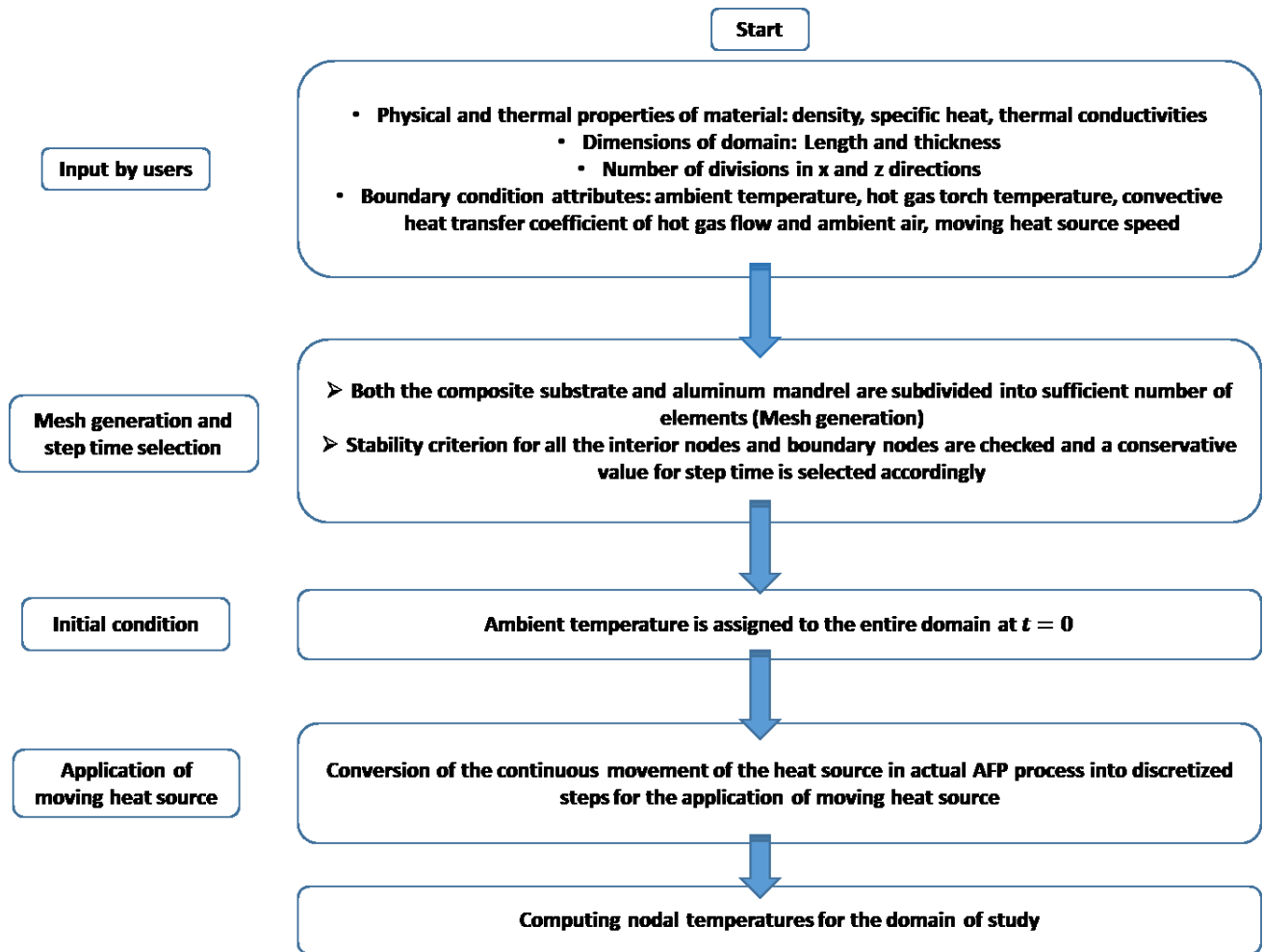


Figure 16. Flow chart of the FD program code in MATLAB

3.3.1 Input Values Directory

At the first stage, the input values are entered by the user. These include physical and thermal properties of the material, dimensions of domain, number of divisions in x and z directions and the attributes of the boundary conditions. For the case of this study, AS4/APC-2 carbon fiber/PEEK composite material is selected for the composite substrate and aluminum is considered as the mandrel's material. The physical and thermal properties for AS4/APC-2 were reported in literature [5] and those values are used in this study as input parameters as presented in Table 4 and 5. The corresponding properties of the aluminum mandrel were reported based on [50]. Experimental values and boundary condition attributes are also required to proceed the model. Temperature of the hot gas torch and the nitrogen gas flow rate are selected to be 875 °C and 60 standard liter per minute respectively. The convective heat transfer coefficient for free convection (h_c) is selected to be 10 W/m²K [30]. The heating length, where the h_{HGT} is applied, is selected to be 10 mm based on the experimental setup. Different values of the h_{HGT} were reported by several authors in literature [38,55,56,59]. In these studies, an initial value of h_{HGT} was assumed to start the calculations. A few thermocouples were utilized to obtain the temperature data experimentally. A comparison between experimental and numerical results was done; a few iterations were carried out until a good match is found to obtain the h_{HGT} . In this study, following a procedure similar to what was presented in literature, the maximum temperature corresponding to the position of TC3, embedded one layer beneath the top surface, obtained experimentally. It was then compared with the maximum temperature predicted numerically at that location. Following this procedure, the value of h_{HGT} of 990 W/m²K was obtained. In order to ensure that the selection of this value can lead to numerical results with reasonable accuracy, the temperatures at two other through-thickness locations were also monitored using two other embedded thermocouples (TC1 and TC2) and results were compared with numerical predictions. A summary of all input parameters for the FD code is presented in Table 6.

Table 4. Temperature dependent physical properties of AS4/APC-2 [5]

Temperature T(°C)	Specific heat C_p (J/kg°C)	Density ρ (Kg/m ³)	Viscosity μ (Mpa.s)
0	800	1601	7.03
50	930	1598	1.31
100	1040	1593	0.38
150	1260	1586	0.15
200	1300	1575	0.07
250	1400	1563	0.04
300	1550	1551	0.02
350	1650	1537	0.02
400	1700	1524	0.01

Table 5. Temperature dependent physical properties of AS4/APC-2 [5]

Temperature T(°C)	Conductivity		Diffusivity	
	k_x (Axial) W/m °C	k_z (Transverse) W/m °C	α_x (Axial) J/m ³ °C	α_z (Transverse) J/m ³ °C
0	3.5	0.42	2.733e-06	3.2792e-07
50	4.6	0.52	3.095 e-06	3.499 e-07
100	5.1	0.6	3.078 e-06	3.6216 e-07
150	5.9	0.7	2.952 e-06	3.5028 e-07
200	5.9	0.7	2.882 e-06	3.4188 e-07
250	6.1	0.7	2.788 e-06	3.1989 e-07
300	6.7	0.75	2.787 e-06	3.1197 e-07
350	6.8	0.68	2.681 e-06	2.6813 e-07
400	7	0.65	2.702 e-06	2.5088 e-07

Table 6. Input parameters for the FD code

	Properties	Value	Reference
Composite	Density (ρ)	1524 - 1601 Kg/m^3	[5]
	Specific Heat (C_p)	800 - 1700 $J/kg.K$	[5]
	Longitudinal Thermal Conductivity (K_x)	3.5 - 7 $W/m.K$	[5]
	Transverse Thermal Conductivity (K_z)	0.42 - 0.65 $W/m.K$	[5]
Tool	Density (ρ_m)	2700 Kg/m^3	[50]
	Specific Heat (C_{pm})	905 J/K	[50]
	Thermal Conductivity (K_m)	237 $W/m.K$	[50]
Experimental Variables and Boundary Conditions			Reference
	Moving Heat Source Velocity (v)	25.4 mm/s (1 in/s)	-
	Heated Length	10 mm	-
	Temperature of the Hot Gas Torch (T_{HGT})	875 °C	-
	Convective Heat Transfer Coefficient of the Hot Gas Flow (h_{HGT})	990 W/m^2K	-
	Ambient Temperature	25 °C	-
	Initial Temperature	25 °C	-
	Convective Heat Transfer Coefficient of the ambient air (h_C)	10 W/m^2K	[30]
Finite Difference Size and Mesh Configuration			
Composite	Analyzed Length in x direction (L_C)	508 mm (20 inch)	
	Analyzed Thickness in z direction (W_C)	1 mm (equivalent to 8-layer composite)	
	Number of nodes in x direction (M_C)	508 (mesh size = 1 mm)	
	Number of nodes in z direction (N_C)	3 nodes per layer	
Tool	Analyzed Length in x direction (L_m)	508 mm (20 inch)	
	Analyzed Thickness in z direction (W_m)	50.8 mm (2 inch)	
	Number of nodes in x direction (M_m)	508	
	Number of nodes in z direction (N_m)	20	

3.3.2 Procedure for The Analysis of Heat Transfer by A Moving Heat Source

In actual AFP process, the heat source moves continuously. However, in the FD simulation, the continuous movement of the heat source needs to be discretized into specified steps. Assume that the sample has a total length of $L = 508$ mm (20 inch). The speed of travel of the torch (moving heat source) is $v = 25.4$ mm/sec (1 inch/sec). The total time for the complete process is $L/v = 20$ seconds. The length of the heating region is 10 mm. Concerning the fact that the length of the sample is subdivided into 508 nodes (the distance between nodes is 1 mm), the heating region encompasses 10 successive nodes as shown schematically with red circles in Figure 17 [18].

The way that the moving heat source is modeled in this study is based on the fact that the heat source moves one node at a time. This means if at step 1 the center of the heating length is at $x(t_1) = 5$ mm, at step 2, the center of the heating length would be at $x(t_2) = 6$ mm (since the distance between nodes is 1 mm). As such, the time which takes for the moving heat source to move from step 1 to step 2 is equal to the distance between nodes (i.e., 1 mm) divided by the speed (i.e., 25.4 mm/s), so the time interval is $1/25.4 = 0.04$ seconds. In other words, the heat source moves every 0.04 seconds from one node to the adjacent node to simulate the speed of 25.4 mm/s of the heat source [18].

Based on the above analysis, the procedure for the analysis of the moving heat source for $L = 508$ mm (20 inch), speed $v = 25.4$ mm/sec (1 in/sec) and heating length 10 mm is as follows:

- Step 1: During the first time increment (first stop), the center of the heating length is at $x(t_1) = 5$ mm. Duration of stop = 0.04 seconds. The time step at which the temperature of each node is re-calculated is equal to 0.0004 seconds which is determined by stability criterion for the problem. This means that at each stop, there are 100 time increments for the heat transfer analysis. Subsequently, the heat source moves one node (1 mm) and the calculation continues. The temperatures at different points in the structure at the end of this stop period are used as input to the next heating analysis in step 2 below.
- Step 2: Heating length travels so that the new position of the center of the heating length is at $x(t_2) = 6$ mm. Duration of stop = 0.04 seconds. Using the temperature from the previous step

(step 1) as initial conditions, the finite difference analysis is carried out. The temperature at the end of this step is used as input for the initial conditions for the analysis in the next step.

The same procedure is carried out until as far as necessary. This procedure is shown schematically for four first successive steps in Figure 17 [18].

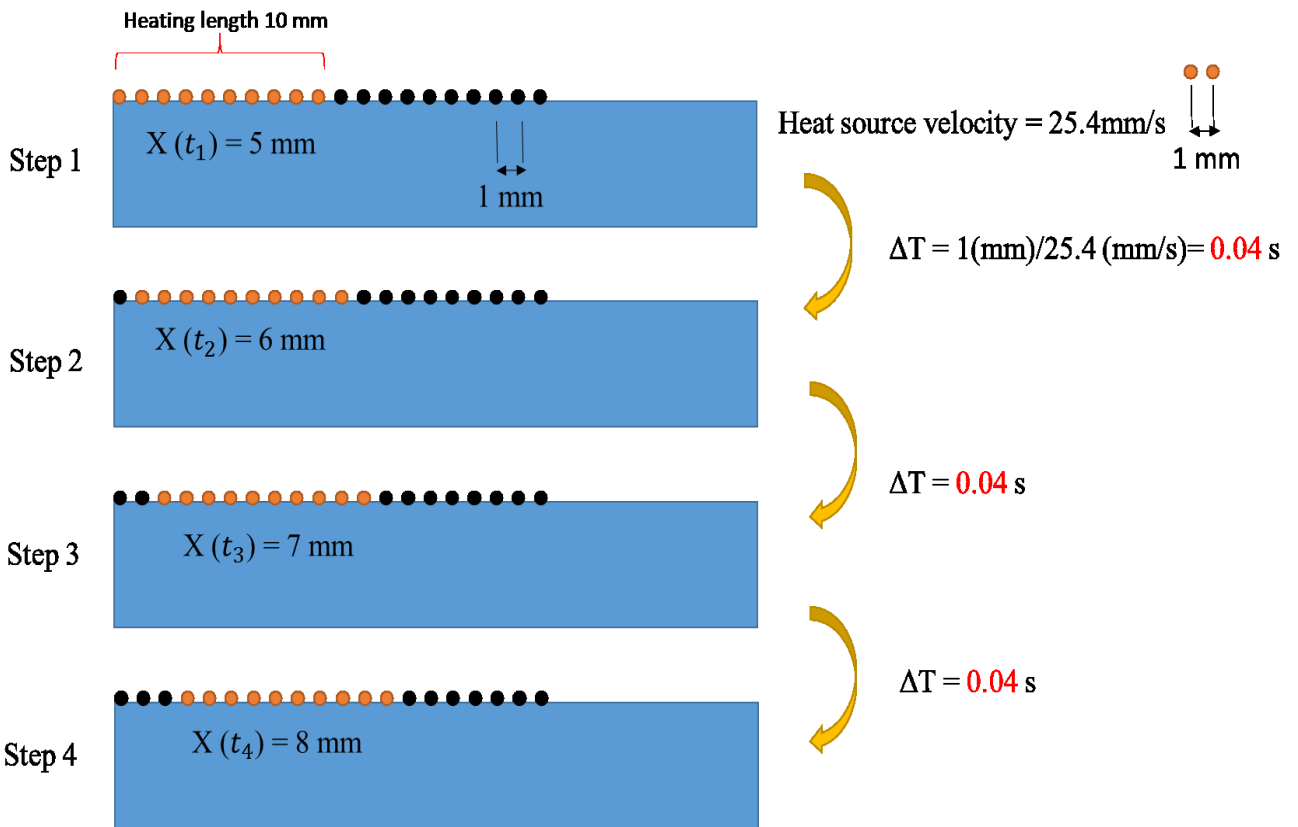


Figure 17. Procedure for the analysis of heat transfer by a moving heat source implemented in FD code in MATLAB [18]

3.4 Mesh Size Study (Mesh Convergence)

In this study, a continuous process is converted into a discrete process. It is not known exactly which mesh size would be sufficient to obtain the numerical results from the heat transfer analysis. Using a sufficiently refined mesh is important to ensure that numerical results do not deviate from the actual results. Coarse mesh may yield erroneous results and needs to be refined. This will guarantee that numerical results are independent of the mesh size and results are valid.

Table 7 presents different meshes used for the mesh size study (mesh convergence), including the number of divisions and total number of nodes for the heating length for each mesh size, the jump distance (the distance the heat source is moved each time) and the stop time (the time which the heat source rests at each stop).

Table 7. Description of different mesh sizes [18]

Number of divisions for the heating length	Total number of nodes for the heating length	Mesh size (the distance between nodes in mm)	Jump distance (mm)	Stop time (seconds)
10	11	1	1	0.0394
9	10	1.1111	1.11	0.0437
8	9	1.25	1.25	0.0492
7	8	1.4285	1.43	0.0562
6	7	1.6666	1.66	0.0656
5	6	2	2	0.0787
4	5	2.5	2.5	0.0984
3	4	3.3333	3.33	0.1312
2	3	5	5	0.1968
1	2	10	10	0.3937

In order to see how the mesh size would affect the numerical results, temperature distribution results are presented in Figure 18 for four values of number of divisions for the heating length, i.e., 10, 8, 6 and 4 (corresponding to the mesh sizes of 1, 1.25, 1.66 and 2.5 mm). Assume that we have a total length of 508 mm (20 inches) and the heat source (heating length of 10 mm) moves with the speed of 25.4 mm/s (1 inch/sec) from the left to the right of the sample. Temperature variation for the node located in the middle of the sample ($x=10$ inch), underneath 9th layer is presented in Figure 18. The horizontal axis is limited from 8000 ms to 14000 ms to be able to distinguish the difference between results from different numbers of divisions. Looking at Figure 18, it can be noticed that the difference between the temperatures from different mesh sizes varies with time. The difference is largest when the maximum temperature occurs (at around 11000 ms) and decreases as the time moves on. As such, if one waits long enough for the structure to cool down, the mesh size has smaller effect [18].

A summary of numerical results for all mesh sizes considered in this study is provided in Figure 19. As can be seen from Figure 19 (Left), as the number of divisions for the heating length increases from 1 to 10 (corresponding to variation of mesh size from 10 mm to 1 mm), the maximum temperature results converge. Furthermore, in order to see how fast or how slow is the rise from room temperature to the maximum temperature at each layer, times to reach maximum temperature values are plotted for different mesh sizes in Figure 19 (Right). A similar trend can be observed, and results converge for the mesh size of 1 mm (number of divisions for the heating length=10). Overall, it can be noticed that as the mesh size decreases and reaches 1 mm, the difference between the results is insignificant and it can be concluded that the number of divisions for the heating length of 10 (corresponding to mesh size of 1 mm) is satisfactory to be used to generate numerical results in subsequent sections in this study.

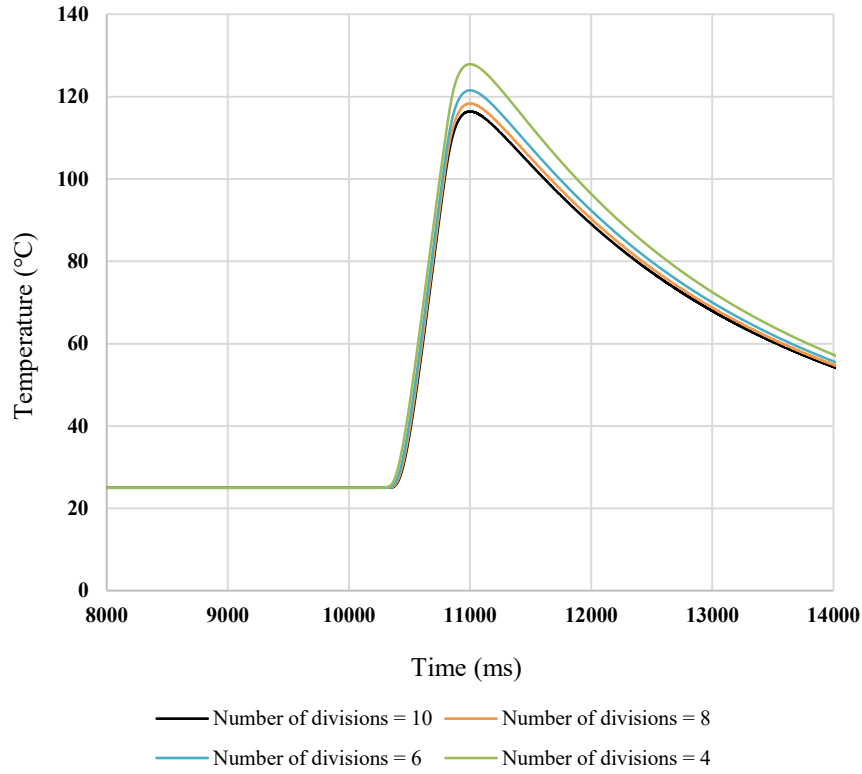
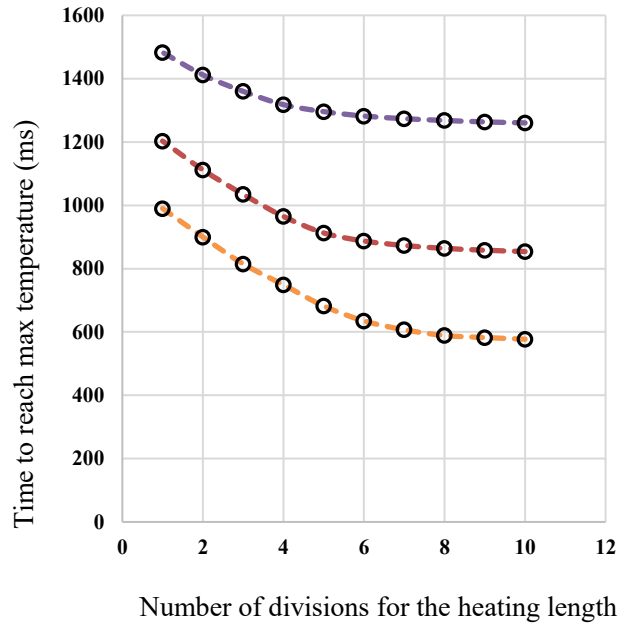
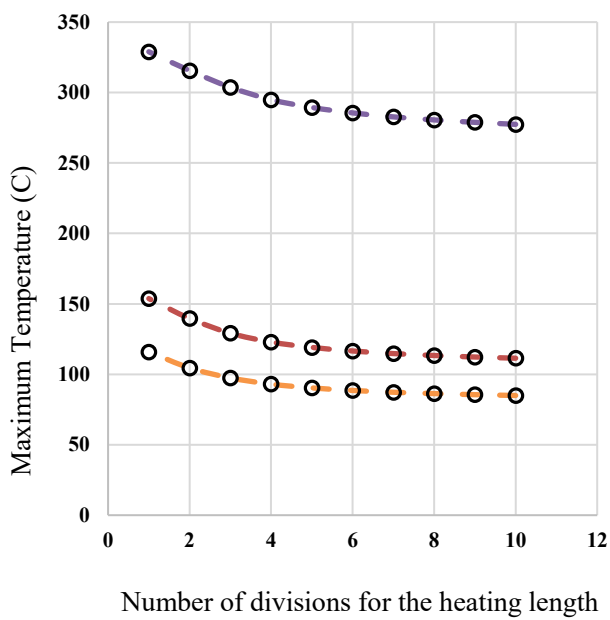


Figure 18. Temperature variation at underneath 9th layer for different number of divisions for the heating length at $x = 254$ mm (10 inch) [18]



-○- underneath 1st layer -○- underneath 9th layer -○- underneath 12th layer

Figure 19. Mesh size study (mesh convergence); (Left) maximum temperature (Right) time to reach maximum temperature in the laminate in three different layers for different number of divisions for the heating length [18]

In summary, in this chapter, thermal analysis model of the process was presented. The heat transfer mechanism in AFP thermoplastic composites process was introduced. It was stated that both heat convection due to the hot gas torch and heat diffusion through the composite substrate are of paramount importance in the thermal analysis of the process. Using the energy balance approach, finite difference formulation of the heat transfer problem was introduced. Depending on type of the nodes i.e., interior nodes or boundary nodes, appropriate formulations were derived. The stability criteria were introduced for the explicit methodology employed in the problem. Based on the formulations derived, a solution algorithm for moving heat source problem in MATLAB was presented. The procedure for the analysis of heat transfer by a moving heat source was discussed in detail. Eventually, the mesh size study was presented as for the mesh convergence.

Chapter 4: EXPERIMENTAL SETUP

4.1 Automated Fiber Placement Setup

Automated Fiber Placement work cell and flat Aluminum paddle tool at Concordia Centre for Composites (CONCOM) obtained from Automated Dynamics Corporation (ADC) are used in this thesis to perform the experimental studies. Close-up of the thermoplastic fiber placement head is illustrated in Figure 20. The incoming tape is first guided and positioned by material guide eyelets. The material is then driven through a tape guide where a feed roller is mounted to apply tension on the tape. The feed roller is connected to a feed motor which supplies energy in the feed system. Depending on the tape being used, the feed system including tape guides and feed rollers can be adjusted. Afterwards, the tape is driven towards a compaction roller. The compaction assembly consists of compression springs, bearings, carriage and a compaction roller [2,6,12,13,28,57,66–70]. The compaction assembly is used to consolidate the material i.e., the incoming tape onto the substrate at the Nip point. Nip point refers to the contact point of the consolidation roller with the incoming tape. The pneumatic force is used to apply pressure on the consolidation roller. It is necessary to maintain full contact throughout the entire length of the compaction roller to achieve good and uniform bonding between the incoming tape and pre-consolidated composite layers. Pressure is also necessary to remove the voids developed during the process. However, it should be noted that too much pressure is also not desirable as it may increase the waviness of the fibers [2,6,12,13,28,67–69]. The single curvature compaction roller is selected in this study as it is generally used for unidirectional layup configurations as shown in Figure 21. The roller material can be a stiff material such as steel (for hot gas assisted AFP) or it can be a soft material such as silicone (for laser assisted AFP) [13]. In this study, hot gas assisted AFP is employed to perform the experimental trials and therefore, a steel roller is used to consolidate the composite layers. The steel roller can also withstand high temperature and it is a promising candidate for the case of hot gas torch [13]. The selection of roller material is of paramount importance since the hot gas directly

points towards the roller along with the incoming tape. The AFP machine used in this thesis is equipped with a single roller for consolidation as shown in Figure 20.

As mentioned earlier, a HGT is integrated in the AFP head which is employed to heat up the incoming tape and a certain area of the substrate during the process. The main purpose of the HGT is to heat up the material in order to reduce the viscosity (enhance formability) and increase the tackiness (enhance intimate contact) [1,30,69]. The HGT is positioned in a way that it points towards the lower half of the consolidation roller. This helps to heat up both the incoming tape and the substrate in the vicinity of the nip point. Nitrogen gas is used in this setup to provide heat to the material. Nitrogen as an inert gas helps to protect the tapes from oxidation [2,6]. A nitrogen line (Figure 22 (left)) supplies nitrogen on the back of the torch housing where the nitrogen gas is passed through. Prior to the torch housing, an HGT nitrogen regulator is embedded to adjust the pressure as shown in Figure 22 (right). Inside the torch housing, there are a few heating elements which enable the control of the temperature of the nitrogen gas. The heated nitrogen is then guided through the torch nozzle where the hot gas is directed onto the material. The nozzle exit cross-sectional area is relatively small compared to the torch housing diameter which creates very high-speed flow of the gas while leaving the nozzle. The temperature of the hot gas at the nozzle exit is measured by a K-type thermocouple (Figure 20). The temperature and nitrogen gas flow rate can be set independently through an operator interface as shown in Figure 23. Depending on the type of the material being used, the lay-up speed, the geometry and the lay-up configuration, each of these parameters can be set [2,6,13,28,38,58,68,69,71,72].

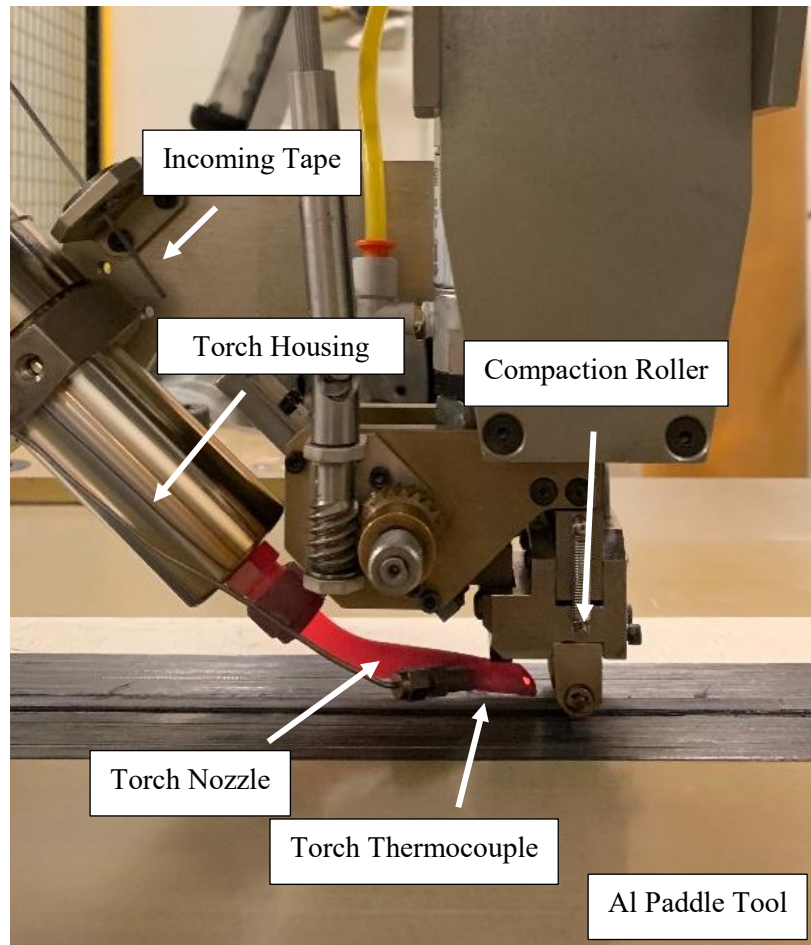


Figure 20. Thermoplastic Fiber Placement Head



Figure 21. Consolidation roller of AFP setup



Figure 22. Nitrogen supply line (Left); HGT nitrogen regulator (Right)

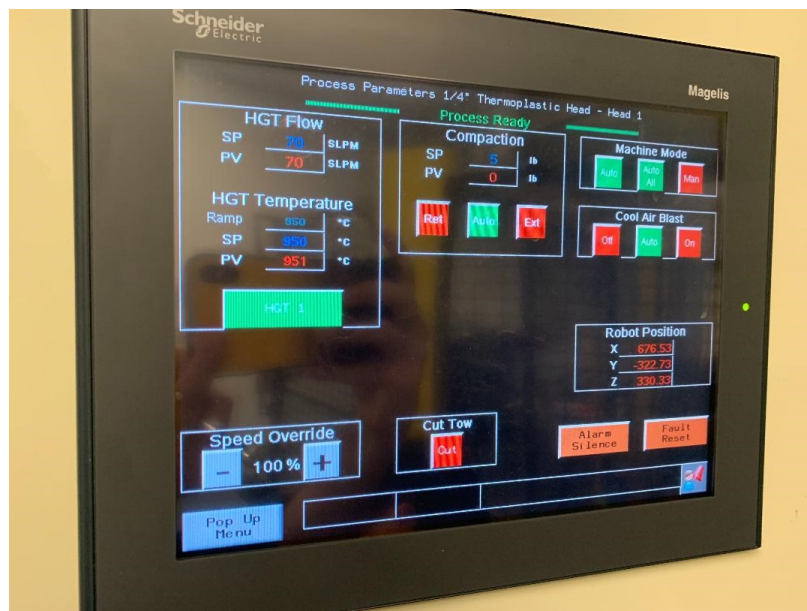


Figure 23. AFP Operator interface

4.2 Prepreg Material

Fully impregnated ¼ - inch wide AS4/APC-2 carbon fiber/PEEK tapes supplied by CYTEC Engineered Materials are used as the prepreg material in the experimental layup trials in this thesis. The thermoplastic matrix of these tapes is based on poly-ether-ether-ketone known as PEEK. It is a semi-crystalline thermoplastic matrix with a glass transition temperature (T_g) of 143 °C. It exhibits outstanding resistance to moisture, chemicals, impact and wear, as well as high temperature stability and high service temperatures of up to 250 °C [2,6,73–75]. Owing to excellent properties of the thermoplastic matrix and complete wetting of the fibers in the impregnation process, APC-2 can be processed using wide range of manufacturing techniques and thus can be used in a variety of applications [76–80]. The unidirectional tape consists of a 68:32 weight percentage mixture of carbon fiber (AS4) and PEEK matrix (APC-2). The nominal value of fiber volume fraction is 61% [6,12,81]. The unidirectional tape has standard width of 0.25 inch and standard thickness of 0.05 inch. A complete data sheet of APC-2-PEEK thermoplastic polymer can be found in [75]. A summary of important mechanical properties is also provided in the Appendix A and B.

Examination of CYTEC prepregs performed by Hoang [6] indicated that there were some resin rich area and small amount of voids in the prepreg material. Looking at Figure 24 (left), it can be noticed that at the edge, prepregs exhibit some level of roughness. He performed the differential scanning calorimetry (DSC) of the prepregs and it was found that the glass transition temperature of prepregs was around 143 °C and the degree of crystallinity was found to be approximately 16.5 %. Heat flow curve of the prepreg is shown in Figure 24 (right) [6].

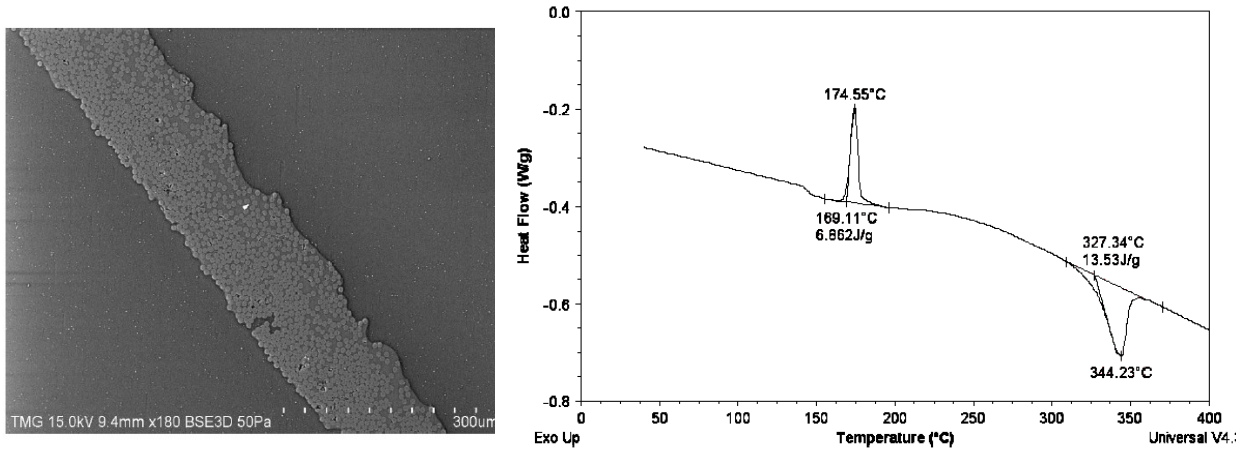


Figure 24. Micrograph of CYTEC prepreg (Left); Heat flow curve of APC-2/AS4 prepreg (Right) [6]

4.3 Thermal Measurement Apparatus

Thermocouple is the most common sensor for measuring temperature due to its unique features. These include low cost, versatility and durability. Depending on the type and size of the thermocouple, it can be used for wide range of applications ranging from heavy industrial usage with high level of chemical and environmental exposures to typical laboratory testing conditions [82]. These make the thermocouple a promising candidate as a sensor in temperature measurement. In this section, the major criteria for selection of the thermocouple for the case of this study will be discussed. Selection of fast-response K-type thermocouples will be presented. Eventually, other thermal measurement apparatus which will be used in the experimental setup will be discussed.

4.3.1 Selection Criteria of Thermocouple

The structure of the thermocouple is based on two dissimilar metal wires which are covered by a sheath and are joined at one end. Depending on the type of the thermocouple, the metal wires can be from Iron, Aluminum, Nickel and Copper alloys for typical applications to Platinum, Rhodium and Rhenium for specific applications. When the thermocouple wires are heated up, electrical

current flows in the thermoelectric circuit. As such, heating up the thermocouple junction induces a voltage in the circuit, and this can be further correlated back to the temperature. This is the principal of thermocouples' performance which is common among different types of thermocouples [82].

Calibration	Tem Range
J	0°C to 750°C (32° F to 13382°F)
K	-200°C to 1250°C (-328° F to 2282°F)
E	-200°C to 900°C (-328° F to 1652°F)
T	-250°C to 350°C (-328° F to 662°F)

Figure 25. Common thermocouple temperature ranges [82]

In order to choose a thermocouple for the application of experimental studies in this thesis, there are two major criteria which need to be considered. First, is the temperature range that the thermocouple can withstand. Common thermocouple temperature ranges are presented in Figure 25. As can be seen, the temperature can be set in a wide range i.e., from very low temperatures (-250°C) to very high temperatures (1250°C). Considering the fact that for the case of fiber placement using the hot gas torch, the temperature is very high (close to 1000°C), among different types of available thermocouples, K-type thermocouple is a promising candidate which can withstand very high temperatures up to 1250°C. The second criterion is the response time of the thermocouple. For the case of this study, the thermocouple will be exposed to instantaneous application of the hot gas torch while depositing the material onto the substrate during the cyclic process. Since the automated fiber placement is performed under relatively high laying up speeds, it is extremely important to employ thermocouples that can capture the true temperature that occurs during the process. There are two main factors that can have influence over the response time of thermocouples:

First is the type of junction. Looking at Figure 26, different junction types of thermocouples including insulated, grounded and exposed can be noticed [82]. Thermocouple wires are typically covered using the sheath as can be seen in Figure 26. The sheath acts like a shield to protect the wires in very high temperatures or in corrosive environments. Regardless of the wires' sheath, the junction itself can be housed inside a shield [82]. In the first category i.e., insulated junctions, the thermocouple junction is not attached to the probe wall. The insulation provides electrical isolation. However, because of the gap between the junction and the wall along with outer shelter, this type of junction exhibits slow response time. This type is typically used for corrosive environments where the thermocouple needs to be electrically isolated from the outside [82]. In the second category (grounded junctions), the junction is physically attached to the inner side of the protective sheath. Because of the good contact between the junction and the probe wall, the heat can be easily transferred through the boundaries. This type exhibits faster response time compared to insulated junctions. It can be used for static gas and liquid temperatures and also in applications subjected to high pressure [82]. Eventually, in the last category, exposed junctions can be seen. In this type, the junction is out of the protective sheath and is directly imposed to the surrounding environment. This type offers the highest response time among all the types and therefore, it can be used in applications which fast response time is required [82]. Based on the discussion above, the exposed junction type is selected as the best type for the case of automated fiber placement where the response time is crucial in temperature measurements.

The second factor which can greatly affect the response time of the thermocouple is the wire diameter [82]. As the thermocouple's wires become thinner and thinner, it can respond faster and faster. Depending on the type of the junction, one can refer to the available diagrams such as the one shown in Figure 27 to determine the response time of the thermocouple at the corresponding wire diameter [82]. As such, it can be concluded that theoretically, if we aim at measuring the temperature with fast response time, we should consider the thinnest possible thermocouple available in the market. However, there are numerous limitations which makes the usage of very thin thermocouples impossible in the real applications. These include the handling the thermocouple itself, availability of protective sheaths for extremely thin wires, fragility of the thermocouple in very high temperatures and its susceptibility to the application of compaction force. Considering the discussion above, in the next section, the selection of fast-response K-type thermocouple for the application of automated fiber placement will be discussed.

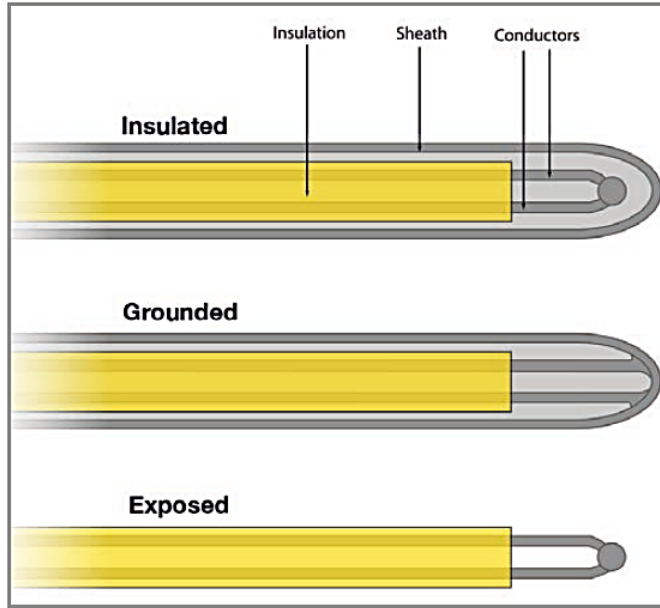


Figure 26. Different junction types of thermocouples [82]

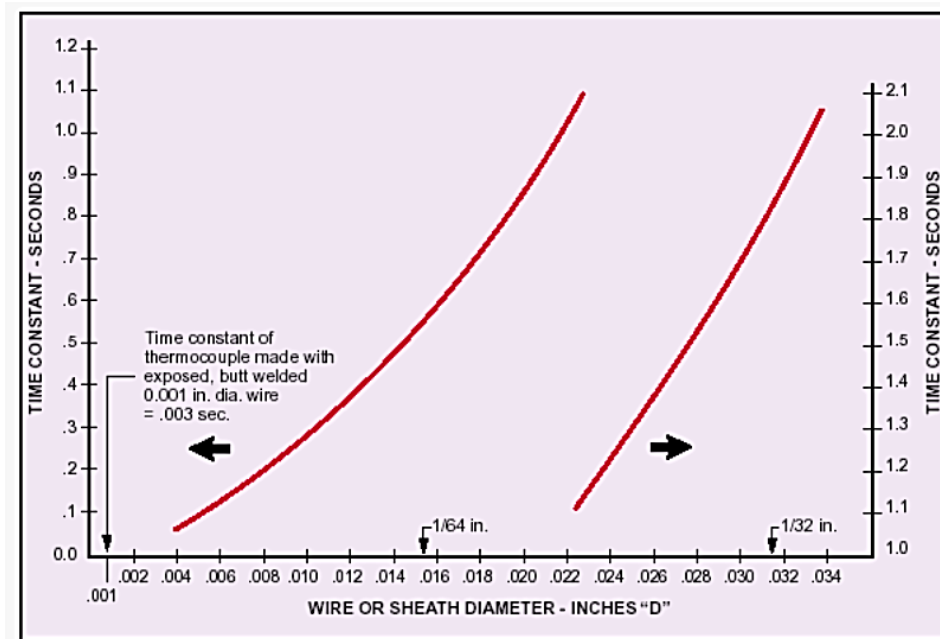


Figure 27. Thermocouple response time for different wire diameters [82] (the vertical axis is subdivided into two parts, from 0 to 1.1 in the left and from 1.1 to 2.1 in the right)

4.3.2 Selection of Fast-Response K-Type Thermocouple

The thermocouples have time lag in terms of response to the input. If the response time of the thermocouple is noticeable, this may have effect on the meaning of the measurement. In previous section, it was discussed that there are two major factors affecting the response time of the thermocouple, thermocouple junction type and its wire diameter. It was mentioned that among available junction types, exposed type exhibits the fastest response time and thus it was selected. Regarding the wire diameter, it was stated that although by decreasing the wire diameter, one might achieve a thermocouple with faster response time, there are some limitations which make it challenging. In the following, the procedure to overcome these challenges will be discussed.

Typical thermocouples used in industry have wire diameters of 0.254 – 0.508 mm (0.01 – 0.02 in) which theoretically exhibit response time of 0.3 – 0.8 seconds [82]. This response time is too slow for this type of measurement during the AFP process. For the purpose of this study, CHAL-002 from Omega is selected. This type of the thermocouple is among the thinnest possible thermocouples available in markets. Its wire diameter is about 0.05 mm (0.002 in). Compared to typical thermocouples used in industry, this thermocouple is about 5-10 times thinner which is expected to response much faster. CHAL-002 thermocouple is a type of unsheathed fine gauge thermocouples. This category of thermocouples is known to provide fast and accurate temperature measurement on a miniature scale for some specific applications [82]. These include internal combustion engines, gas chromatography, scientific instruments and biophysics. The wire diameter of these thermocouples can vary from 0.025 mm to 0.8 mm. Due to their extremely thin junctions, they enable accurate temperature measurements by keeping the heat transfer via the leads to a minimum possible amount [82]. Despite numerous benefits, there are some challenges in handling the thermocouple. Because of the extremely thin wires, there is no protective sheath for this type, and this can limit the usage of these thermocouples for very high temperatures and the applications with compaction force due to their fragility. However, these limitations are overcome by utilizing the setup as shown in Figure 29. In this setup, some modifications are applied in order to handle the thermocouple and its fragility. The thermocouple's wires are initially mounted on a glass epoxy sheet which is considered as an insulation. Subsequently, the wires are separated and covered by Flashbreaker tapes supplied by Airtech [83]. The tape consists of high temperature polyester films coated with a pressure sensitive silicone. This tape is typically used for oven/autoclave curing at

high temperatures [83]. In the right side, positive and negative leads are labelled with yellow and red marks respectively. The positive lead consists of a Chromel alloy (Nickel and Chromium) while the negative lead consists of a Alumel alloy (Nickel and Aluminum) [82]. The leads are welded to thicker wires using fine wire welder. This is done to facilitate the connection of the thermocouple leads to the connector for data recording. The thermocouple junction as noticed in the left side, will be embedded inside the composite layers to measure the temperature during the process.

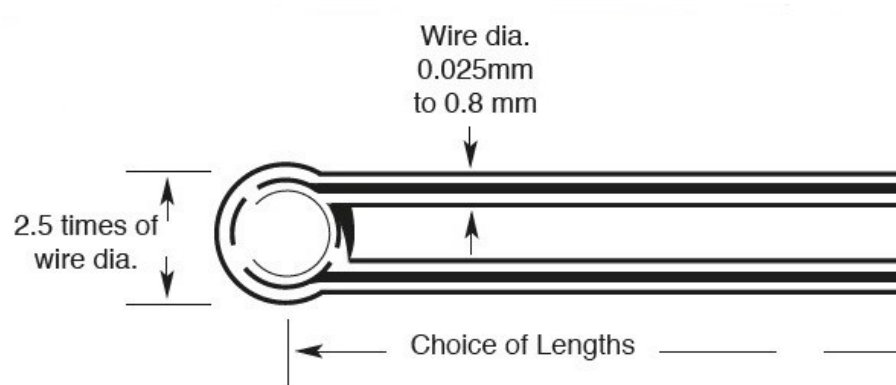


Figure 28. Schematic of unsheathed fine gauge thermocouple [82]



Figure 29. Fast-response K-type thermocouple assembly

4.3.3 Comparison of Response Time of Thermocouples

One way to check the response time of the thermocouple is to use a hot oil bath. In this method, the oil is heated up to a certain temperature. A thermometer is used to measure the temperature of the oil. Then by immersing the thermocouple inside the oil bath, the response time of the thermocouple i.e., 63.2% of the plateau could be measured. The response time can be correlated with the dynamics of the measurement process. Following this method, the response time of two thermocouples, one from typical type of thermocouples (GG-K-36 Omega) and the thermocouple developed for the purpose of this study (CHAL-002 Omega) is compared. The experimental setup used for measuring the response time and results are presented in Figure 30 (left) and (right) respectively. Looking at results, it can be noticed that the suggested thermocouple (CHAL-002) exhibits the response time of around 0.05 seconds while the one for the typical thermocouple is around 0.53 second. In other words, the suggested thermocouple is able to respond approximately 10 times faster than typical thermocouples. This can highlight the importance of employing fast-response time thermocouple for the application of this study.

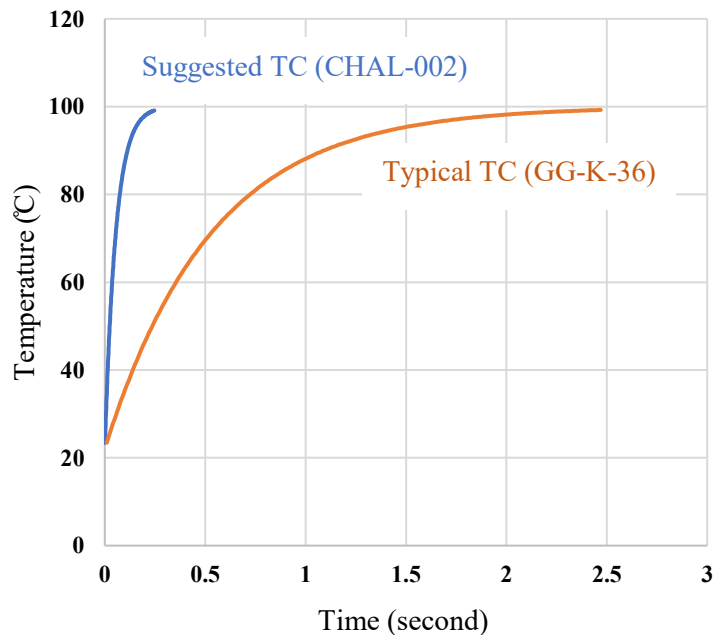
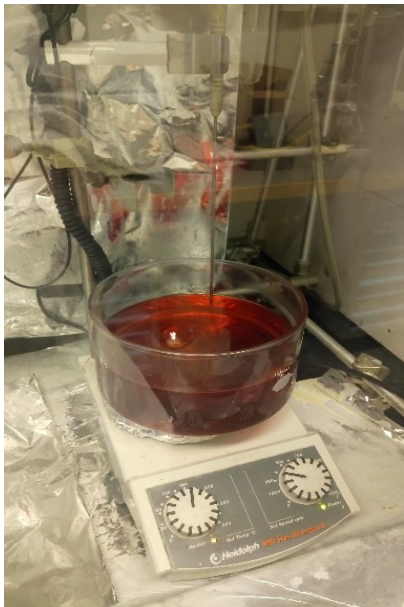


Figure 30. Oil bath for response time measurement (Left), temperature versus time for typical and developed thermocouples (Right)

4.3.4 Other Measurement Instruments

Along with the thermocouple which is the most important component in the temperature measurement setup, there are some other components as shown in Figure 31. The thermocouple wires are welded at one end which forms the junction of the thermocouple for temperature measurement. At the other end, wires are connected to a connector as a thermocouple-capable device to record the thermal data. Schematic of the thermocouple wires arrangement with the connector is shown in Figure 32. The connector plays an important role in providing good resistance while handling the thermocouple [82]. The connector, on the other side, is connected to a data acquisition system (DAQ) which converts the voltage readings of the thermocouple into the temperature. The DAQ can have multiple channels to record the thermal data from multiple thermocouples simultaneously. The one used in this study has 8 channels. At the end, a personal computer is required to adjust the recording settings and to monitor the thermal data. A logging software developed by the Omega is installed on the personal computer. The software is able to adjust the settings such as type and number of the thermocouples, duration of recording etc. and is able to display the data from multiple thermocouples while being recorded by the thermocouples in the experimental setup.

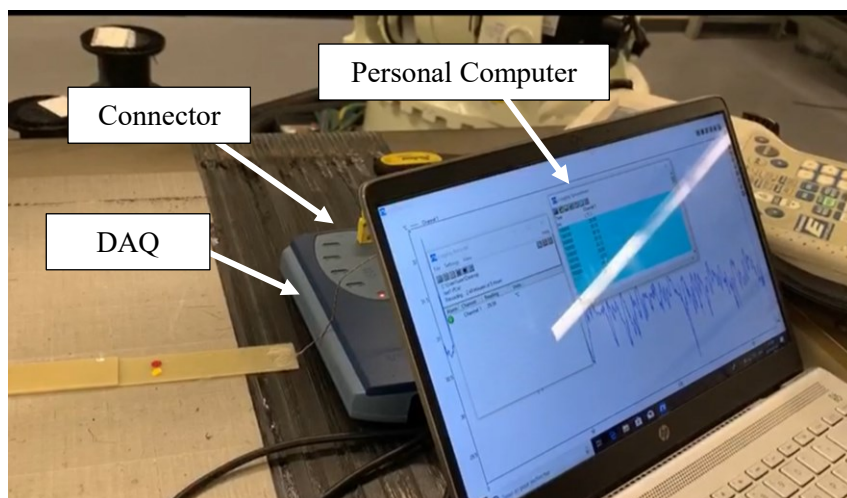


Figure 31. Temperature measurement apparatus

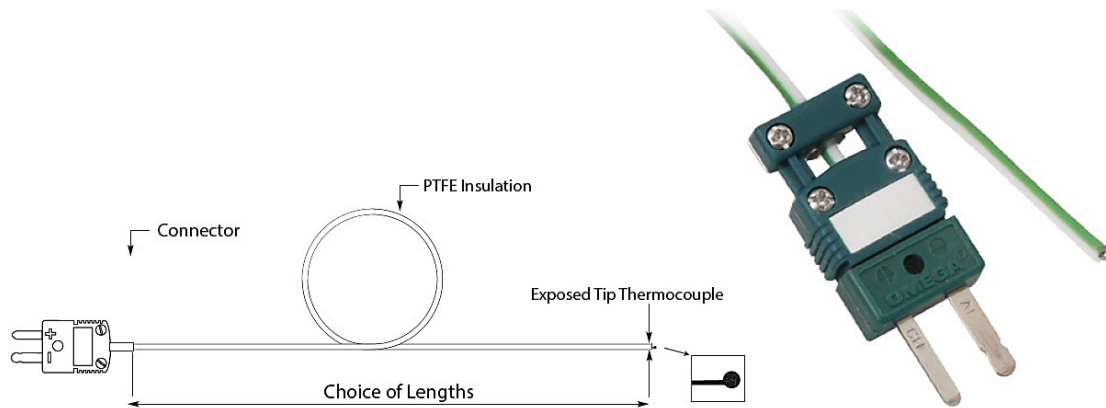


Figure 32. Connector assembly to the thermocouple wires [82]

4.4 Manufacturing Procedure

In previous sections, thermal measurement apparatus was discussed in detail. The selection criteria for the thermocouple for the purpose of this study were stated and it was demonstrated that CHAL-002 thermocouple could be employed as a fast-response thermocouple which satisfies the requirements of temperature measurement in this study. Furthermore, the necessity for other instruments including connector, DAQ and the personal computer was mentioned. In this section, the manufacturing procedure for the composite laminate and the way the thermocouples are embedded inside the composite laminate to record the temperature during the process is discussed.

Figure 33 depicts the experimental trials setup used in this study to obtain experimental results to provide validation for numerical results. The main focus of the study is on the way how temperature gradient develops through the thickness of the composite laminate during the process. Unidirectional composite strips of 508 mm (20 inch) long making up 20 layers are manufactured to investigate the temperature distribution in various locations through the thickness of the composite laminate when the moving heat source travels across the upper side of the laminate. To do so, 8 unidirectional composite strips of 508 mm (20 inch) long making up 8 layers are first manufactured, and the laminate is allowed to cool down to room temperature. This is of paramount importance to avoid thermal accumulation inside the composite laminate. Afterwards, on the upper

side layer, a fast-response K-type thermocouple (TC; Omega CHAL-002) is mounted on top of the 8th composite strip using a Kapton® tape. Subsequently, the 9th layer is deposited. When the NIP point of the roller arrives on top of the thermocouple, it deposits the composite layer and the TC becomes embedded into the composite substrate. The thermocouple data is measured by Data Acquisition system (DAQ) at 100 Hz. It is important to have a thermocouple with fast response time. Otherwise, the temperature reading is not accurate, and it cannot measure the actual temperature during the process. The aforementioned thermocouple is denoted by TC1 in Figure 34. Then, 3 more layers are deposited on top of the previously laid composite substrate along with another thermocouple (denoted by TC2 in Figure 34). The system is allowed to cool down to reach room temperature. Another 8 layers are deposited afterwards on top of TC2 to form 19 layers of composite laminate with two embedded thermocouples. Eventually, the third thermocouple is mounted, and the last layer is deposited, and the entire system is allowed to cool down for 24 hrs. The entire layup consists of 20 layers of unidirectional composites with three embedded thermocouples of the same type to capture the temperature variation during the experimental trials. In order to compare the numerical results from moving heat source with experimental results, the material deposition is deactivated in AFP setup and the nozzle temperature is set at 875 °C and is kept constant during the experimental trials. The distance between the torch beginning position and thermocouple is 254 mm (10 inches). The heat source moves from one end to the other end with speed of 1 in/s without material deposition and the temperature is recorded by thermocouples which are embedded into the composite substrate, underneath layers of composite material. After completing one pass, the setup is allowed to cool down to room temperature. The process is repeated five times to ensure readings are repeatable, and the data are consistent [18].

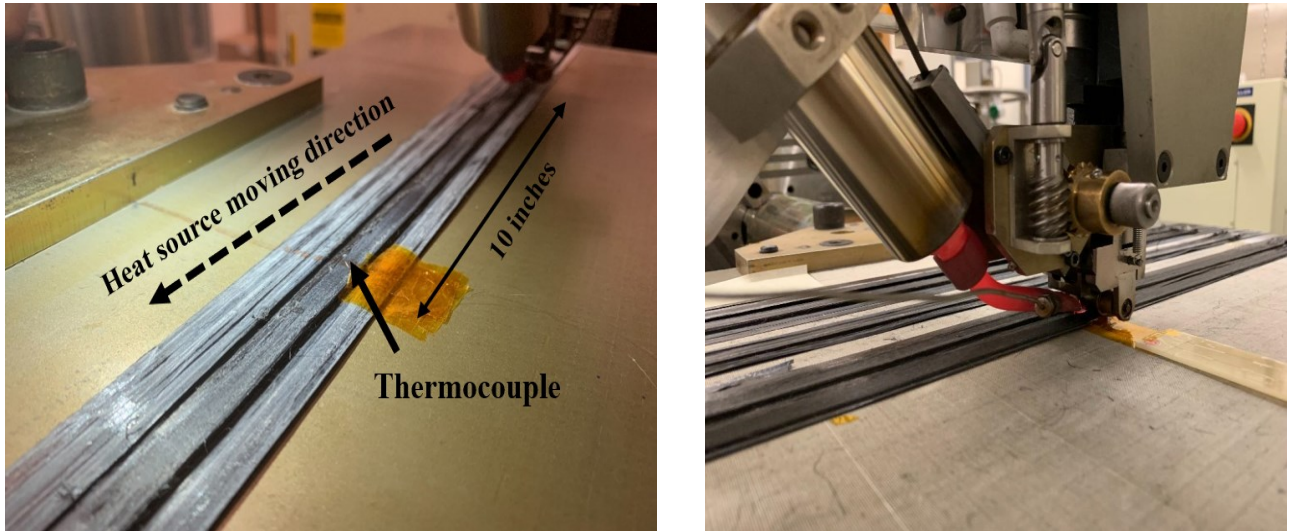


Figure 33. Experimental setup; location of AFP head (Left) at the beginning of the pass (Right) over the embedded thermocouples [18]

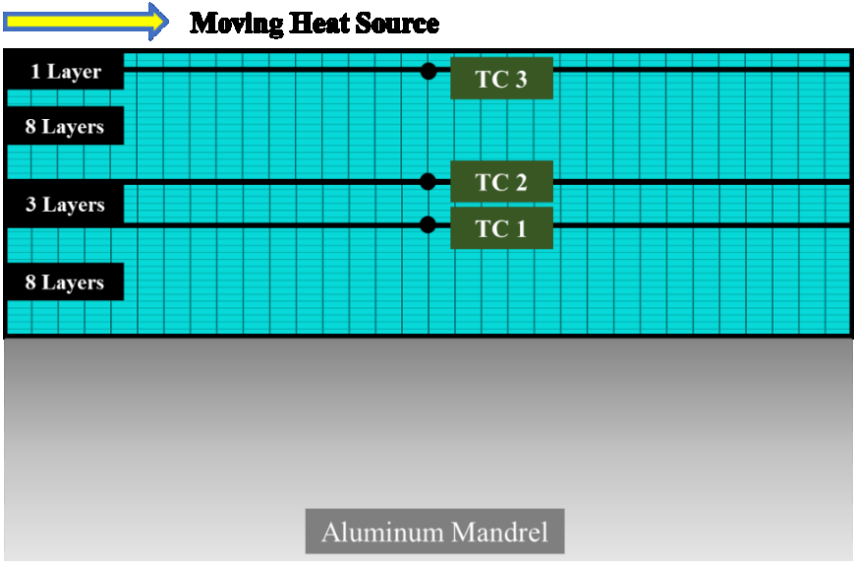


Figure 34. Schematic illustration of 20-layer composite laminate with embedded TCs [18]

Chapter 5: RESULTS AND DISCUSSION

In Chapter 2, it was discussed that because of the rapid heating and cooling of the thermoplastic composites during the process, there are many issues to be addressed and it was stated that among those, the development of the temperature distribution in different directions is of paramount importance since it gives rise to the temperature gradients. The temperature gradients emerge as a result of different cooling rates in different layers of the composite laminate. Consequently, they can affect the residual stresses during the process which can lead to the distortion of the composite laminates. In order to understand the heat transfer in the composite laminate subjected to a moving heat source, in Chapter 3, the finite difference formulation of the transient heat transfer problem in a two-dimensional rectangular domain was presented. Using the energy balance approach, the finite difference formulations for all the interior nodes and boundary nodes of the domain were presented. Eventually, a computer code was developed in MATLAB to be able to solve the system of the finite difference equations numerically. In this section, using the numerical method developed in Chapter 3, the nodal temperatures at different locations of the composite laminate will be generated. In order to provide validation of the numerical results, experimental results will be also presented. In Chapter 4, the experimental setup was described in detail. The importance of usage of fast-response thermocouples was mentioned. Unidirectional composite strips were manufactured using AFP and fast-response K-type thermocouples were used to determine the thermal profiles in various locations through the thickness of the composite laminate subjected to a moving heat source. Schematic illustration of the manufactured composite laminate with embedded thermocouples is presented in Figure 35. In this chapter, results from both experimental trials and numerical method are presented and compared. The results can be classified into three categories: a) temperature variations as time progresses for three different through-thickness locations of the composite substrate at a constant x location; b) temperature distribution in the vicinity of the heat source along the lay-up direction at different through-thickness locations at a specific time during the process; c) temperature variations through the thickness of the composite substrate at five

different x locations at a specific time during the process. At the end of the chapter, the main conclusions of results will be presented.

5.1 Numerical and Experimental Temperature Variations for Different Through-Thickness Locations of The Composite Substrate

Temperature distribution results are shown in Figure 36. Family of curves with solid lines represent numerical results while the dashed lines describe experimental results. Looking at the graph, it can be noticed that the transient temperature profile can be divided into 3 different stages. As the heat source moves from left towards the embedded thermocouples, the temperature maintains room temperature ($25\text{ }^{\circ}\text{C}$) for the first few seconds (*Stage 1*). This is because of the fact that the heat source is at the beginning of the pass and the downstream region is not heated up yet. When the heat source approaches the location of the thermocouple, the temperature starts to rise up and reaches a maximum temperature (*Stage 2*). Once the heat source (the center of the heating length) passes the spot, that spot begins to cool down (*Stage 3*). Although the temperature of the gas is about $875\text{ }^{\circ}\text{C}$, the maximum temperature of TC3 is only $277\text{ }^{\circ}\text{C}$. This is because TC3 is embedded below one layer of the composite, and this layer of composite shields TC3 from the high temperature. It was shown in [30] that the temperature of a thermocouple placed on top of the laminate reaches to around $800\text{ }^{\circ}\text{C}$ when the hot gas torch passes over it.

The speed of the torch (moving heat source) is 25.4 mm/s (1 inch/sec); as such it would take 10 seconds for the heat source (center of the heating length) to reach the embedded thermocouples which are placed in the middle of the substrate length ($x = 254\text{ mm}$). Looking at the results for TC3, it can be noticed that the maximum temperature occurs at around 10.3 seconds from the numerical results and 10.5 seconds from the experimental results. The time difference between points “B” (the point on the graph corresponding to 10 seconds) and “C” (the point where the temperature reaches maximum) is denoted as delay time. Note that at 10 seconds, the center of the heating length passes over the position $x = 254\text{ mm}$ (10 inch). The remaining 5 nodes of the heat length would take 0.2 seconds ($5\text{mm}/25\text{mm/s}$) to pass away from the position of $x = 254\text{ mm}$ (10 inch). As such out of the delay of 0.3 seconds, the non-heating time is only 0.1 seconds. The heat energy provided by the heat source needs to be transferred and absorbed by the material and thus

the maximum temperature occurs with a time delay. The experimental data indicate the effect of other influential parameters which result in longer time delay (0.5 second) as compared to the numerical results. This is because of the fact that the thermocouple has a response time and cannot measure the temperature instantaneously. As such, due to the response time of the thermocouple, there is a slight difference between the time delay prediction based on numerical results and experiments. Another interesting point is the fact that temperature starts to rise up at around 6 seconds (for TC3) i.e., before the heat source reaches the embedded thermocouple. This phenomenon is denoted as rise time which is the time difference between points “A” (where temperature deviates from the horizontal line) and “B” as shown in Figure 36. The rise time is attributed to the heat transfer through the material along the direction of travel of the moving heat source [18].

In Figure 36, the numerical method is able to capture the maximum temperature with good agreement with experimental results. However, there is significant difference in the rate at which the temperature rises. The numerical results show much sharper rise in temperature from the ambient as compared to experimental results. This can be due to the way how the h_{HGT} is applied. In Chapter 3, it was demonstrated that the top surface of the composite substrate is divided into region 1 and region 2. The boundary between these regions is sharp in the numerical method whereas in reality, it may not be that sharp. Also, h_{HGT} is assumed to be constant over the heating length but it may not be. These can be the reasons for the significant difference in the rate of cooling between the numerical results and experimental results. This is the subject of a further investigation [18].

Looking at temperature variations through the thickness (Figure 36), it can be noticed that as one goes through the thickness, the maximum temperature becomes lower and lower. For instance, the maximum temperature recorded by TC2 was 124 °C i.e., 55% lower temperature than TC3. The corresponding nodal temperature predicted by numerical code was around 112 °C (9.6% error). Furthermore, TC1 would reach the peak temperature of 93 °C which is almost 66% lower temperature compared with TC3. Overall, the temperatures measured experimentally during the heating pass, using embedded thermocouples into the composite substrate, underneath layers of the composite material, show consistent trends with the generated temperatures from the numerical model [18].

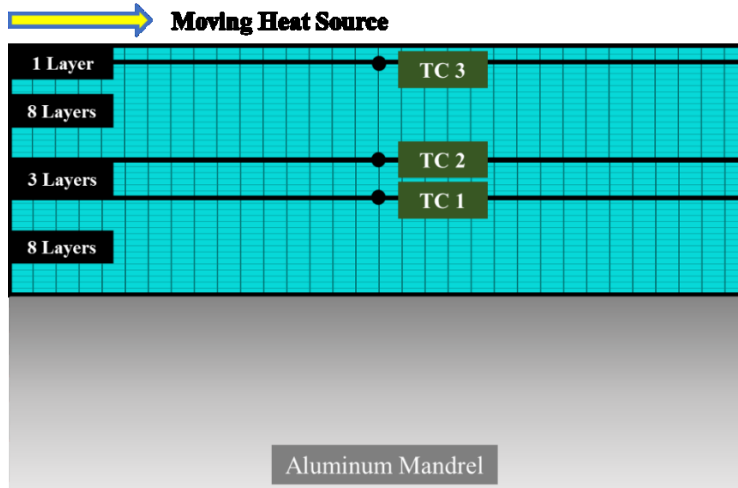


Figure 35. Schematic illustration of 20-layer composite laminate with embedded TCs [18]

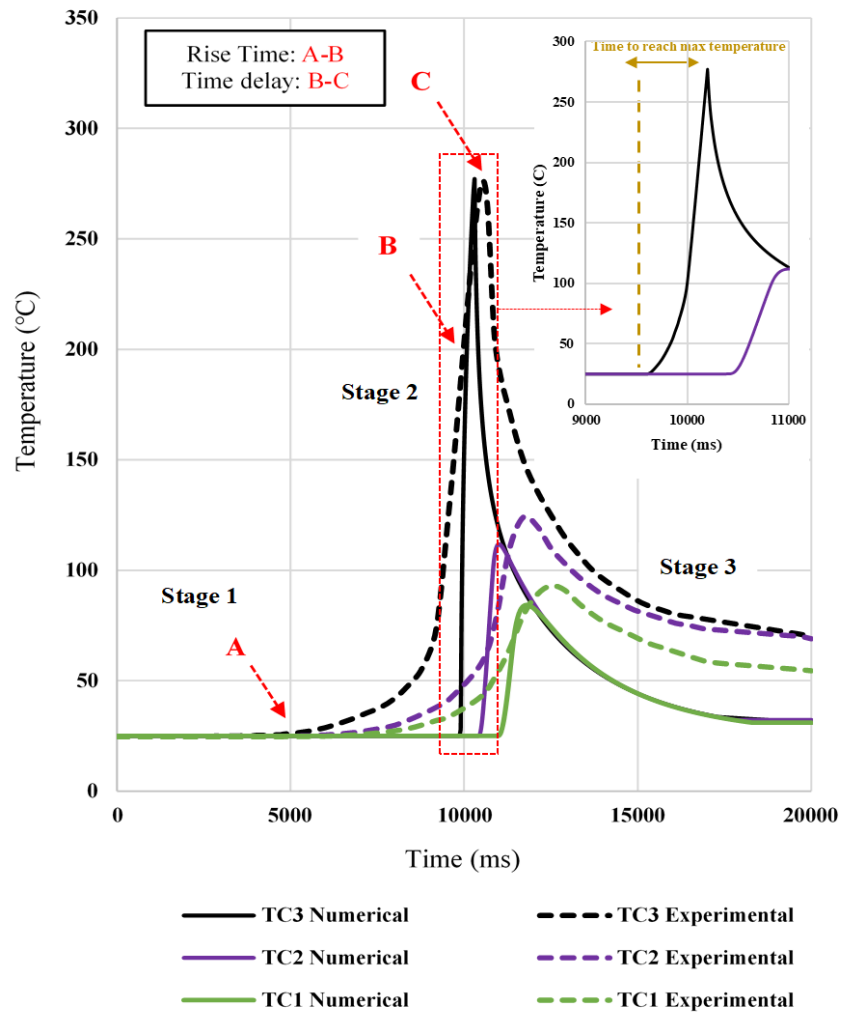


Figure 36. Temperature variations; numerical simulation versus experimental results at $x = 10$ inch [18]

5.2 Temperature Distribution in the Vicinity of the Heat Source Along the Lay-Up Direction at Different Through-Thickness Locations

Using the developed numerical model, the temperature distribution for the structure was determined. Figure 37 represents the temperature distribution in the vicinity of the heat source along the lay-up direction at different through-thickness locations. Zeta ($\xi = x - vt$) is a transformation on the x-axis indicating the distance between the heat source and the target point in the lay-up direction (heat source moves with the speed of v and its mid length has the same x position as the target point when $\xi = 0$). The negative values ($\xi < 0$) indicate the upstream region which was heated up by the heat source while the positive values ($\xi > 0$) demonstrate the downstream region where the mid length of the heat source has not reached yet. As it can be seen from Figure 37, the temperature gradient in downstream region is sharper than the one in upstream region. The reason is because the upstream region was affected by the heat source before the center of the heat arrives at $x = 254$ mm (10 inch), while the downstream region was not [18].

Looking at Figure 37, it can be noticed that as one goes through the thickness, the maximum temperature becomes lower and lower until after 5 layers, the temperature is not above glass transition temperature T_g (143 °C) anymore. For regions where the temperature is below T_g , the material becomes stiff and this contributes to the development of residual stresses and distortion due to the temperature gradients. This is also of practical importance for repass treatment (reconsolidation pass) which has been reported in literature [12,43] to improve bonding quality, reduce void content and improve surface finish of in-situ consolidated thermoplastic composites. Repass refers to the application of heat and pressure using the AFP head to the laminate without addition of a new layer. It can be seen from Figure 37 that repass treatment can be effective in improving bonding interface between layers where the temperature is above glass transition temperature T_g (i.e., up to 5 layers below the top surface). Another interesting point, which is obtained from the observation of Figure 37, is the fact that the maximum temperature occurs at later time as one goes through the thickness. This is due to the heat diffusion mechanism inside the composite domain. A localized heat flux resulting from the hot gas flow diffuses through the thickness of the composite substrate. As such, it takes time for the heat energy provided by the hot gas flow at the upper side layer to be diffused, transferred and absorbed by the material at

underneath layers. This can be interpreted as the delay time in peak temperatures at underneath layers [18].

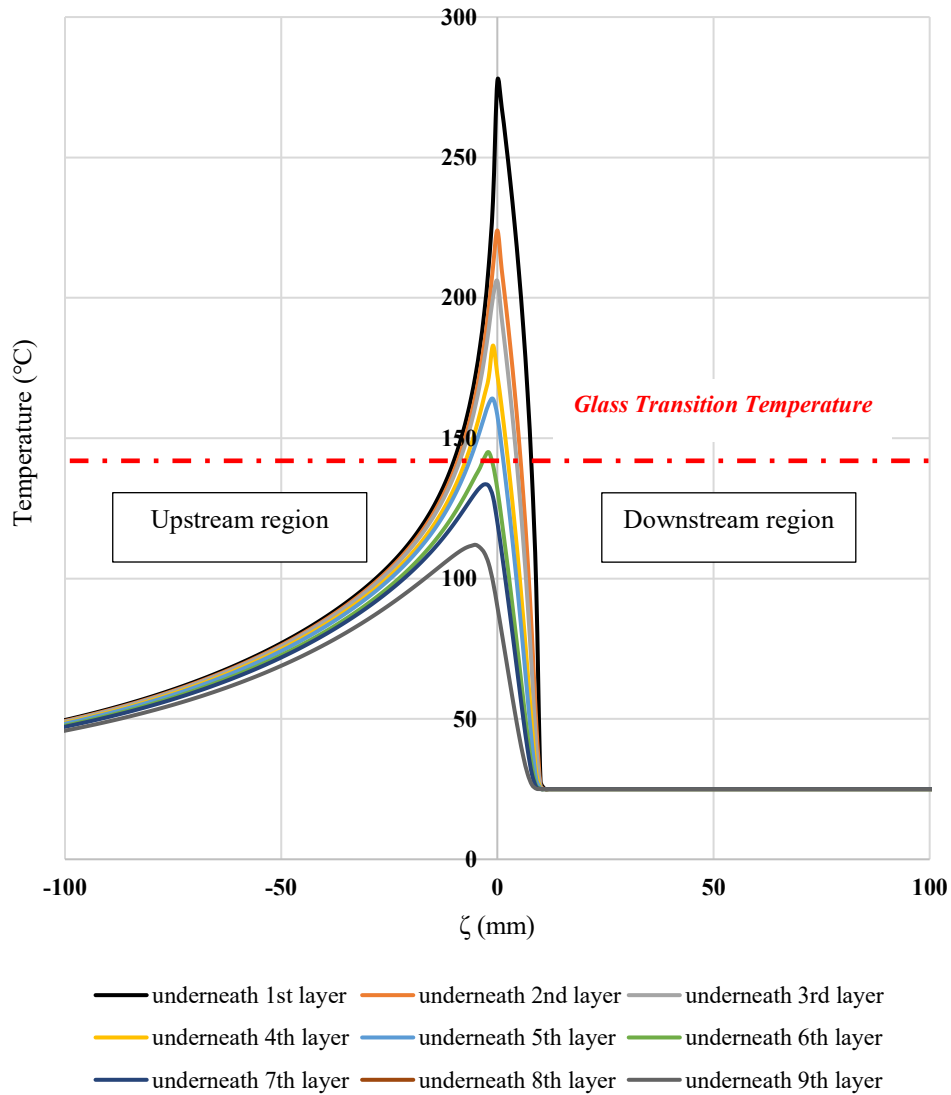


Figure 37. Temperature distribution in the vicinity of the heat source along the lay-up direction at different through-thickness locations at $t = 10$ seconds [18]

5.3 Temperature Variations Through the Thickness of the Composite Substrate at Different Locations Along the Layup Direction

Further investigation of through-thickness temperature distribution is illustrated in Figure 38. When the mid length of the heat source is located at $x(t_n) = 254$ mm (10 inch) at $t = 10$ seconds, the variations of temperature through the thickness (z direction) from 0 mm (top of the composite laminate) to 2.5 mm (bottom of the composite laminate) at five different x locations are presented in Figure 38. For $x(t_n) = 254$ mm (10 inch), this location of the composite laminate experiences the maximum temperature because it is directly below the mid length of the heat source. This temperature variation demonstrates a sharp temperature drop until 1mm (8 layers below) through the thickness where the temperature reaches below 100 °C followed by a gradual temperature reduction until it stabilizes. The curve for $x = 249$ mm (9.8 inch), shows the temperature variation in the upstream region which was previously heated up by the heat source and it is exposed to the surrounding ambience in the cooling stage. As can be seen, the temperature curve for $x = 249$ mm (9.8 inch), initially shows lower temperature than the curve at $x(t_n) = 254$ mm (10 inch). However, as z increases, there is a cross over (“A”) and within the lower half of the thickness, the temperature at $x = 249$ mm (9.8 inch) is higher than the temperature at $x(t_n) = 254$ mm (10 inch). A similar trend can be observed from the curve at $x = 9.6$ inch (plotted at $x(t_n) = 10$ inch). The temperature is initially lower than the temperature at both $x(t_n) = 254$ mm (10 inch) and $x = 249$ mm (9.8 inch); however, as z increases, there is a cross over with the curve at $x(t_n) = 254$ mm (10 inch) at $z = 0.75$ mm (“B”) and another cross over with the curve at $x = 249$ mm (9.8 inch) at $z = 1$ mm (“C”). The curve at $x = 259$ mm (10.2 inch) represents the downstream region as elaborated in Figure 37. Looking at this temperature distribution, it can be noticed that the temperature at $x = 259$ mm (10.2 inch) is lower than the temperature at $x(t_n) = 254$ mm (10 inch). The curve at $x = 264$ mm (10.4 inch) is also plotted to confirm the trend for the curve at $x = 259$ mm (10.2 inch). The reasons for these are as follows [18]:

Considering the surrounding of two positions, $x = 249$ mm (9.8 inch) and $x = 254$ mm (10 inch). At time $t = 10$ seconds, both the left side and right side of position $x = 249$ mm (9.8 inch) are at high temperature because they were previously heated, particularly for positions of higher z values. However, at time $t = 10$ seconds, the left side of $x = 254$ mm (10 inch) is hot while its right

side has not been heated previously. As such, while for positions at lower z values, the temperatures are high due to immediate exposure to heating, positions at higher z values have lower temperatures since there was no previous heating to allow the heat to soak in. This same reason applies to all other positions.

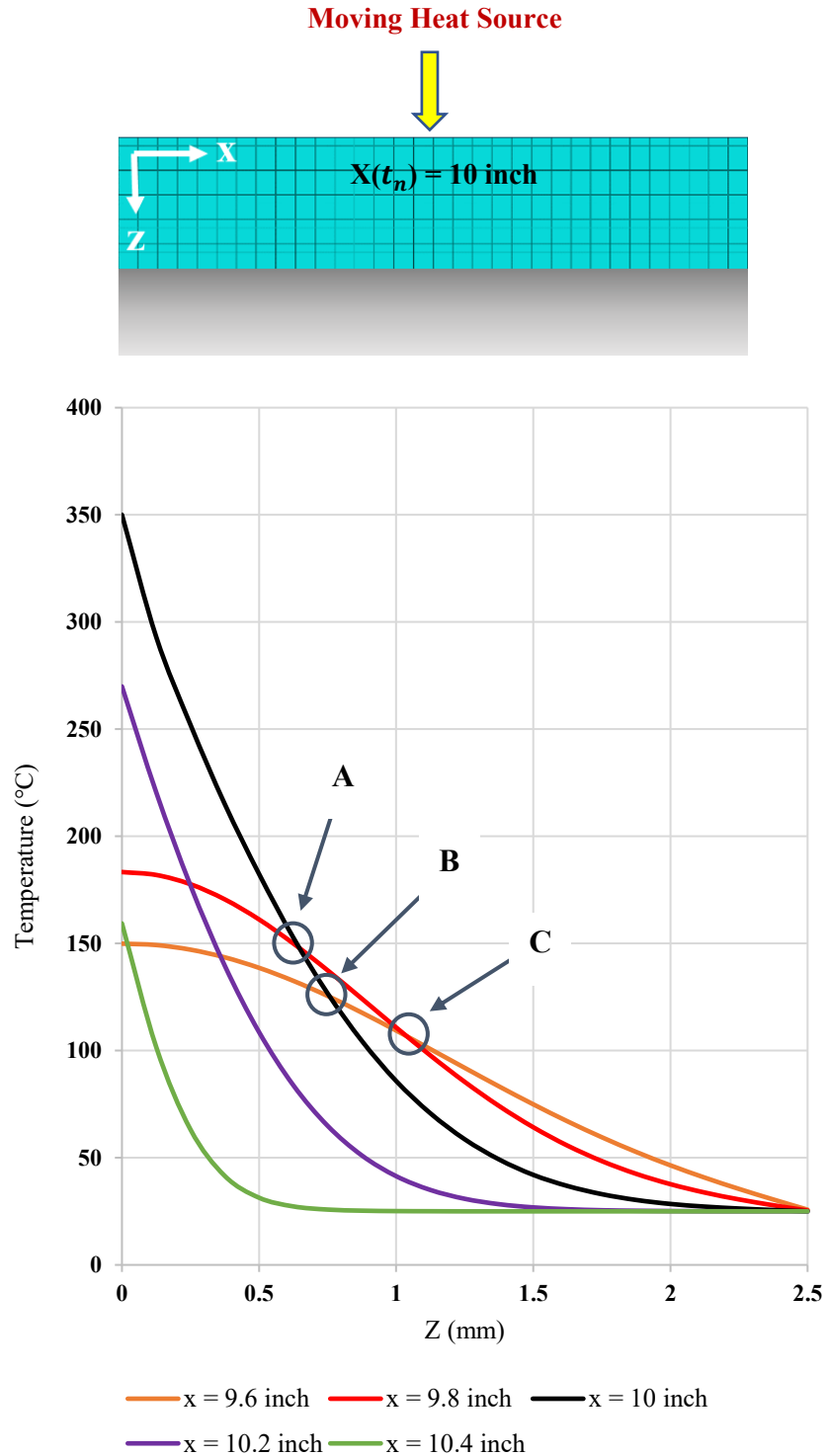


Figure 38. Temperature variations through the thickness (z direction) of the composite substrate at five different x locations at $t = 10$ seconds [18]

In summary, in this chapter, results from numerical method developed for the case of the moving heat source were presented. In order to provide validation of numerical results, experimental trials were performed and results from both numerical method and experimental trials were compared. Numerical and experimental temperature variations for different through-thickness locations of the composite substrate indicated that the numerical method was able to capture the maximum temperature with good agreement with experimental results. The general trend for the temperature distribution also showed agreement. It was also shown that as one goes through the thickness, the maximum temperature becomes lower and lower until after 5 layers the temperature is below glass transition temperature. Results from the temperature distribution in the vicinity of the heat source along the lay-up direction at different through-thickness locations indicated that the downstream region experienced sharper temperature gradient than the upstream region. At the end, temperature variations through the thickness of the composite substrate at different locations along the layup direction were demonstrated. It was shown that the temperature drop in the first few layers was sharp where the temperature reached below 100 °C followed by a gradual temperature reduction until it is stabilized. Overall, results provided significant insight into the distribution of the temperature due to a moving heat source. The results showed significant temperature gradients which explain why there are so much distortion even during the manufacturing process.

Chapter 6: EFFECT OF AFP PROCESS PARAMETERS ON CONVECTIVE HEAT TRANSFER COEFFICIENT

6.1 Overview of The Chapter

In heat transfer analysis of AFP process using a hot gas torch, the convective heat transfer which occurs between the hot gas flow generated by a torch nozzle and a composite substrate plays an active role in the heat transfer mechanism. As mentioned in Chapter 3, in order to model the convective heat transfer, a local heat flux equation $q'' = h (\Delta T)$ is utilized where q'' is the energy flow per unit of area per unit of time, h is accountable for the convective heat transfer coefficient between the hot gas torch and the composite surface, and for the conversion of a portion of the kinetic energy of the gas upon impact with the surface of the composite material; and ΔT accounts for the temperature difference between the two media. This coefficient is dependent on various number of parameters such as nozzle geometry, gas flow rate, temperature of the gas, type of the gas etc. Information from the literature shows values of h that vary from 80 W/m²K to 2500 W/m²K. This large range can provide a great degree of uncertainty in the determination of important quantities such as the temperature distributions and residual stresses. The reason for these large differences can be due to the differences in the process parameters in each of the studies. The process parameters can include the volume flow rate of the hot gas, the gas temperature, the distance between the nozzle exit and the surface of the composite plate, the angle of the torch with respect to the surface of the substrate etc. The purpose of this chapter is to investigate the effect of different AFP process parameters on the convective heat transfer coefficient using available theoretical formulations in literature. Experimental technique is introduced at the end to obtain the h values for the case of AFP at different process parameters. The methodology that will be introduced in the experimental part can be used as the guideline for other researchers to determine the convective heat transfer coefficient for each particular setup.

6.2 Literature Review

Heat transfer mechanism in AFP of thermoplastic composites using a hot gas torch is mainly dominated by heat convection because of the significant temperature difference that exists between the torch nozzle (hot gas flow) and the surface of the composite substrate. Looking at literature, several values for the convective heat transfer coefficient (h) were reported by several researchers. In 2004, Toso *et al.* [55] used an infrared camera to measure the temperature of both the incoming tape and the substrate in static position. Then, temperature gradients along two different directions were found from the temperature data. This was then used to estimate the convective heat transfer coefficient. The h was estimated to be around 80-100 W/m²K for both the incoming tape and the substrate. Tierney *et al.* [42] used the available forced jet-impingement theories to obtain the h coefficient in their heat transfer model developed for tow placement process. Despite the introduction of formulations, no particular value was reported in their study for the h coefficient. Using the average heat transfer coefficient values for impinging jets, Kim *et al.* [84] assumed the h coefficient to be 900 W/m²K in the vicinity of the nip point and for the incoming tape to be 250 W/m²K. A few years later in 2004, the same authors [85] employed the finite element method (FEM) to obtain the distribution of the convection heat transfer coefficient over the composite surface. The flow analysis was conducted for the region between the incoming tape and the composite substrate. Heat transfer coefficient distribution exhibited two peaks within the range of 400 – 500 W/m²K right before the nip point. The values reported, however, were only valid for the test parameters considered in their study. Li *et al.* [51] in 2015, used birth and death of elements technique in ANSYS to obtain the temperature field during the processing of thermoplastic composites. The h coefficient values used as an input in their model were within the range of 900-1000 W/m²K depending on the nozzle temperature. Sonmez *et al.* [48] assumed a coefficient of 2500 W/m²K in their study to investigate the effect of different process parameters in thermoplastic composite tape placement process on crystallization behavior and consolidation condition of the composite parts.

An experimental method, on the other hand, was used by several researchers to estimate the h coefficient for the case of AFP. In this method, first a value for convective heat transfer coefficient is assumed. The temperature distribution is measured experimentally using embedded thermocouples. The calculated temperature distribution from thermal analysis models for the

similar processing parameter is obtained and compared with experimental results. The h coefficient is modified through an iterative process until the predicted numerical temperature results match the experimental temperature values. Using this technique, the h coefficient was found to be $350 \text{ W/m}^2\text{K}$ for the filament winding process [56,59]. Khan [38] used the same technique for AFP of thermoplastic composites and reported a range of $180 - 280 \text{ W/m}^2\text{K}$ for a variety of gas volumes in his study. The experimental setup used in his study is shown in Figure 39. In order to determine the convective heat transfer coefficient, temperatures were measured using the embedded K-type thermocouples mounted through the thickness of the already placed carbon fiber/PEEK composite laminate. In order to predict the temperature numerically, a one-dimensional heat transfer model was used to predict the temperature through the thickness of the composite laminate. Having assumed a value for the h coefficient, through an iterative process, it was modified until the predicted temperature profiles matched well with the experimentally measured temperatures [38]. More recently, in 2019, Tafreshi *et al.* [18] investigated the temperature distribution due to the moving heat source in AFP of thermoplastic composites. A finite difference (FD) code was generated in MATLAB based on the energy balance approach and the temperature gradient in both lay-up and through-thickness directions were predicted numerically. Unidirectional composite strips were manufactured using AFP and fast-response K-type thermocouples were embedded in various locations through the thickness to determine thermal profiles experimentally. It was shown that $h = 990 \text{ W/m}^2\text{K}$ yielded good agreement to match the maximum temperatures measured experimentally with predicted numerical results. The h coefficient was close to the ones reported in literature [51,84].

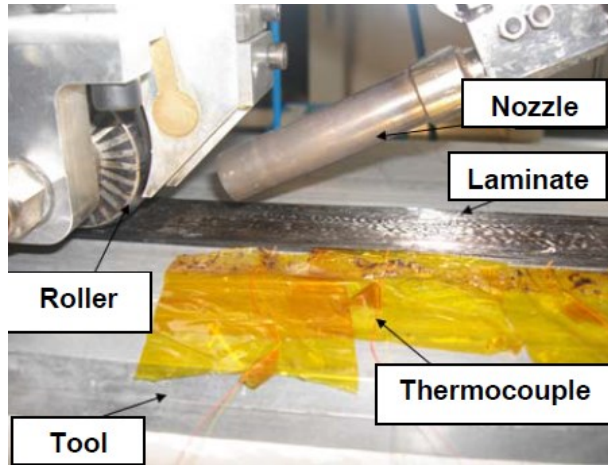


Figure 39. Experimental setup for the determination of the convective heat transfer coefficient [38]

While the research to date has shown some distinct values for convective heat transfer coefficient, much of these has been attributed to the specific set of process parameters in their experimental setup and results cannot be generalized for other configurations. To our knowledge, the effect of AFP process parameters on the convective heat transfer coefficient has not been reported in depth in literature. This chapter is concerned with fundamental heat transfer mechanism that occurs in an impinging jet flow with the focus on its application in AFP processing of thermoplastics using a hot gas torch. An important objective of this chapter is to reveal the convective heat transfer mechanism that influences the temperature distribution developed during the processing of thermoplastic composites and to investigate the variation of the convective heat transfer coefficient with various AFP process parameters.

To achieve this objective, the organization of this chapter is as following:

- (i) In order to understand the convection heat transfer mechanism, one first needs to understand the impinging flow. This provides the fundamental concepts in the impinging flow like an introduction to characteristic regions of the flow.
- (ii) A discussion on Reynolds number and Nusselt number is provided which relates the variety of parameters involved in the problem such as nozzle geometry, gas temperature, flow rate of the gas etc. This will be followed by the presentation of theoretical formulations to compute Reynolds and Nusselt numbers. These relations

will enable the determination of convective heat transfer coefficient (h) for different set of parameters.

- (iii) From the numerous variables in the problem, it will be discussed that only three of them i.e., gas temperature, flow rate of the gas, and nozzle to plate spacing are of paramount importance for the case of this study. Then, the effect of these parameters will be investigated. This helps to reveal the significance of each parameter.
- (iv) The experimental setup is introduced in detail. A methodology is then presented to obtain the h experimentally. Design of experiments in this section is performed based on the significance of each parameter discussed in previous step.
- (v) Results are presented following by the discussion and conclusion at the end.

6.3 Introduction to Impinging Flow

Impinging jets are widely used for heating and/or cooling of large surface areas where high local heat transfer is required. They are used in a variety of applications including heat treatment, cooling of turbine blades and other turbomachinery components, glass manufacturing, heating of optical surfaces, and in electronics [86–88]. In this method, a single or array of nozzles in different geometries (round/slot) are used to impinge air or another type of gas upon the surface of interest to induce high local heat transfer rates [89,90]. The heat transfer mechanism involved in this method is forced convection in which an external means (impinging jet or torch nozzle) is utilized to create temperature gradients [64,91].

Schematic of the impinging flow is illustrated in Figure 40. As can be seen, flow field of impinging flow from single nozzle can be subdivided into three characteristic regions: (a) free jet region, (b) stagnation flow region, and (c) wall jet region. The free jet region develops from the exit of the nozzle with nearly rectangular velocity distribution. The flow in this region is often turbulent until it reaches a limiting distance z_g (about 1.2 times the nozzle diameter) from the surface where the stagnation flow region begins. In stagnation flow region, as the flow approaches the surface, the vertical component of the velocity becomes lower and lower (normal flow is decelerated) and it is transformed into the horizontal component (transverse flow is accelerated). The boundary layer thickness δ_0 in the stagnation zone is around 0.01 of the nozzle diameter for

most of the engineering applications where the Reynolds number is higher than an order of magnitude of 10^4 . Wall jet region represents the region of lateral (or radial) flow outside the stagnation zone. The radial component of the velocity will reach a maximum value and eventually will tend to zero. The main variables for jet impingement heat transfer are the shape (round/slot) and size (diameter or width) of the nozzle, the height of the nozzle above the impingement surface, the nozzle temperature, the gas flow rate, type and thermodynamic state of the gas, the jet Reynolds number and the angle of impingement [64,86,87,89,91,92].

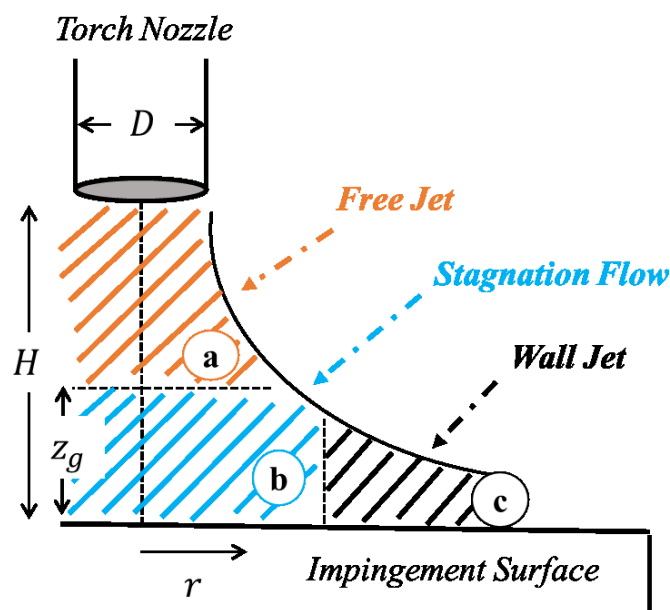


Figure 40. Schematic of the impinging flow by a torch nozzle (a: free jet region, b: stagnation flow region, c: wall jet region)

6.4 Theoretical Formulations

In this section, an introduction into some of important concepts and parameters in convection heat transfer by an impinging jet is presented. The calculation of Reynolds and Prandtl numbers as two major dimensionless parameters is discussed, and appropriate formulations are presented to compute the Nusselt number and it is correlated to the convective heat transfer coefficient involved in the heat transfer mechanism.

6.4.1 Assumption

The formulations presented in this section is based on the following assumptions [86,90,38]:

- The velocity profile of the gas at the torch nozzle exit is uniform.
- The temperature is assumed to be constant over both the torch nozzle exit and the impingement surface.
- It is assumed that at the impact point, where the impinging flow approaches the impingement surface, the fluid is at rest i.e., all velocity components tend to zero [86,90].
- The influence of the turbulence level at the torch nozzle exit is not taken into account. As suggested by Martin [90], inserting turbulence parameter into an engineering correlation for heat transfer is not logical as it is not controllable and cannot be included in design variables. Although the inclusion of turbulence may affect the heat transfer in different flow regions, the equations presented in this section, still can be used for most engineering applications.
- The AFP lay-up speed is assumed to have insignificant effect on the flow condition. Considering the fact that the lay-up speed is much less than the jet impact velocity, this assumption is reasonable [38].
- Instability of the flow velocity and temperature which may result in fluctuations and instabilities in flow is ignored.

6.4.2 Reynolds And Prandtl Numbers

Reynolds number (Re) is defined as the ratio of inertia to viscous forces. The former is associated with an increase in the momentum of a moving fluid while the latter represents the shear forces. For large values of Re , inertia forces are dominant while for small values of Re , viscous/shear forces have more influence in the flow regime [64,91]. In order to determine whether the flow is laminar or turbulent for certain process parameters, one needs to determine the Re number. In a fully developed flow, $Re = 2300$ corresponds to the onset of turbulence regime. In the hot gas torch, Reynolds number can be described as [55]:

$$Re = \frac{V_T \cdot D}{\nu_T} \quad (15)$$

Where D is the inside diameter of the torch nozzle, V_T is the temperature dependent flow velocity at the torch nozzle exit, and ν_T is the temperature dependent kinematic viscosity of the gas.

Knowing the torch nozzle cross-sectional area (A) and the volumetric flow rate of gas at high temperature (Q_T), the temperature dependent flow velocity V_T can be calculated as following [55]:

$$V_T = \frac{Q_T}{A} \quad (16)$$

Where $Q_T = \frac{\rho_{RT}}{\rho_T} Q_{RT}$. Having the gas density at high temperature (ρ_T) and at room temperature (ρ_{RT}) along with the volumetric flow rate of the gas at room temperature (Q_{RT}), V_T and thus Re can be calculated from equations (16) and (15) respectively.

A sample calculation of hot gas torch parameters for selected process parameters is summarized in Table 8. Looking at calculated Reynolds numbers in this table, it can be noticed that the flow in the vicinity of the hot gas torch is turbulent. The Prandtl number (Pr) reported in Table 8 is defined as the ratio of the kinematic viscosity (ν_T) to the thermal diffusivity (α_T) i.e., $Pr = \frac{\nu_T}{\alpha_T}$. It is therefore a measure of the relative effectiveness of the momentum and the energy transport by diffusion in the velocity and thermal boundary layers, respectively [64,91].

Table 8. Parameters of the hot gas torch for three different set of process parameters (Thermophysical properties of Nitrogen gas in different temperatures can be found in Appendix C)

T_{HGT} (°C)	A (mm^2)	ρ_T (kg/m^3)	Q_T (m^3/s)	V_T (m/s)	ν_T (m^2/s)	α_T (m^2/s)	Pr	Re
25	28.27	1.1233	1.25 e-3	44.21	15.8 e-6	22.1 e-6	0.716	16700
600	28.27	0.386	3.63 e-3	128.65	96 e-6	133 e-6	0.722	8041
800	28.27	0.314	4.47 e-3	158.15	133.3 e-6	186 e-6	0.716	7118

6.4.3 Nusselt Number

The heat transfer coefficient could be described in dimensionless form known as Nusselt number. This dimensionless parameter can be interpreted as the dimensionless temperature gradient at the surface which provides the measurement of the convection heat transfer at the surface [64,91]. Based on the definition, this number is a function of various parameters as shown below:

$$Nu = F (Re, Pr, \text{geometric relations}) \quad (17)$$

which Re and Pr are Reynolds and Prandtl numbers respectively. Equation (17) indicates that for a given geometry, the Nusselt number is a function of Re, Pr and some geometric parameters. For different fluid conditions (different gas flow rate, temperature and type of the gas), and different nozzle shapes and sizes, the value of Nu could be computed providing the function above is known [64,90].

Equation (17) could be used for computing the local value of Nu and accordingly the local convection coefficient h . In other words, it addresses the condition at a particular location on the surface. For practical engineering calculations, surface heat transfer in the vicinity of the stagnation zone and the wall jet is important and therefore, the integral mean heat transfer coefficient is often needed. Hence, the average Nusselt number (\overline{Nu}) is obtained by integrating over the surface area. From knowledge of \overline{Nu} , the average convection heat transfer coefficient (\bar{h}) could be found and the average heat flux may then be calculated. The overbar points out an average from $r = 0$ where the boundary layer begins to develop, to the location of interest. The average Nusselt number can be represented as following [64,91]:

$$\overline{Nu} = \frac{\bar{h} L}{k} = F (Re, Pr, r/D, H/D) \quad (18)$$

In this equation, L is the characteristic length which is selected here to be the nozzle diameter ($L=D$) and k is the thermal conductivity of the gas. Since beside the nozzle diameter D, the vertical distance H between the nozzle exit and surface and the lateral (or radial) distance r from stagnation

point are involved in the problem, two dimensionless geometrical parameters of H/D and r/D are included in formulation above [64,89–91].

An extensive review of the impingement heat transfer was performed by Neil *et al.* [88] as well as Viskanta [93]. In these reviews, it is mentioned that depending on the nozzle type (round or slot), number of nozzles (single or array of nozzles), the range of Reynolds number and the nozzle height, one can refer to the appropriate formulations for their particular study. A summary of different sources in literature ([90,94–106]) can be found in Table 9. In these studies, the experimental approach was employed to obtain the local convective heat transfer coefficient and the local Nusselt number. In this approach, heat and/or mass transfer measurements are performed under controlled laboratory conditions. Different geometries and flow conditions are investigated and by correlating the data in terms of dimensionless parameters, appropriate formulations are introduced [64,88,91,93]. Considering the nozzle type used in this study (round nozzle), and the practical range of Reynolds number and nozzle height, formulations presented by Martin [90] and Lytle *et al.* [100] will be employed to investigate the effect of different parameters. Lytle *et al.* [100] suggested the following formulation for calculating the Nusselt number at stagnation point:

$$Nu_{stag} = 0.726 Re^{0.53} (H/D)^{-0.191} \quad (19)$$

Where H is the distance between the nozzle and the target plate (nozzle to plate spacing) and D is the nozzle diameter. For nozzle to plate spacings lower than 0.5, it was found that the following formulation can predict the Nusselt number with slightly better accuracy [100]:

$$Nu_{stag} = 0.663 Re^{0.53} (H/D)^{-0.248} \quad (20)$$

For the case when the nozzle to plate spacing is greater than 2, the formulation presented by Martin [90] can be used as shown below:

$$\frac{\overline{Nu}}{Pr^{0.42}} = \frac{D}{r} \frac{1 - 1.1 D/r}{1 + 0.1 \left(\frac{H}{D} - 6\right) D/r} F(Re) \quad (21)$$

This equation was obtained by integrating the local heat transfer coefficients over the surface area and in this equation, the function $F(Re)$ can be represented by the following smooth curve expression as suggested by Martin [90]:

$$F(Re) = 2Re^{\frac{1}{2}} \left(1 + \frac{Re^{0.55}}{200}\right)^{0.5} \quad (22)$$

Table 9. List of relevant publications in literature for Nusselt calculation [88]

Source	Nozzle type	Provides	Reynolds number, nozzle height range
Goldstein and Behbahani [99]	Single round nozzle	Nu_{avg}	$35,200 \leq Re \leq 120,500$ $H/D = 6 \text{ or } 12$
Goldstein <i>et al.</i> [94]	Single round nozzle	Nu_{avg}	$61,000 \leq Re \leq 124,000$ $2 \leq H/D \leq 12$
Lytle and Webb [100]	Single round nozzle	Nu_0 and Nu_{avg}	$3600 \leq Re \leq 27,600$ $0.1 \leq H/D \leq 1$
Martin [90]	Single round nozzle	Nu_{avg}	$2000 \leq Re \leq 400,000$ $2 \leq H/D \leq 12$
Meola <i>et al.</i> [101]	Single round nozzle	Nu_{avg}	$10,000 \leq Re \leq 100,000$ $10 \leq H/D$
Mohanty and Tawfek [102]	Single round nozzle	Nu_0	$4860 \leq Re \leq 34,500$ $6 \leq H/D \leq 58$
Tawfek [103]	Single round nozzle	Nu_{avg}	$3400 \leq Re \leq 41,000$ $6 \leq H/D \leq 58$
Wen and Jang [104]	Single round nozzle	Nu_{avg}	$750 \leq Re \leq 27,000$ $3 \leq H/D \leq 16$
Martin [90]	Single slot nozzle	Nu_{avg}	$3000 \leq Re \leq 90,000$ $2 \leq H/(2B) \leq 10$
Chan <i>et al.</i> [105]	Single slot nozzle (convex target)	Nu_0	$5600 \leq Re \leq 13,200$ $2 \leq H/B \leq 10$
Florschuetz <i>et al.</i> [106]	Array of round nozzles (inline orifice nozzles)	Nu_{avg}	$2500 \leq Re \leq 70,000$ $1 \leq H/D \leq 3$
Gori and Bossi [95]	Single slot nozzle (on cylinder)	Nu_{avg}	$4000 \leq Re \leq 20,000$ $2 \leq H/B \leq 12$
Huber and Viskanta [96]	Array of round nozzles	Nu_{avg}	$3400 \leq Re \leq 20,500$ $0.25 \leq H/D \leq 6$
Martin [90]	Array of round nozzles	Nu_{avg}	$2000 \leq Re \leq 100,000$ $2 \leq H/D \leq 12$
San and Lai [97]	Array of round nozzles (staggered orifice nozzles)	Nu_0	$10,000 \leq Re \leq 30,000$ $2 \leq H/D \leq 6$
Goldstein and Seol [98]	Row of round nozzles (square orifice)	Nu_{avg}	$10,000 \leq Re \leq 40,000$ $0 \leq H/D \leq 6$
Martin [90]	Array of slot nozzles	Nu_{avg}	$1500 \leq Re \leq 40,000$ $1 \leq H/(2B) \leq 40$

6.4.4 Angle of Impact

The angle of the torch with respect to the surface of the substrate or angle of impact is one of the important parameters affecting the heat transfer especially for the case of AFP in which the torch nozzle is often inclined to be able to heat up the incoming tape as well as the surface of the composite substrate. Figure 41 defines some of the terms used in an inclined impinging jet. The impact point (I.P.) is the point of intersection between the jet mid-axis (L1) and the surface of impingement (L2). θ is the angle of impact which is the acute angle between L1 and L2. The positive direction is called uphill direction which is towards the acute angle that the jet mid-axis makes with the impingement surface. The downhill direction (negative direction) is the direction of the main flow. The distance between the nozzle exit and the impact point is denoted by H, and z represents the normal distance between the impingement surface and the nozzle exit. For the case of normal impingement where $\theta = 90$, H is equal to Z [86].

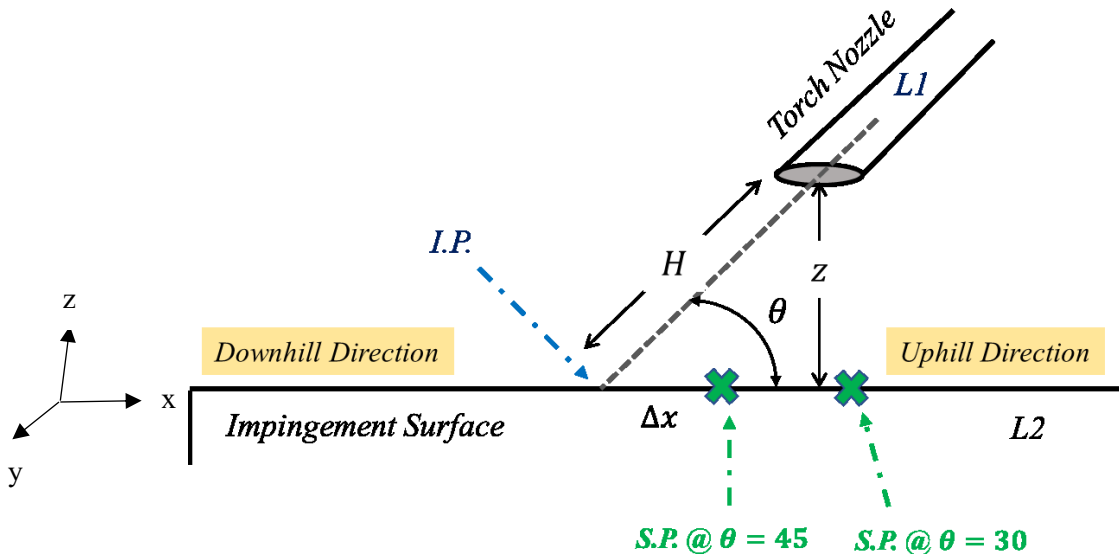


Figure 41. Schematic of Inclined Impinging Jet

Relative displacement of the stagnation point (S.P.) to the impact point is illustrated in Figure 42 for different angles of impact. Various investigations on inclined impinging jets yielded to the fact that the point of maximum heat transfer (stagnation zone) does not occur at the intersection

point (impact point). In other words, the stagnation point shifts by a certain length (Δx) in the uphill direction [89,93]. As shown schematically in Figure 41, the displacement of the stagnation point (Δx) varies with θ . As the angle of impact increases, the stagnation point becomes closer to the impact point and for the case of normal impingement ($\theta = 90^\circ$), the stagnation point coincides with the impact point (S.P.=I.P.). This was reported by various authors in literature [86,90,92,107]. Among those, Goldstein *et al.* [87] investigated the dependency of the stagnation point displacement on impingement angle experimentally. They investigated the effect of different angles of impact i.e., 30° , 45° , 60° and 90° on Nusselt distribution. Looking at Nu distribution contours (Figure 42 (right)), they found that for normal impingement where the angle of impact is 90° , contours exhibit circular pattern which indicates that the flow impinged on the surface is distributed evenly in all lateral directions. The circular and symmetrical pattern of the flow, however, is restricted to the normal impingement. As the impinging jet becomes inclined (angle of impacts $< 90^\circ$), the contours exhibit quasi-elliptical patterns as shown in Figure 42 (right). Asymmetry distribution of flow indicates that the majority of the flow is in the downhill direction and only portion of the flow approaches the uphill direction. This, however, is a function of angle of impact. The more acute the impingement is, the more asymmetry the flow is, and greater portion of the flow approaches the downhill direction. Having obtained the distribution of local Nu for different angles of impact, an empirical correlation was suggested to determine the average Nu for different configurations. The displacement of the stagnation points from the impact point (Δx) for different angles of impact was summarized from their study and is presented in Figure 42 (Left). These are, however, only valid within the range of parameters reported in their study [87]. A more extensive research on inclined impinging jets was conducted by O'Donovan *et al.* [86]. Following a similar experimental method to [87], yet by utilizing particle image velocimetry technique, they showed the displacement of the stagnation point in the uphill direction as the angle of impact became more acute. They concluded that the angle of impact was the parameter of paramount significance which could affect the location of stagnation point. However, they stated that the height of the jet above the surface and variation of Reynolds number in the range of their study had insignificant influence on displacement of the stagnation point.

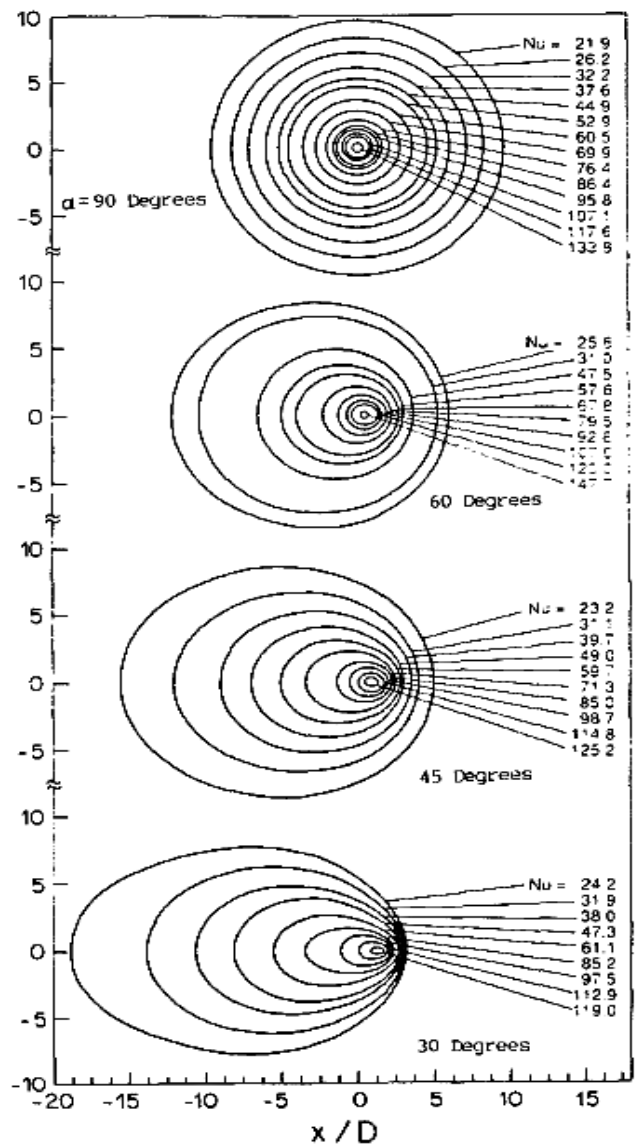
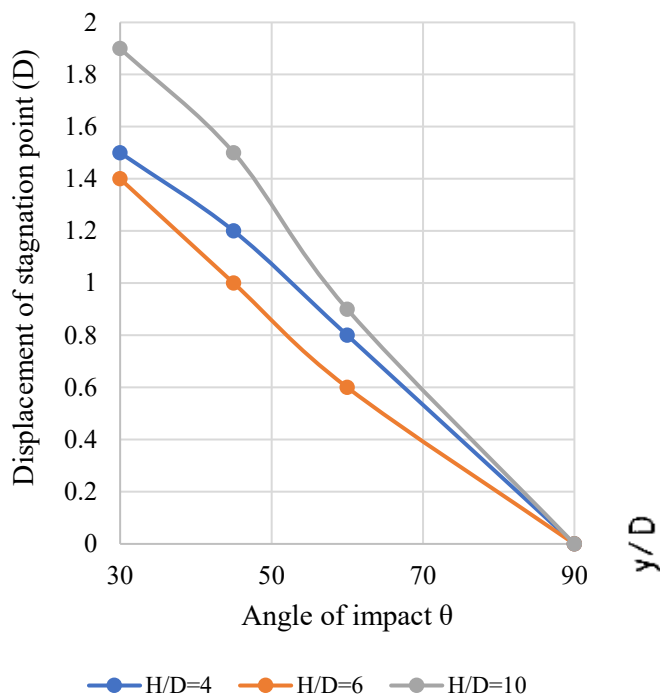


Figure 42. Displacement of stagnation point from impact point for different angle of impacts (Left); Asymmetry distribution of Nu number in acute angles of impact (Right) [87]

Along with the influence of the angle of impacts on displacement of the stagnation point, different studies pointed out that it can also affect the Nusselt number distribution [107,108]. Sparrow *et al.* [107] studied the heat transfer characteristics of the obliquely impinging circular jet experimentally. In their study, Reynolds number, the distance between the nozzle and the impingement plate, and the angle of inclination of the nozzle were considered as variables. The Reynolds number was varied in the range of 2500 to 10000 while the nozzle to plate spacing was chosen among three different values (7, 10 and 15 nozzle diameters). The angle of inclination of

the nozzle was varied from 90 degrees (normal impingement) to 30 degrees in 15 degrees interval. Similar to previous studies, they found that the point of maximum heat transfer does not coincide with the impact point (geometrical impingement point) and as the jet inclination becomes greater, the displacement of the point of maximum heat transfer would extend. For example, it was found that when the angle of impact (θ) is 30 degrees, the displacement is 1.05 nozzle diameter (1.05D) for the nozzle to plate spacing of $H/D = 7$. They measured the maximum heat transfer coefficients and presented results as shown in Table 10. The effect of angle of impacts at different H/D for a constant $Re=5000$ can be seen from Table 10 (left). As can be noticed, with increasing the nozzle inclination, the maximum heat transfer coefficient decreases within the range of 15 to 20 %. It, however, depends on the nozzle to plate spacing. At larger H/D values such as 15, the decrease is less significant which is in the order of 5%. The influence of Reynolds number can be seen from Table 10 (right). The maximum heat transfer coefficient is very sensitive to the Reynolds number. By increasing the Re from 2500 to 10000 when the angle of impingement is 60 degrees, the increase of about 140 % (from 39 to 94.5) can be noticed from the results. They pointed out, however, the average heat transfer coefficient (averaged over a square with a side equal to 4 nozzle diameter) is not very sensitive to the angle of impingement. Similar study performed by Perry [108] confirmed that the effect of angle of impingements on the average heat transfer coefficient is not significant.

Overall, looking at Nu number distribution results for various configurations discussed in above studies, the following concluding remarks for inclined impingements can be stated [86,87,89,90,107,108]:

- Nu distribution is asymmetric, and the peak occurs at a location in the uphill direction i.e., it shifts from the impact point. The asymmetry distribution of the Nu is more significant in greater nozzle inclination.
- The majority of the flow is in the downhill direction and it vanishes quickly in the uphill direction. The reason can be due to the fact that the flow does not have sufficient momentum to climb the uphill direction.
- The magnitude of the peak heat transfer is a function of angle of impingement, Reynolds number and nozzle to plate spacing. Although the maximum heat transfer is very

sensitive to the angle of impingement, the average heat transfer is essentially unchanged.

Table 10. Maximum Nusselt number in different angle of impingements, the effect of nozzle to plate spacing (H/D) at a constant $Re=5000$ (Left), the effect of Reynolds number for constant nozzle to plate spacing ($H/D = 10$) [107]

θ (deg)	Nu_{max}		
	$H/D=7$	$H/D=10$	$H/D=15$
90	93.0	62.0	43.0
75	91.5	63.1	40.5
60	85.5	60.0	40.2
45	80.0	58.0	39.5
30	75.0	53.8	34.5

Reynolds	Nu_{max}		
	$\theta =90$ deg	$\theta =60$ deg	$\theta =30$ deg
2500	43.0	39.0	34.5
5000	62.0	60.0	53.8
10000	101.5	94.5	71.5

6.5 Theoretical Results

In this section, the theoretical formulations presented in previous section are used to investigate the effect of different parameters on Reynolds number, nozzle exit flow velocity, and more importantly the convective heat transfer coefficient. As mentioned earlier, there are many parameters that affect the convective heat transfer by the hot gas torch. These parameters include shape and size of the nozzle, type of the gas, thermodynamic properties of the gas, nozzle temperature, volumetric flow rate of the gas, turbulence level, nozzle to plate distance, and angle of impact. In the current investigation, the effect of shape and size of the nozzle and type of the gas are not investigated since the shape and size of the nozzle, and the type of gas are fixed for one particular experiment. However, the effect of nozzle geometry is briefly presented based on the available studies in literature. The values used for generating the results in this section are tabulated in Table 11.

Table 11. Parameters values used in this study

Nozzle cross-sectional area (mm ²)	Nozzle shape	Gas type	Angle of impact	Nozzle to plate spacing (H/D)
28.3	Round	Nitrogen*	90° (Normal)	1
Torch nozzle temperature °C	Volumetric flow rate of gas	Gas density @RT (kg/m ³)	Gas thermal conductivity @RT (W/m.K)	Gas thermal diffusivity @RT (m ² /s)
Variable	Variable	1.1233	25.9 E-3	22.1 E-6

* Thermophysical properties of Nitrogen gas at higher temperatures are obtained by interpolating the available data in the reference [64] as presented in the Appendix C

6.5.1 Effect of Nozzle Geometry

The effect of nozzle geometry can be classified into the effect of nozzle shape and the effect of nozzle dimensions (nozzle diameter for the case of round nozzle). These two categories can be studied independently. Long pipe or channel type nozzles can have different shapes including circular, square and rectangular as shown in Figure 43 (left). Singh *et al.* [109] studied the effect of nozzle shape on the heat transfer when a cylindrical surface is the target. They considered air as the working fluid and performed experimental and numerical parametric study on the heat transfer for circular, square and rectangular nozzle shapes with similar hydraulic diameters (equal to nozzle diameter for circular cross-section). In their study, the Reynolds number was varied in the range of 10000 to 25000. According to their parametric study, it was concluded that the Nusselt number at stagnation point increases as the Re_{hyd} (Reynolds number defined based on the hydraulic diameter) increases for different nozzle shapes (Figure 43 (right)). It was also pointed out that for a constant Re_{hyd} , the circular nozzle provides higher Nusselt number at stagnation point compared to other shapes of the nozzle. Following a similar experimental procedure, Gulati *et al.* [110] investigated the effect of nozzle shape, nozzle to plate spacing and Reynolds number on heat transfer characteristics for a flat plate. They found that the rectangular nozzle exhibited higher Nusselt number in the stagnation region compared to circular and square nozzles. However, the average

Nusselt number was found to be consistent for different nozzle shapes in their study. The effect of nozzle dimension, on the other hand, was addressed in literature [111–114]. Among those, Lee *et al.* [111] studied the effect of nozzle diameter for the case of round nozzle on fluid flow characteristics of the impinging jet. They conducted the experiments for different nozzle diameters ranging from 1.36 to 3.40 cm. The study was performed under a constant Reynolds number and variable nozzle to plate spacings. They observed that for a larger nozzle diameter, the Nusselt number at stagnation point was higher compared to smaller diameters. The heat transfer increase was correlated to the increase in the flow momentum as impinged by the jet. However, it was observed that the effect of nozzle diameter on heat transfer for further radial locations i.e, $r/d > 0.5$ (r is the radial location and d is the nozzle diameter) was not significant.

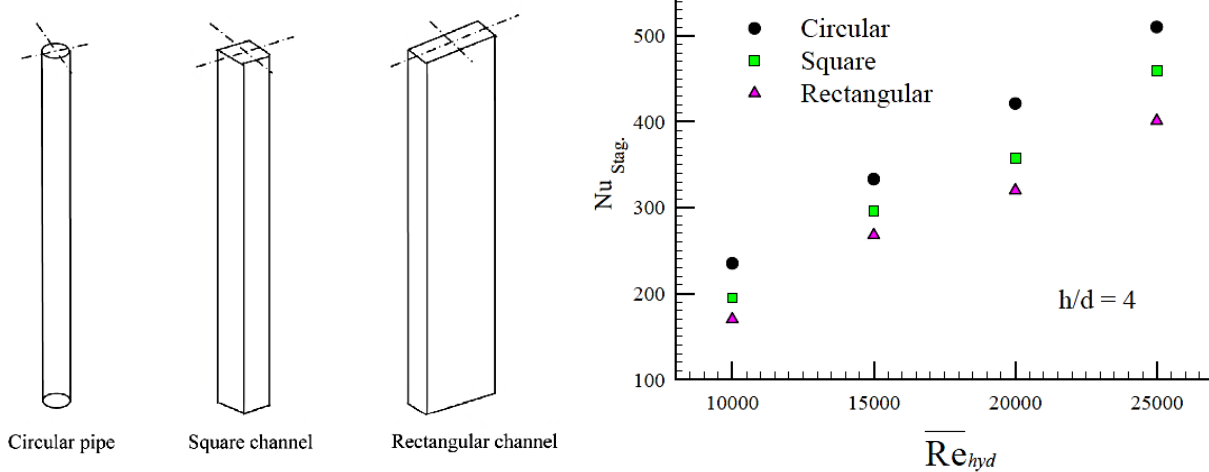


Figure 43. Different nozzle shapes in impingement studies (Left); Effect of different nozzle shapes on Nusselt at stagnation point (Right) [109]

6.5.2 Effect of Nozzle Temperature

The effect of nozzle temperature on nozzle exit flow velocity (V_T) and Reynolds number (Re) is shown in Figure 44. As can be seen, the increase of nozzle temperature from 600 °C to 900 °C, results in around 35% increase in V_T and 15% reduction in Re number. This is attributed to the variation of volumetric flow rate and kinematic viscosity of the gas at different nozzle temperatures. In Figure 45, variation of the convective heat transfer coefficient (h) at stagnation point at different nozzle temperatures is presented. The procedure to calculate the h coefficient at stagnation point (h_{stag}) for different process parameters is as following:

At each nozzle temperature, thermophysical properties of the Nitrogen gas are obtained from the table presented in Appendix C. From this table, properties such as density, thermal diffusivity, kinematic viscosity, and Prandtl number need to be recorded. According to the gas flow rate in which you aim at calculating the h coefficient, the volumetric flow rate of the gas is then found using equation (16). Having the nozzle cross-sectional area and the gas flow rate, the nozzle exit flow velocity can be computed. Then, using equation (15) and the values obtained for flow velocity and kinematic viscosity of the gas, the Reynolds number can be calculated. Afterwards, we need to refer to equations (19) to (21) where the Nusselt number is given. The final step is to refer to equation (18) to determine the h coefficient at stagnation point. In this equation, the characteristic length is given as the nozzle diameter and k is also given as the thermal conductivity of the gas. Having found the Nusselt number in previous step, the convective heat transfer coefficient h can be calculated. The same procedure is repeated for all the other process parameters to obtain different values for the h coefficient.

Looking at results in Figure 45, it can be seen that by increasing the nozzle temperature, the h coefficient at stagnation point increases. For example, for the gas flow rate of 50 SLPM, the h_{stag} increases by about 16%. The amount of increase is in the same range for other gas flow rates. Overall, it can be stated that the variation of h_{stag} versus nozzle temperature exhibits similar trend for all the gas flow rates.

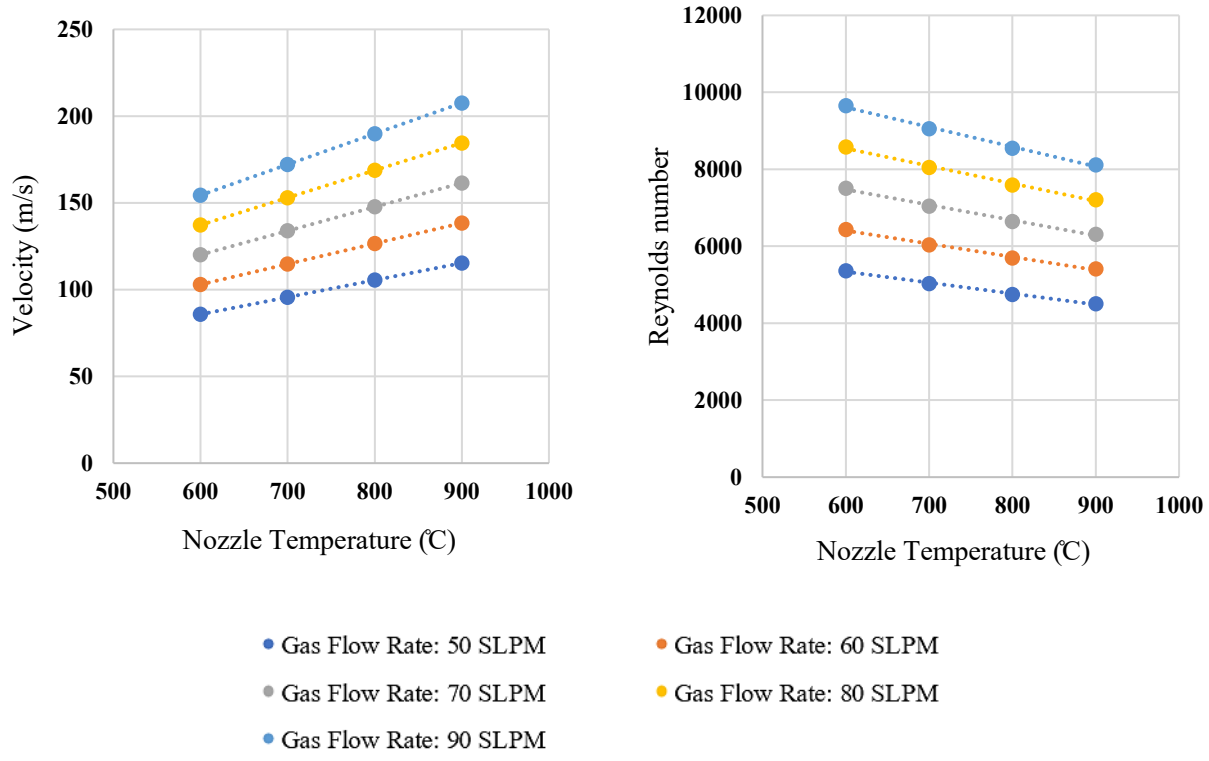


Figure 44. Effect of nozzle temperature on gas velocity at nozzle exit (left) and Reynolds number (right) at different gas flow rates

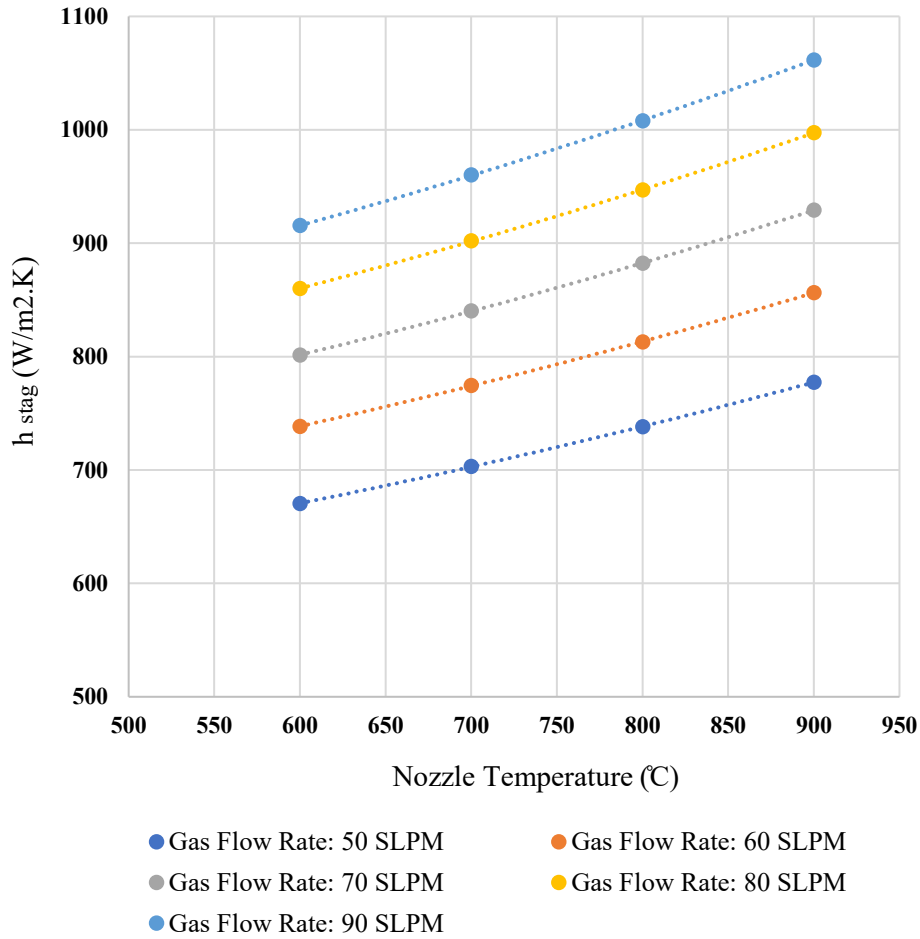


Figure 45. Effect of nozzle temperature on convective heat transfer coefficient at stagnation point h_{stag} at different gas flow rates

6.5.3 Effect of Gas Flow Rate

Investigation the effect of volumetric flow rate of the gas is presented in Figure 46 and Figure 47. As the nitrogen gas flow rate increases from 50 to 90 standard liter per minute (SLPM), both the nozzle exit flow velocity and Re number increase around 80%. These two parameters are directly affected by the volumetric flow rate of the gas. In a similar manner to Figure 45 by obtaining the thermophysical properties of the nitrogen gas at different nozzle temperatures, and by considering the gas flow rate, the nozzle exit flow velocity and the Reynolds number are

calculated. Having obtained the Nusselt number, h coefficients for different process parameters are calculated.

Comparing to results presented in Figure 45, the effect of nitrogen gas flow rate is more significant than the effect of nozzle temperature on h_{stag} results. By increasing the gas flow rate from 50 to 90 SLPM, the h_{stag} can be increased by about 36 % while by increasing the nozzle temperature from 600 to 900 °C, it can be increased by about 16 %. Results from different nozzle temperatures show similar trend. For example, at nozzle temperature of 600 °C, the h_{stag} can be increased by 36 % by increasing the flow rate. And the similar amount of increase can be noticed for other graphs. Overall, it can be concluded that the influence of gas flow rate on results is approximately two times the influence of the nozzle temperature.

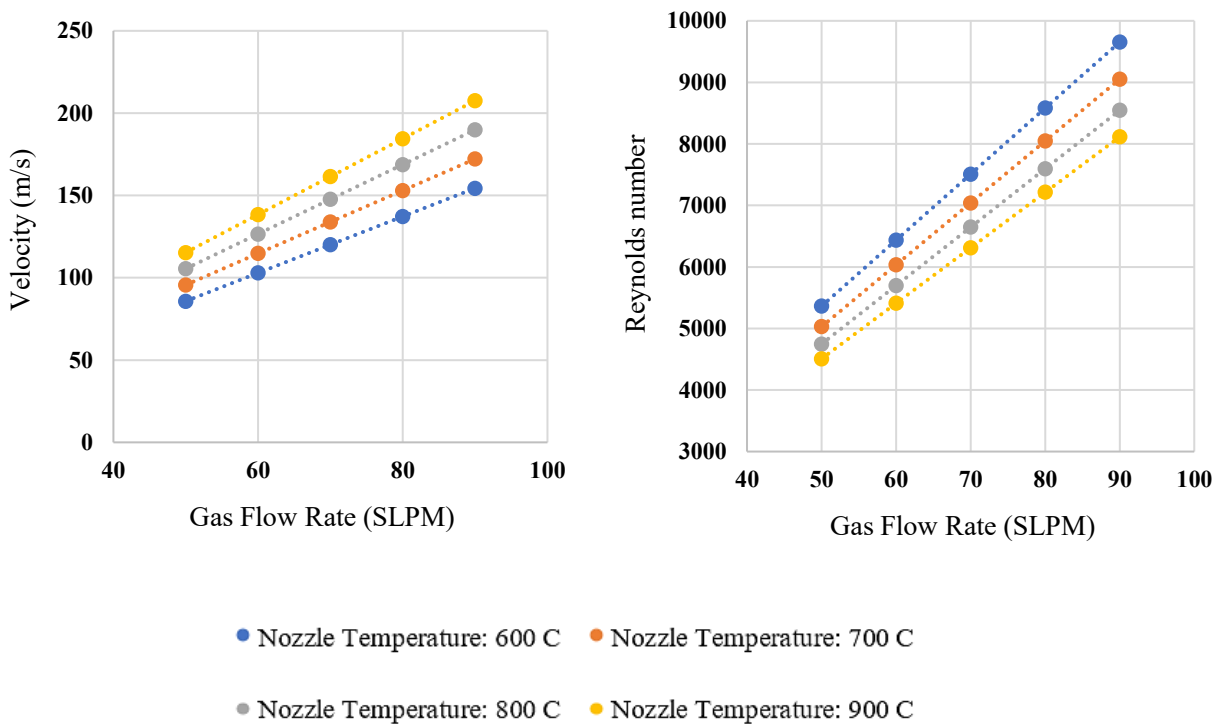


Figure 46. Effect of Nitrogen gas flow rate on gas velocity at nozzle exit (left) and Reynolds number (right) at different nozzle temperatures

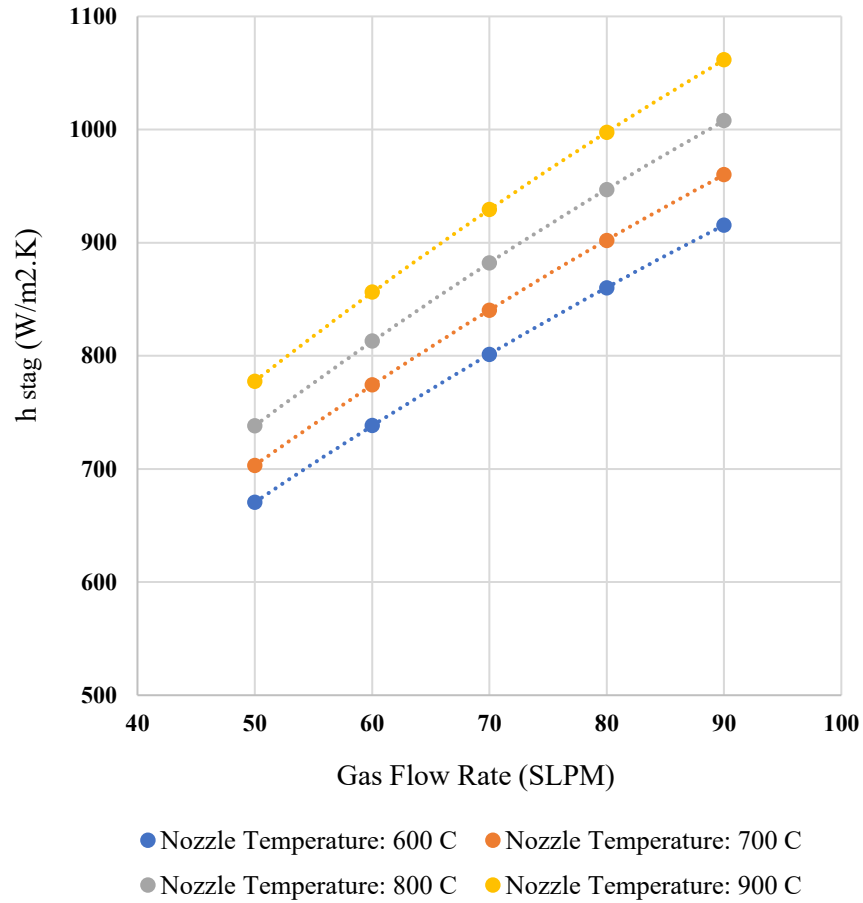


Figure 47. Effect of Nitrogen gas flow rate on convective heat transfer coefficient at stagnation point h_{stag} at different nozzle temperatures

6.5.4 Effect of Nozzle to Plate Spacing

Figure 48 shows the effect of nozzle to plate spacing on the heat transfer results. The horizontal axis represents the non-dimensionalized spacing which is the nozzle to plate distance (H) divided by the nozzle diameter (D). The results are obtained for different process parameters i.e., for different nozzle temperatures at a constant gas flow rate for the range of H / D between 0.1 and 1 and presented in Figure 48. The reason for the selection of such a small range, is that for the case of AFP, the distance between the nozzle and the target plate is typically very small and is in the similar range. As can be seen, the convective heat transfer coefficient at stagnation point decreases by increasing the nozzle to plate spacing for all the process conditions. The reduction is in the range of about 35%. Therefore, it can be assumed that for the range of parameters considered in practice, the effect of smaller nozzle to plate spacing on the heat transfer results is within 35% which is noticeable and needs to be considered.

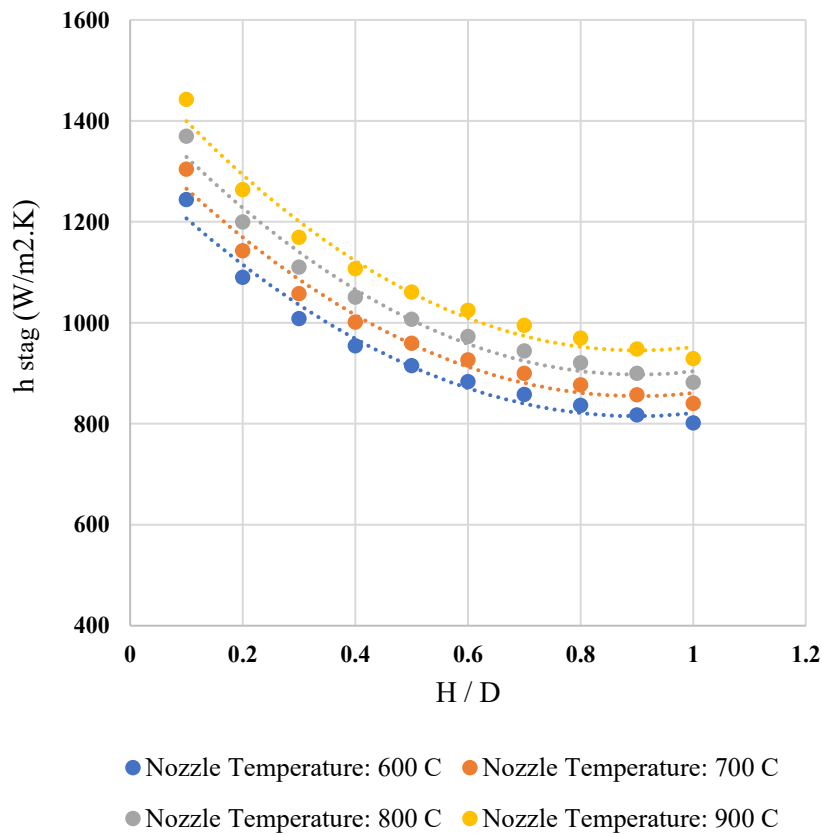


Figure 48. Effect of non-dimensionalized nozzle to plate spacing (H/D) on the h coefficient at stagnation point for nozzle temperatures at a constant gas flow rate of 70 SLPM

6.6 Discussion

The theoretical results presented in previous sections provided good insight on the heat transfer characteristics of the impinging jet problems. It is important to obtain the theoretical results using the available formulations in literature prior to performing the experimental trials. This should be done mainly because of three reasons:

1. To understand what type of parameters are involved in the problem.
2. To investigate the influence of each parameter on heat transfer results. This can be of paramount importance in design of experiments. Considering the fact that investigation of all possible parameters is time consuming, determination of most influential parameters can be helpful in narrowing down the experimental parameters in practice.
3. To understand how the convective heat transfer coefficient varies with each parameter and whether different process parameters have similar level of influence on the results.

In the following section, based on the theoretical results, design of experiments is performed. The details of the experimental setup and the methodology to investigate the effect of each process parameter on the convective heat transfer coefficient will be presented.

6.7 Experimental Methodology

6.7.1 Experimental Setup

AFP work cell and flat Aluminum paddle tool at Concordia Centre for Composites (CONCOM) obtained from Automated Dynamics Corporation (ADC) are used to perform the experimental studies (Figure 49). Close-up of the thermoplastic fiber placement head is illustrated in Figure 49 (right). The details of the experimental setup and the AFP machine were provided in Chapter 4. In this setup, the incoming tape is first guided and positioned by material guide eyelets. The material is then driven through a tape guide where a feed roller is mounted to apply tension on the tape. Afterwards, the tape is driven towards a compaction roller. The compaction assembly is used to consolidate the material i.e., the incoming tape onto the substrate at the Nip point. A hot gas torch (HGT) is integrated in the AFP head which is employed to heat up the incoming tape and a certain area of the substrate during the process. As mentioned earlier, the main purpose of the HGT is to heat up the material. The HGT is positioned in a way that it points towards the lower half of the consolidation roller. This helps to heat up both the incoming tape and the substrate in the vicinity of the nip point. Nitrogen gas is used in this setup to provide heat to the material. Inside the torch housing, there are a few heating elements which enable the control the temperature of the nitrogen gas. The heated nitrogen is directed onto the material using the torch nozzle. The temperature and nitrogen gas flow rate can be set independently through an operator interface [6,13,18,28,69].

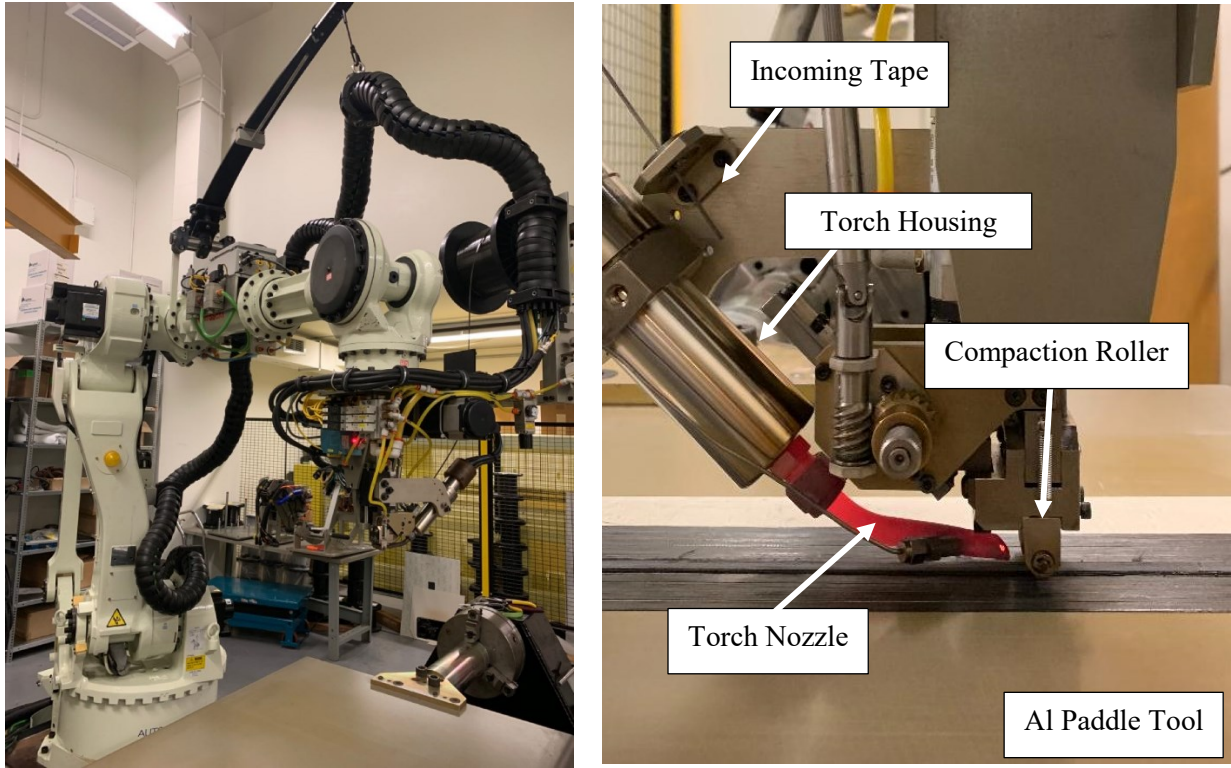


Figure 49. Automated Fiber Placement at Concordia Center for Composites (Left); Thermoplastic Fiber Placement Head (Right)

6.7.2 Design of Experiment

The main objective of this chapter is to determine the convective heat transfer coefficient under different process parameters. As discussed in previous sections, there are variety of parameters that can affect the convective heat transfer coefficient “h” and thus many possibilities exist in the design of experiment. A list of all parameters that may affect the results are presented in Table 12. The parameters are classified into four major groups: a) nozzle, b) gas, c) configuration of the nozzle, roller and the substrate and d) the layup velocity. It is also indicated that whether they are variable in a study or not. Among these, shape and size of the nozzle, type and state of the hot gas are the parameters which are dominated by the experimental setup used in this chapter and thus they are fixed. Nitrogen gas is used as the hot gas coming out of the torch and the thermophysical properties of the hot gas at different temperatures are listed in Appendix C. The layup speed is considered to

be fixed. There are two major parameters in the gas category in Table 12 which are considered variables. These include the nozzle temperature and the volumetric flow rate of the gas. In the AFP setup, these two parameters can be set independently through the AFP operator interface. Studies on impinging jet theories in previous sections revealed the presence of two parameters of nozzle temperature and gas flow rate in heat transfer formulations. These parameters can affect the thermophysical properties of the gas, the Reynolds number, the flow speed at the nozzle exit, the Nusselt number and more importantly the convective heat transfer coefficient. The theoretical results presented in sections 6.5.2 and 6.5.3, revealed that the h coefficient increases by increasing the nozzle temperature. The variation was shown to be within 16 %. Similarly, it was found that by increasing the gas flow rate, the h coefficient can increase. The significance of gas flow rate, however, was found to be greater than nozzle temperature as it exhibited around 36 % variation. As such, it can be concluded that these two parameters are of paramount importance to be investigated in experimental trials and they are considered variable in this chapter.

Table 12. List of AFP parameters

Nozzle	
Shape of section	Fixed
Section diameter	Fixed
Gas	
Type of gas (Nitrogen)	Fixed
State of the gas (thermophysical properties)	Fixed
Volume flow rate	Variable
Gas temperature	Variable
Configuration of nozzle, roller and substrate	
Distance between nozzle and roller	Fixed
Distance between nozzle and substrate	Variable
Angle between torch and substrate top surface	Fixed
Lay up velocity	
	Fixed

In the third category in Table 12, configuration of the nozzle, roller and the substrate are presented. Positioning of the torch nozzle with respect to the consolidation roller and the surface of the substrate may also affect the results. The parameters involved in positioning of the torch are illustrated in Figure 50. The nozzle to mid-roller spacing is denoted by “A” while the distance from the tip of the torch nozzle to the surface of the composite substrate is denoted by “H”. Using the theoretical formulations, it was shown that for the range of H/D between 0.1 and 1 (H is the normal nozzle to substrate spacing), by increasing the nozzle to substrate spacing, the convective heat transfer coefficient decreases. For these range of parameters, it can be assumed that the effect of smaller nozzle to plate spacing on the heat transfer results is within 35% of the values calculated using large distances which is noticeable. Therefore, it is necessary to perform experiments for each particular setup to investigate the effect of nozzle to plate distance at very close spacings. Considering the discussion above, the parameter “H” i.e., the distance between the torch nozzle and the surface of the composite substrate is considered to be variable in this chapter. In practice, the torch nozzle can be positioned at various locations relative to the consolidation roller in the AFP setup. This parameter can be variable during the cases of different studies. However, the experimental trials in this study are performed so that the torch nozzle is mounted at a fixed location with respect to the consolidation roller. The distance between the tip of the nozzle to the roller mid point is recorded to be 10.4mm as shown in Figure 50. The angle of the torch with respect to the substrate is also kept constant and is about 8 degrees.

In summary, among all the potential parameters of the process, in this experimental study, it is decided to investigate the effect of nozzle temperature, gas flow rate and nozzle to substrate spacing on convective heat transfer coefficient. The nozzle temperature is varied between 50 and 90 SLPM for three different values while the torch nozzle temperature is varied between 600 and 900 °C for four different values. As for the nozzle to substrate spacing, three different distances of 2.5, 5 and 10 mm are selected to perform the experimental trials. The design of experiment and the values assigned for each case are summarized in Table 13. In total, 36 cases are considered in this study.

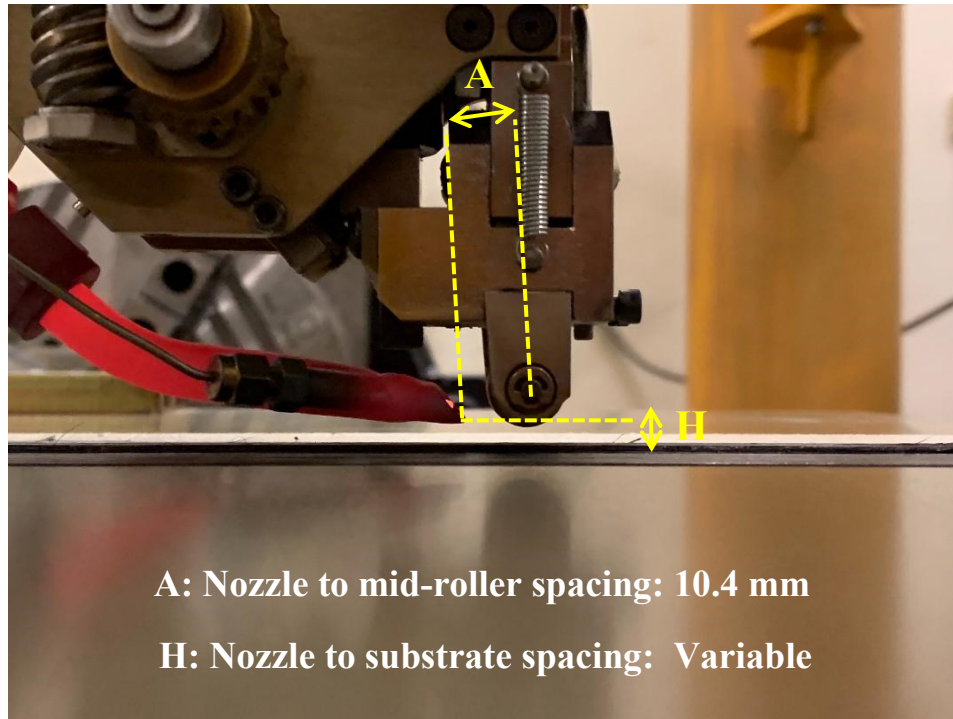


Figure 50. Positioning of the torch nozzle with respect to the consolidation roller and the composite substrate

Table 13. Design of experiments

Nozzle to plate spacing : 2.5 mm	Nitrogen Gas Flow Rate (SLPM)			
		50	70	90
Torch Nozzle Temperature (°C)	600	<i>Case 1</i>	<i>Case 2</i>	<i>Case 3</i>
	700	<i>Case 4</i>	<i>Case 5</i>	<i>Case 6</i>
	800	<i>Case 7</i>	<i>Case 8</i>	<i>Case 9</i>
	900	<i>Case 10</i>	<i>Case 11</i>	<i>Case 12</i>
Nozzle to plate spacing : 5 mm	Nitrogen Gas Flow Rate (SLPM)			
		50	70	90
Torch Nozzle Temperature (°C)	600	<i>Case 13</i>	<i>Case 14</i>	<i>Case 15</i>
	700	<i>Case 16</i>	<i>Case 17</i>	<i>Case 18</i>
	800	<i>Case 19</i>	<i>Case 20</i>	<i>Case 21</i>
	900	<i>Case 22</i>	<i>Case 23</i>	<i>Case 24</i>

Nozzle to plate spacing : 10 mm	Nitrogen Gas Flow Rate (SLPM)			
		50	70	90
Torch Nozzle Temperature (°C)	600	<i>Case 25</i>	<i>Case 26</i>	<i>Case 27</i>
	700	<i>Case 28</i>	<i>Case 29</i>	<i>Case 30</i>
	800	<i>Case 31</i>	<i>Case 32</i>	<i>Case 33</i>
	900	<i>Case 34</i>	<i>Case 35</i>	<i>Case 36</i>

6.7.3 Manufacturing Procedure

Experimental trials setup used in this chapter, is illustrated below in Figure 51. Unidirectional composite strips of 508 mm (20 inch) long making up 10 layers are manufactured first under nominal processing parameters (nozzle temperature: 875 °C, nitrogen gas flow rate: 75 SLPM, compaction pressure 80 psi. The laminate is allowed to cool down to reach room temperature to achieve thermal equilibrium. Subsequently, on the upper side layer, a fast-response K-type thermocouple (TC; Omega CHAL-002) is mounted using a Kapton® tape. The thermocouple wires beyond the junction point, may undergo very high temperatures during the experimental trial and sometimes the assembly may degrade due to short circuits. As such, because of Kapton tape’s good insulating and temperature characteristics, it is used to protect the wires (Figure 51 (left)). After the installation of the thermocouple, the last layer is deposited. When the Nip point of the consolidation roller arrives on top of the thermocouple, it deposits the composite layer and the thermocouple becomes embedded into the composite substrate. Figure 51 (right) depicts the AFP head while depositing the last layer over the embedded thermocouple. The TC data is measured by Data Acquisition system (DAQ) at 100 Hz and a personal computer is used to display information and store the thermal data during the process. It is important to have a TC with fast response. Otherwise, the temperature reading is not representative of transient nature of the process. The main objective of this chapter is to determine the convective heat transfer coefficient under different processing parameters. Since the problem is a moving heat source without material deposition, in the AFP setup, the material deposition is deactivated to resemble the case of the moving heat source problem. In this chapter, similar to the main experimental setup introduced in

Chapter 4, fully-impregnated $\frac{1}{4}$ - inch wide AS4/APC-2 supplied by CYTEC is used as the material for the incoming tape [18].

As mentioned in the design of experiments, the torch nozzle temperature is set in the range of 600°C – 900°C and the nitrogen gas volumetric flow rate is selected in the range of 50 – 90 SLPM. Both parameters can be adjusted easily without interfering into the positioning of the torch nozzle and the thermoplastic fiber placement head. These parameters are controlled independently through the AFP operator interface. The nozzle temperature is changed by changing the power input into the electrical heater in the torch housing and the nitrogen gas flow rate is changed by changing the input into the nitrogen line supplying the nitrogen on the back of the torch housing. For all the cases presented in Table 13, at each pass, the heat source moves from one end to the other end of the composite strip with speed of 25.4 mm/s (1 in/s) without material deposition and the temperature signal is recorded by the TC which is embedded into the composite substrate, underneath one layer of composite material. After completing one pass, the setup is allowed to cool down to reach room temperature. For each case (in total 36 cases), the process is repeated five times to ensure readings are repeatable and the data are consistent. As such, in total 180 runs (36×5) are performed. The complete lay up of the composite, the tool, and the location of the embedded thermocouple along with the data acquisition system are shown schematically in Figure 52.

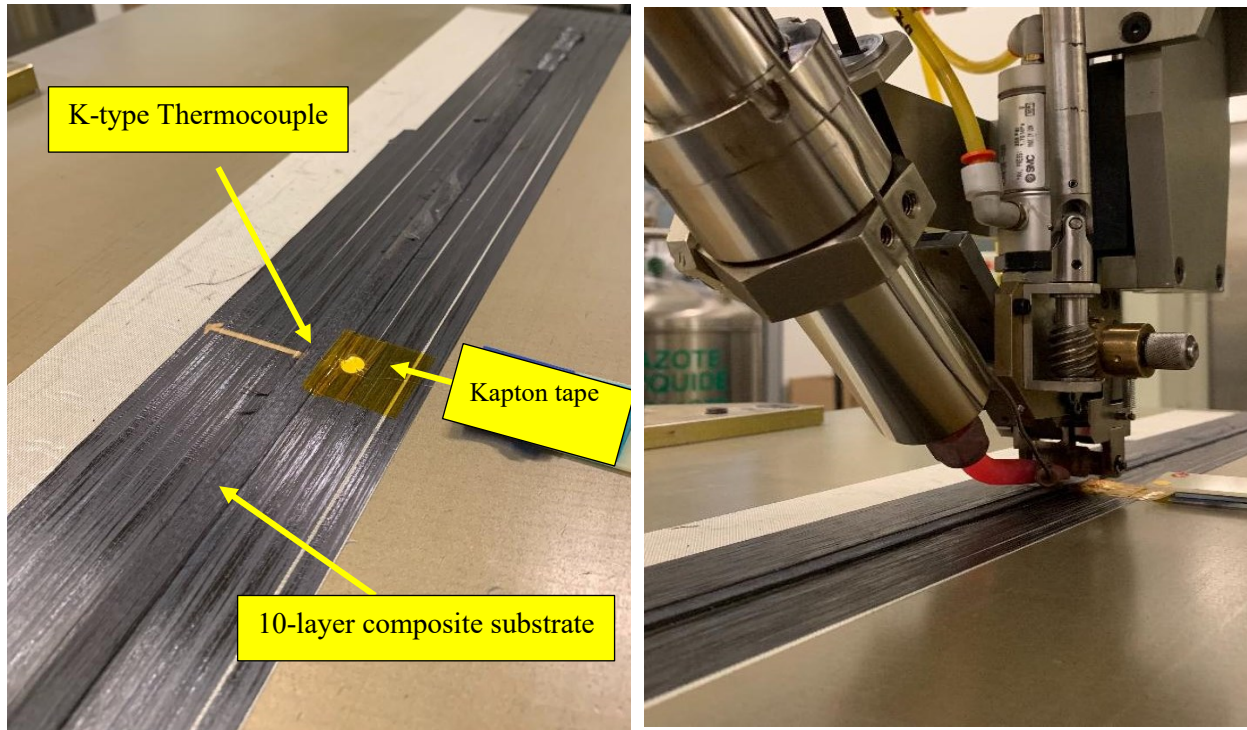


Figure 51. Positioning of the embedded thermocouple inside the composite substrate (Left); AFP head over the embedded thermocouple (Right)

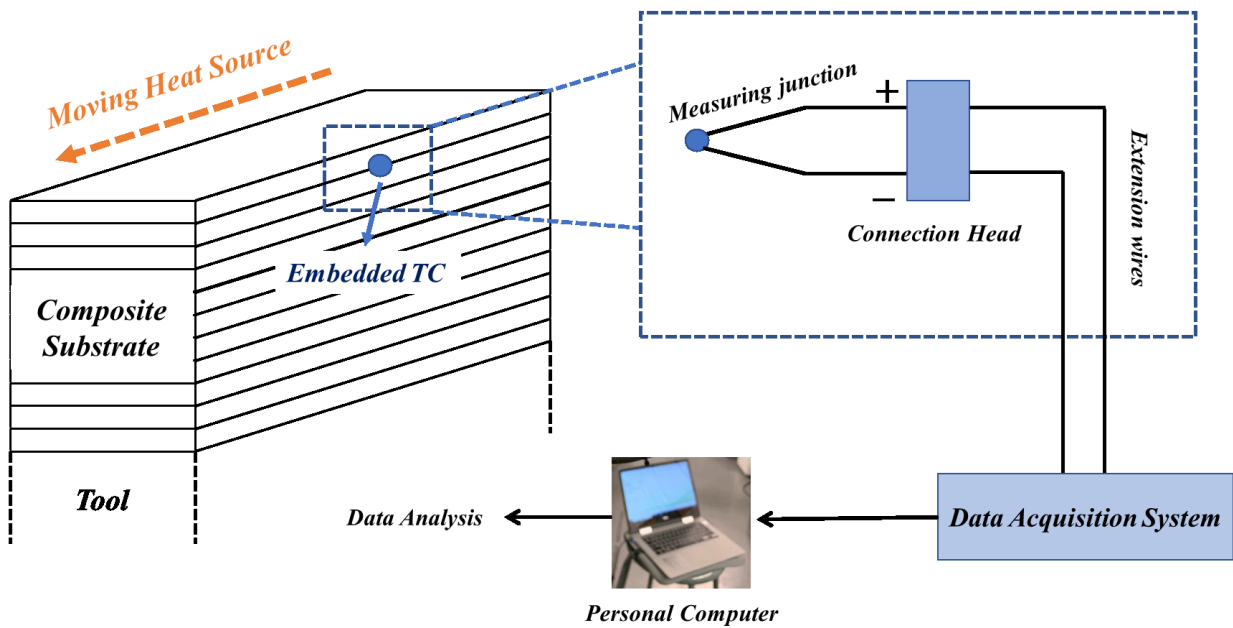


Figure 52. Schematic of the layup of the composite, the tool, location of the embedded thermocouple, data acquisition system and data analysis apparatus

6.7.4 Methodology for Determination of Convective Heat Transfer Coefficient

As stated earlier in previous sections, in this chapter, we aim at determining the convective heat transfer coefficient experimentally for the case of AFP under different operational conditions. The method to be used is similar to the one used in literature by various authors [18,38,55,56,59]. In this method, first a value for h coefficient is assumed. Experimental trials are performed to obtain the temperature data during the process for specific set of operational conditions. The calculated temperature results based on thermal analysis model of the process under similar operational conditions are obtained. The maximum temperature results from both numerical and experimental methods are compared. The h coefficient is then updated and through an iterative process, the best value of h is found in the numerical model to match the maximum numerical temperature with the maximum experimental temperature measured by a fast-response thermocouple embedded underneath one layer of the composite layer. This process is repeated for other operational conditions to determine the coefficient h between the hot gas torch and the composite substrate for a variety of conditions. Figure 53 demonstrates a flow chart to support the explanation of the strategy used in this chapter to determine the h coefficient. The thermal analysis model used in this chapter is essentially the same as the one presented in Chapter 3. In this model, based on the energy balance approach, finite difference formulation of the problem was derived and coded. Numerical results from a moving heat source travelling across the upper side of a composite substrate were obtained. Under the similar set of process parameters, experimental trials were performed using fast-response K-type thermocouples embedded into the composite substrate, underneath layers of the composite material. The experimental results were then used to determine the h coefficient to find the best match between numerical and experimental results. It was shown that using this method, the numerical model was able to capture the maximum temperature in different layers with good agreement with experimental results (Figure 36).

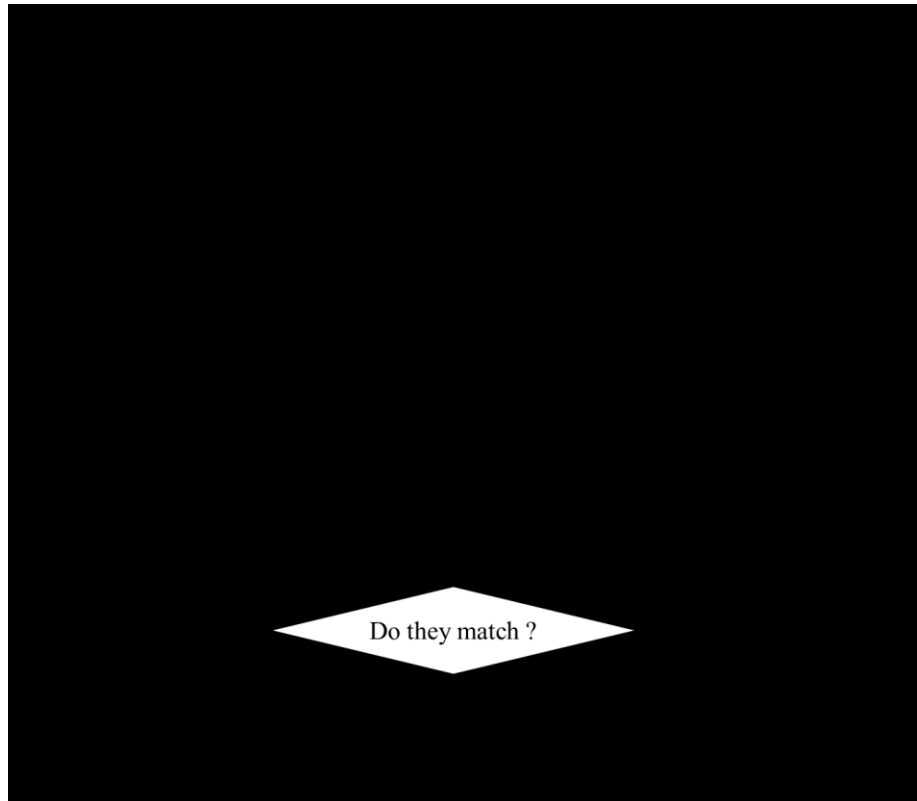


Figure 53. Flow chart of the strategy to determine the convective heat transfer coefficient

In the following, the procedure to determine the convective heat transfer coefficient is thoroughly elaborated through one case. In this case, the iteration of different assumed values of h coefficient and its influence on the resulting temperatures at the location of the thermocouple is shown, and finally the final value (optimum value) of the h coefficient is obtained when there is a match of the maximum temperature between numerical and experimental results. The same methodology will be used to determine the h coefficient under different operational conditions as discussed in the experimental setup.

In order to determine the h coefficient through an iterative process, a scanning algorithm is coded in MATLAB to perform the analysis. In this algorithm, a function is defined in which the coefficient h is an input and the maximum temperature at the location of the thermocouple is selected as an output. A range of variation for the h coefficient is set by the operator. In this case, it is assumed that the h varies between 800 and 1500 W/m²K in 10 intervals. In other words, it is firstly assumed that the unknown coefficient of h has the value of 800 W/m²K as an initial value

to start the iterative process. The maximum temperature at the location of the thermocouple is computed through the thermal analysis using the initial value of the h coefficient. This is regarded as the 1st iteration. As the output, the error percentage is monitored as shown in Figure 54. The error percentage is defined as the difference between the numerical and experimental maximum temperature at the location of the thermocouple divided by the experimental value. For the 1st iteration, as the beginning of the scanning algorithm, the error percentage is computed to be around 25%. In the next iteration (2nd iteration), the h coefficient is updated to 810 W/m²K. This value corresponds to the error percentage of 23.8%. This process is repeated and at each iteration, a new value is assigned to the h coefficient and the error percentage is monitored continuously. Looking at Figure 54, it can be seen that at the 45th iteration, the error percentage tends to zero which means the corresponding h coefficient is the optimum value. Using this value, there is a complete match between the numerical and experimental maximum temperatures at the location of the thermocouple. By further increasing the h coefficient and moving into higher iterations, it can be noticed that the error percentage is increased again and as noted in Figure 54, at the end of the scanning algorithm i.e., at 71st iteration, the error percentage reaches about 11.5%. Eventually, the optimal value of the h coefficient is reported as the optimal case by the algorithm. Figure 55 illustrates the influence of the iteration of different assumed values of the h coefficient on the resulting temperatures at the location of the thermocouple. For comparison, only the results from 5 values are presented. As can be seen, h values of 1000 and 1100 W/m²K i.e., 21st and 31st iterations respectively predict the maximum temperatures as around 259 °C and 275 °C respectively. This can lead to the error percentage of 12.65% and 7.26% respectively. By increasing the h coefficient into 1240 W/m²K at the 45th iteration, the optimum value of the h coefficient is found when there is a match of the maximum temperature between numerical and experimental results. Further increase in the h coefficient to 1400 and 1500 W/m²K, lead to the prediction of the maximum temperatures with 7.11 and 11.37% errors respectively. In summary, it can be stated that the scanning algorithm can be employed to determine the h coefficient through the iterative process. The h values below the optimum value, underestimate the maximum temperatures by predicting values lower than the experimental one, while the h values above the optimum value, can overestimate the maximum temperatures compared to the experimental one.

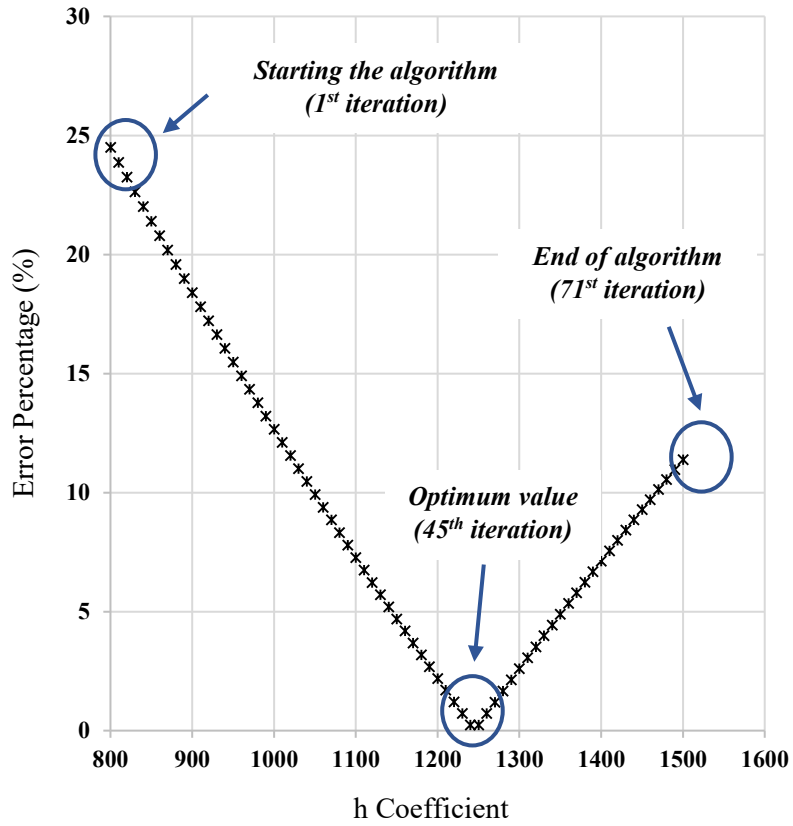


Figure 54. Error percentage versus different h coefficients in scanning algorithm

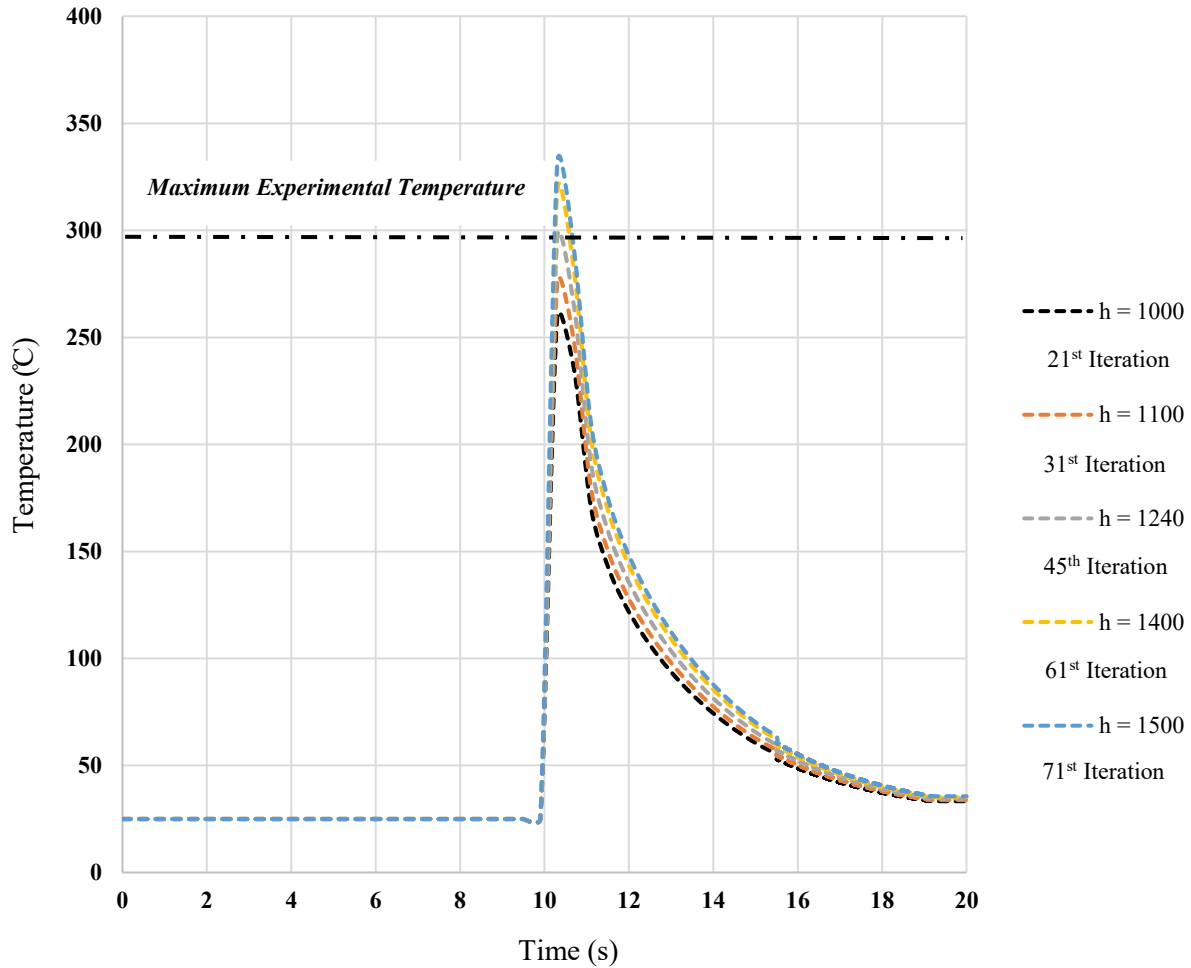


Figure 55. Temperature variations at the location of the thermocouple for iterations of different assumed values of the h coefficient

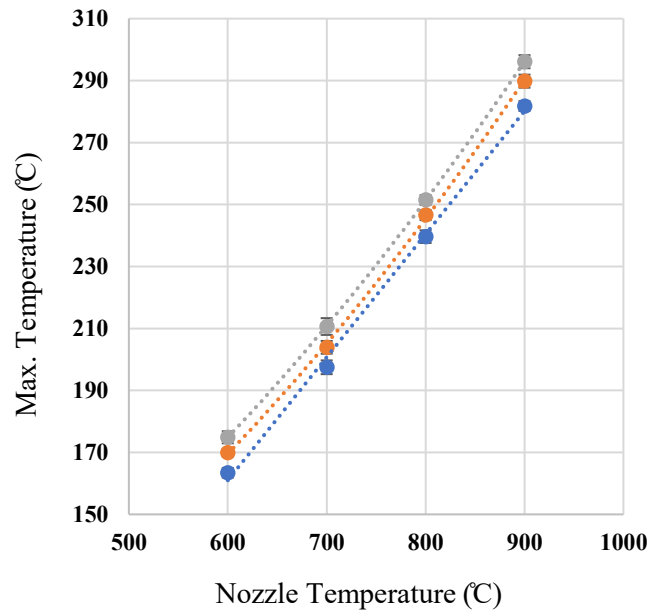
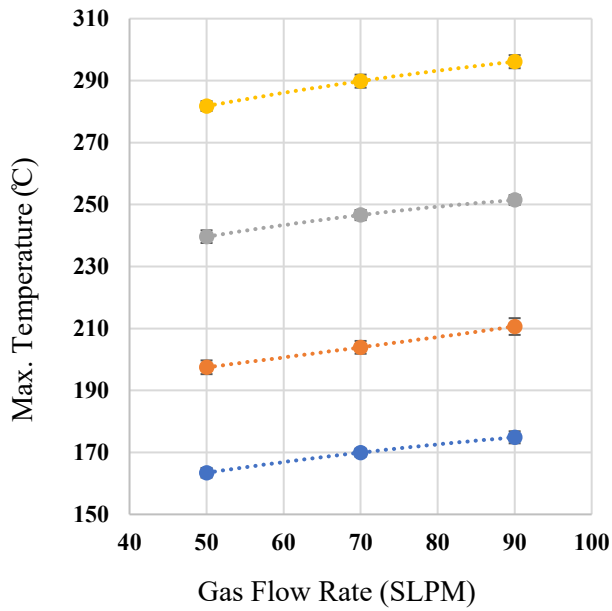
6.8 Results and Discussion

In this section, first the maximum temperature results from the experimental trials are presented for different process parameters as described in the design of experiments. Then, using the methodology introduced to determine the convective heat transfer coefficient, the average h coefficients for different nozzle temperatures and different gas flow rates at different nozzle to substrate spacings are calculated and presented.

6.8.1 Experimental Temperature Results

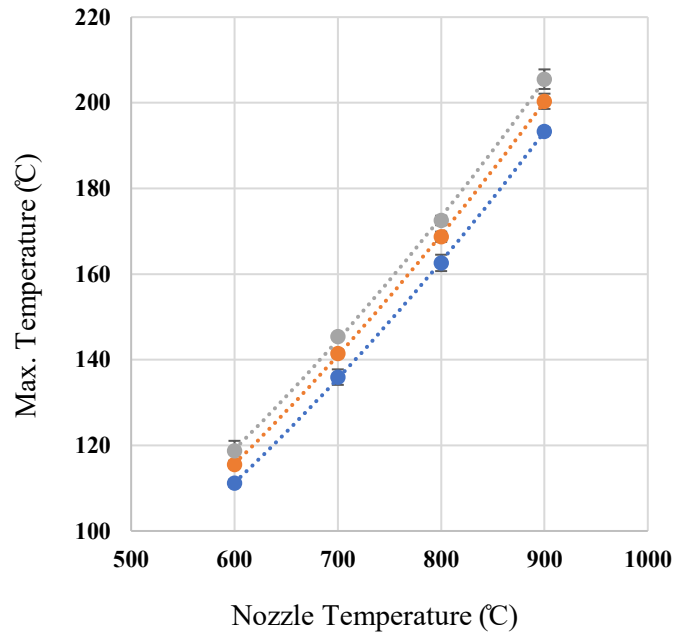
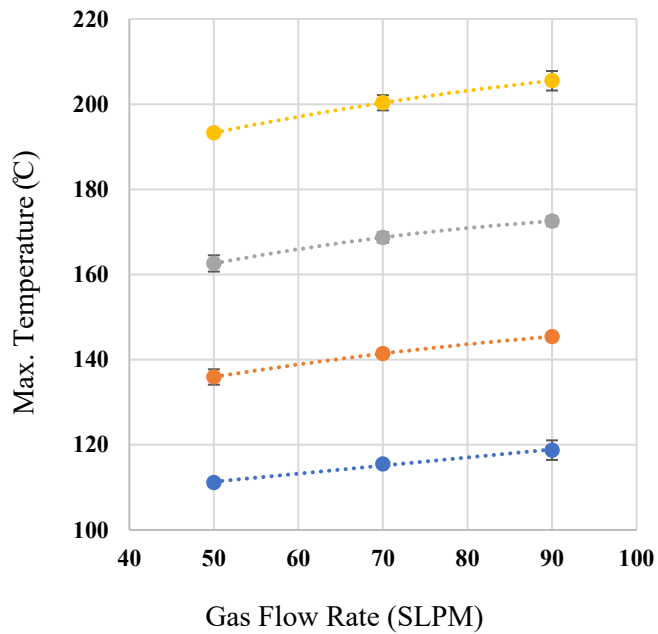
Results from the nozzle to substrate spacing of 2.5 mm are presented in Figure 56. The effect of gas flow rate and the nozzle temperature on the maximum temperature is presented in the left and right respectively. As it can be seen, by increasing the gas flow rate, the maximum temperature increases for all nozzle temperatures. For example, when the nozzle temperature is 600 °C, the maximum temperature increases by about 7 % when the gas flow rate increases from 50 to 90 SLPM. Looking at the right graph in Figure 56, the effect of nozzle temperature on results can be seen. For all the gas flow rates, by increasing the nozzle temperature, the maximum temperature would increase. For example, when the gas flow rate is 70 SLPM, the maximum temperature increases by 70 % when the nozzle temperature increases from 600 to 900 °C.

A similar trend can be observed in Figure 57 and Figure 58. In both figures, by increasing the nozzle temperature and the gas flow rate, the maximum temperature increases. For example, when the nozzle to substrate spacing is 5 mm, by increasing the flow rate from 50 to 90 SLPM, at nozzle temperature of 600 °C, the maximum temperature would increase by 6.8 %. For the similar process parameters when the nozzle to substrate spacing is 10 mm, the maximum temperature increases by about 8 %. Looking at the effect of the nozzle temperature on results, when the nozzle to substrate spacing is 5 mm, the maximum temperature can increase by 73 % at gas flow rate of 70 SLPM. For the same range of nozzle temperature and gas flow rate, the amount of increase is 85 % for the nozzle to substrate spacing of 10 mm. Overall, it can be concluded that both nozzle temperature and gas flow rate have effect on the maximum temperature. However, the effect of nozzle temperature is more significant for all nozzle to substrate spacings considered in this study.



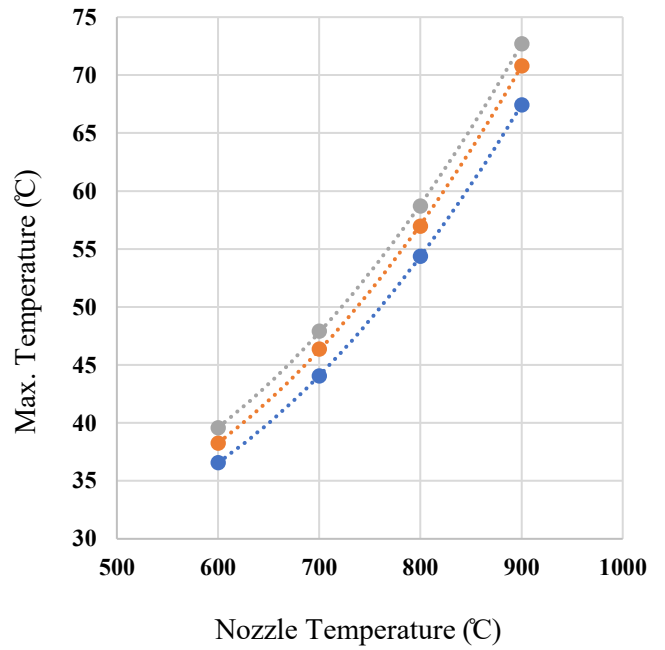
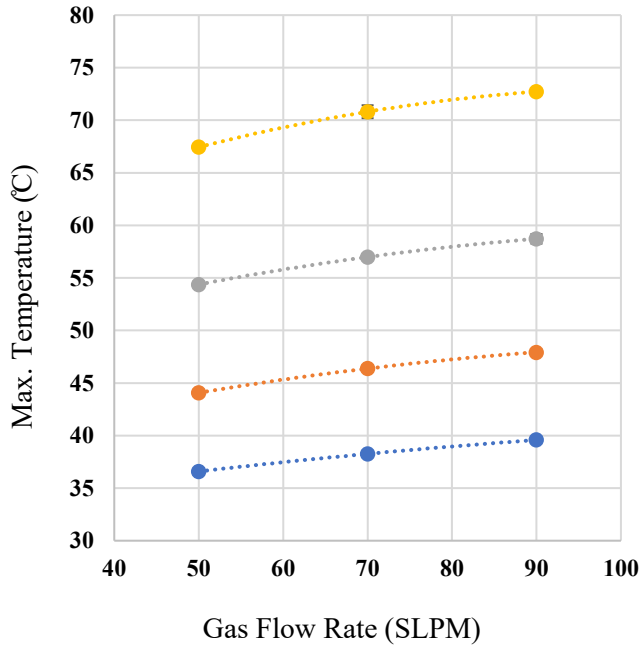
- Nozzle Temperature: 600 C ● Nozzle Temperature: 700 C ● Gas Flow Rate: 50 SLPM ● Gas Flow Rate: 70 SLPM
- Nozzle Temperature: 800 C ● Nozzle Temperature: 900 C ● Gas Flow Rate: 90 SLPM

Figure 56. Effect of gas flow rate (left) and the nozzle temperature (right) on the maximum temperature results for the nozzle to substrate spacing of 2.5 mm



- Nozzle Temperature: 600 C
- Nozzle Temperature: 700 C
- Nozzle Temperature: 800 C
- Nozzle Temperature: 900 C
- Gas Flow Rate: 50 SLPM
- Gas Flow Rate: 70 SLPM
- Gas Flow Rate: 90 SLPM

Figure 57. Effect of gas flow rate (left) and the nozzle temperature (right) on the maximum temperature results for the nozzle to substrate spacing of 5 mm



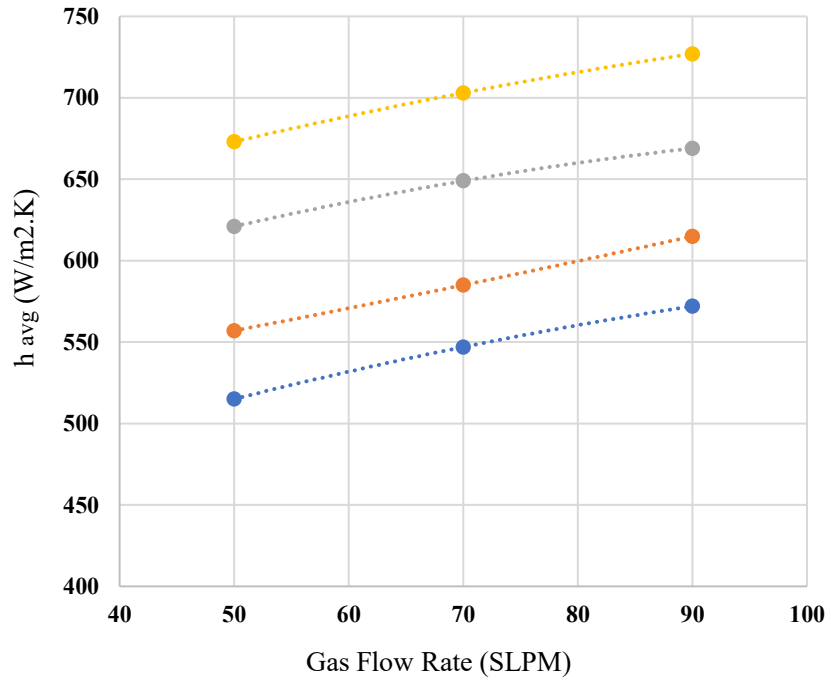
- Nozzle Temperature: 600 C ● Nozzle Temperature: 700 C ● Gas Flow Rate: 50 SLPM ● Gas Flow Rate: 70 SLPM
- Nozzle Temperature: 800 C ● Nozzle Temperature: 900 C ● Gas Flow Rate: 90 SLPM

Figure 58. Effect of gas flow rate (left) and the nozzle temperature (right) on the maximum temperature results for the nozzle to substrate spacing of 10 mm

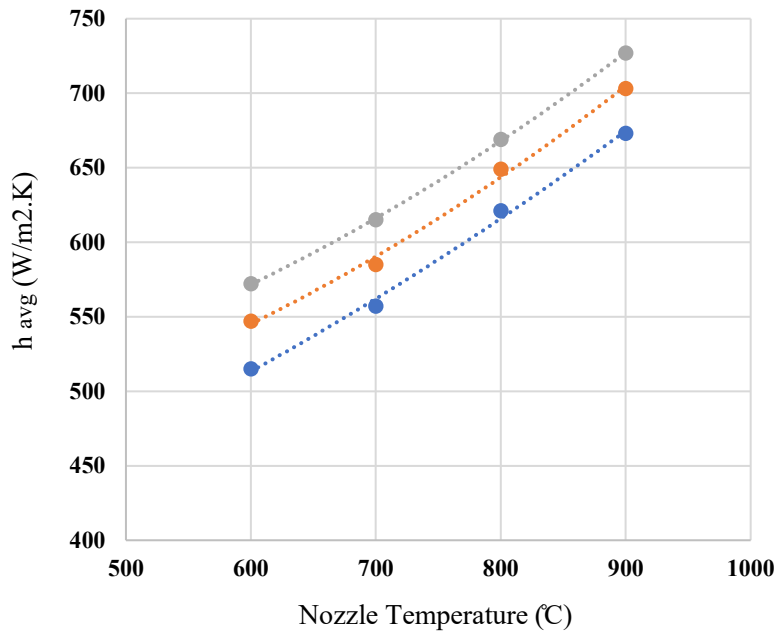
6.8.2 Experimental Convective Heat Transfer Coefficient Results

Using the methodology presented in previous sections, the average h coefficient (h_{avg}) is determined for different process parameters. Results from the nozzle to substrate spacing of 2.5 mm are presented in Figure 59. The effect of gas flow rate and the nozzle temperature on h_{avg} is presented in the left and right respectively. As it can be seen, by increasing the gas flow rate, h_{avg} increases for all nozzle temperatures. For example, when the nozzle temperature is 800 °C, h_{avg} increases by about 7 % when the gas flow rate increases from 50 to 90 SLPM. Looking at the right graph in Figure 59, the effect of nozzle temperature on results can be observed. For all the gas flow rates, by increasing the nozzle temperature, h_{avg} would increase. For example, when the gas flow rate is 70 SLPM, h_{avg} increases by about 28 % when the nozzle temperature increases from 600 to 900 °C.

A similar trend can be noticed in Figure 60 and Figure 61. At both figures, by increasing the nozzle temperature and the gas flow rate, h_{avg} increases. For example, when the nozzle to substrate spacing is 5 mm, by increasing the flow rate from 50 to 90 SLPM, at nozzle temperature of 800 °C, h_{avg} would increase by 9 %. For the similar process parameters when the nozzle to substrate spacing is 10 mm, h_{avg} increases by about 15 %. Looking at the effect of the nozzle temperature on results, when the nozzle to substrate spacing is 5 mm, h_{avg} can increase by about 34 % at gas flow rate of 70 SLPM. For the same range of nozzle temperature and gas flow rate, the amount of increase is about 130 % for the nozzle to substrate spacing of 10 mm. Overall, it can be concluded that both nozzle temperature and gas flow rate have effect on h_{avg} . However, the effect of nozzle temperature is more significant for all nozzle to substrate spacings considered in this study.



- Nozzle Temperature: 600 C
- Nozzle Temperature: 700 C
- Nozzle Temperature: 800 C
- Nozzle Temperature: 900 C



- Gas Flow Rate: 50 SLPM
- Gas Flow Rate: 70 SLPM
- Gas Flow Rate: 90 SLPM

Figure 59. Effect of gas flow rate (top) and the nozzle temperature (bottom) on the average h coefficient for the nozzle to substrate spacing of 2.5 mm

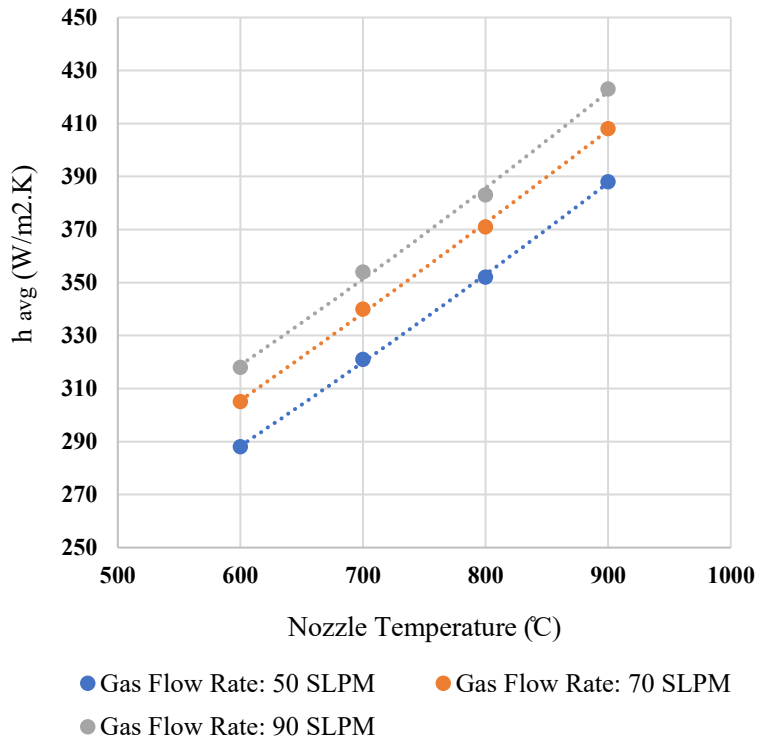
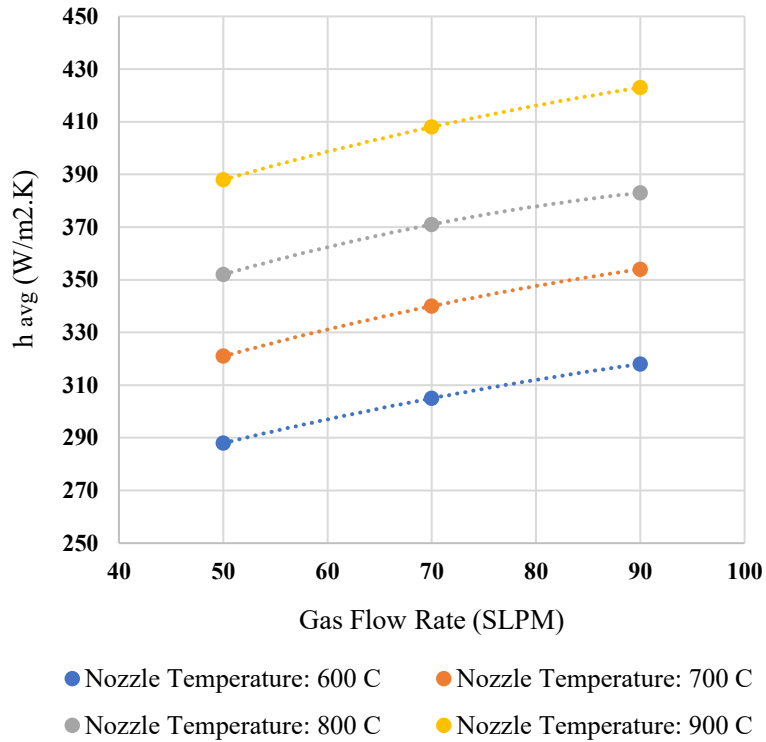


Figure 60. Effect of gas flow rate (top) and the nozzle temperature (bottom) on the average h coefficient for the nozzle to substrate spacing of 5 mm

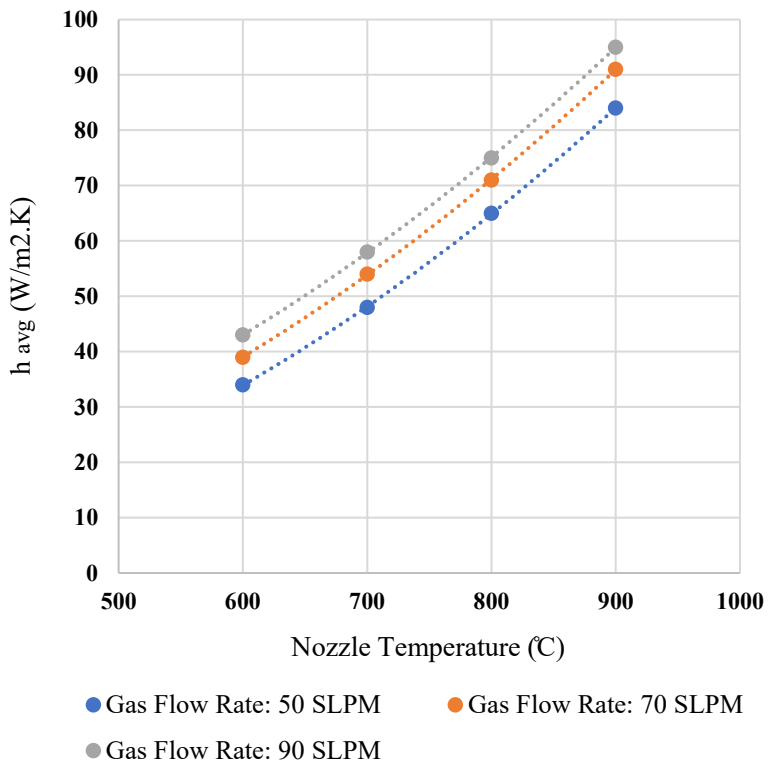
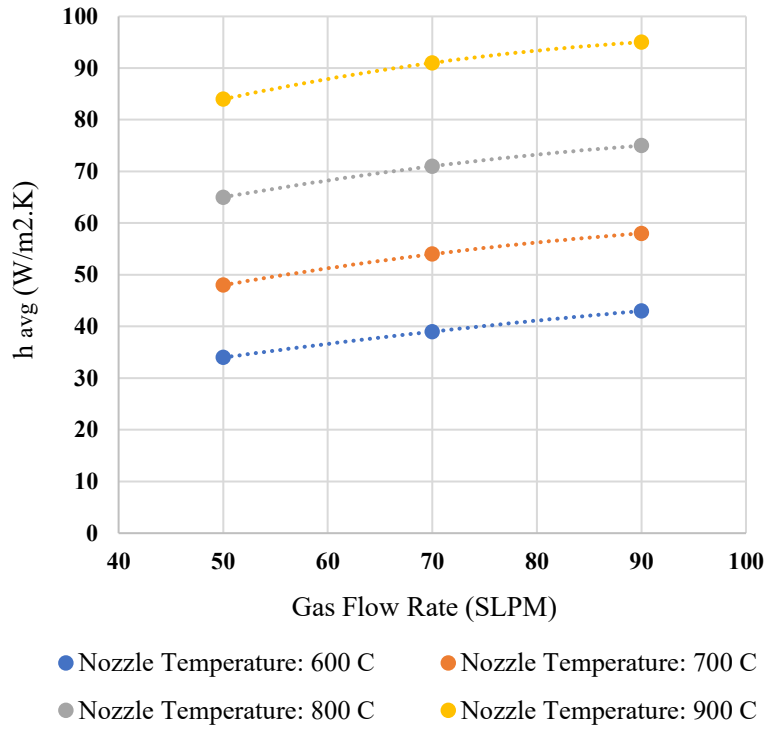


Figure 61. Effect of gas flow rate (top) and the nozzle temperature (bottom) on the average h coefficient for the nozzle to substrate spacing of 10 mm

6.9 Conclusion

Determination of convective heat transfer coefficient (h) is of paramount importance in accurate modeling the heat transfer occurs in AFP. Studies on impingement jet revealed the parameters that can have influence on heat transfer characteristics of the problem. These include nozzle geometry (shape and size of the nozzle cross-section), hot gas temperature, gas flow rate, type and state of the gas, angle of impact and nozzle to plate spacing. The theoretical formulations in literature could provide a great understanding of the problem by investigating the effect of these parameters on the convective heat transfer coefficient. It was found that nozzle temperature, gas flow rate and the nozzle to substrate spacing as the main process parameters can have significant influence. Although the general fluid flow and the heat transfer in typical impingement jet studies could help us in understanding the effect of each parameter and determine the most important ones among the variety of parameters, results cannot be used directly for the case of AFP. The reason is that the heat transfer mechanism in AFP has many characteristics that are unique to this process: the consolidation roller which exists in the AFP can noticeably hinder the flow coming out of the torch nozzle. As the hot gas reaches the vicinity of the nip point, some of the flow experiences instantaneous immobility and part of a hot gas flows backwards. This can be explained by vortexes and re-circulation of the flow in the closed nip region. This can have a significant influence on flow characteristics, pressure and velocity fields, thermal boundary layers and turbulence level in the heating region [55,85,86]. This in turn can result in great amount of heat dissipation into the surrounding. Considering the discussion above, it is necessary to perform an experimental study to better understand the effect of each parameter for the case of AFP. The experimental setup was introduced, and it was discussed that among all the parameters in the setup, the nozzle temperature, gas flow rate and the distance between the nozzle and the substrate were considered as variables for this study. The results for different process parameters were obtained. It was concluded that for a fixed nozzle to substrate spacing, by increasing both the nozzle temperature and the gas flow rate, the h coefficient will increase. The trend, however, is different between the nozzle temperature and the gas flow rate. The nozzle temperature exhibited more influence on the h coefficient rather than the gas flow rate.

The experimental methodology introduced in this study along with the procedure to determine the convective heat transfer coefficient experimentally, can be easily employed to investigate the

effect of other parameters. Although the results presented in this chapter were obtained for the experimental setup used in this study, the same methodology can be used by other researchers to investigate the effect of different process parameters for their particular setup.

Chapter 7:

CONCLUSIONS, CONTRIBUTIONS AND FUTURE WORK

7.1 Concluding Remarks

The development of the fiber placement process offers possibilities to manufacture composite structures in a variety of geometries with and without free edges. In making structures with free edges such as flat plates or flat panels, the issue of distortion is important which leads to the warpage of the final composite part. One of the major reasons that gives rise to the distortion of the laminate is the rapid heating and cooling of the thermoplastic composite material during the process which result in development of the temperature distribution in different directions. The temperature distribution affects the variation in crystallinity, and residual stresses throughout the structure as it is being built. In fact, residual stresses are developed as a result of temperature gradients because of different cooling rates in different layers along the thickness of the laminate. Consequently, the distortion of the composite laminate takes place even during the process. In order to address this problem, to make laminates with free edges with no or minimum distortion, one needs to understand the effect of different parameters on the process. As such, the first thing to look at would be to determine the temperature distribution history during the process. The focus of this thesis is to gain more understanding of the way temperature gradients developed during the AFP process of thermoplastic composites.

Thermal analysis model of the process was presented in Chapter 3. The heat transfer mechanism in AFP thermoplastic composite process was introduced. It was stated that both heat convection due to the hot gas torch and heat diffusion through the composite substrate are important in thermal analysis of the process. Using the energy balance approach, finite difference formulation of the heat transfer problem was introduced. Based on the formulations derived for interior and boundary nodes, a solution algorithm for moving heat source problem in MATLAB was presented. The experimental setup was presented in Chapter 4. To provide validation of numerical results,

unidirectional composite strips were manufactured using AFP and fast-response K-type thermocouples were employed to determine the thermal profiles at various locations through the thickness of the composite laminate subjected to a moving heat source. Results from both experimental trials and numerical method were presented in Chapter 5. The major conclusions can be summarized as follows:

- The numerical method is able to capture the maximum temperature with good agreement with experimental results. The temperatures measured experimentally during the heating pass, using embedded thermocouples into the composite substrate, underneath layers of the composite material, show consistent trends with the generated temperatures from the numerical method.
- As one goes through the thickness, the maximum temperature becomes lower and lower until after 5 layers, the temperature is not above glass transition temperature (T_g) anymore. For regions where the temperature is below T_g , the material becomes stiff and this contributes to the development of residual stresses and distortion due to the temperature gradients.
- The maximum temperature occurs at later time as one goes through the thickness. This is due to the heat diffusion mechanism inside the composite laminate. It takes time for the heat energy provided by the hot gas flow at the upper side layer to be diffused, transferred, and absorbed by the material at underneath layer. This can be interpreted as the time delay in peak temperatures at underneath layers.

In chapter 6, it was noted that information from the literature shows values of the convective heat transfer coefficient (h) that vary from 80 W/m²K to 2500 W/m²K. This large range can provide a great degree of uncertainty in the determination of important quantities such as the temperature distributions and residual stresses. The reason for these large differences can be due to the differences in the process parameters in each of the studies. The process parameters can include the volume flow rate of the hot gas, the gas temperature, the distance between the nozzle exit and the surface of the composite substrate, the angle of the torch with respect to the surface of the substrate etc. The purpose of this chapter was to investigate the effect of different AFP process parameters on the convective heat transfer coefficient using available theoretical formulations in

literature. Experimental technique was introduced at the end to obtain the h values for the case of AFP at different process parameters. From results for the case of AFP, the following conclusions can be noted:

- By increasing the gas flow rate from 50 to 90 SLPM, the h coefficient increases for all nozzle temperatures i.e, 600, 700, 800 and 900 °C.
- For all the gas flow rates, by increasing the nozzle temperature, the h coefficient increases.
- For the practical range of the distance between the nozzle and the surface of the composite substrate in AFP, the effect of nozzle to substrate spacing on h coefficient is considerable.
- Both the nozzle temperature and the gas flow rate have effect on the h coefficient. However, the effect of nozzle temperature is more significant for all nozzle to substrate spacings considered in this study.

7.2 Contributions

Some of the major contributions presented in this thesis can be summarized as following:

- Procedure to handle the heat transfer of a moving heat source. According to the knowledge of the candidate, this is the first time that this procedure is proposed.
- Providing information on temperature distribution in different directions.
- Providing experimental data regarding the thermal analysis of the process by utilizing the fast-response K-type thermocouples. Wide range of thermal data obtained in this thesis can be used as an important reference for future studies.
- Introduction to important criteria for the selection of the fast-response K-type thermocouple and to investigate the role of the thermocouple in accurate temperature profile measurement during the process. The technical data obtained for the fast-response time thermocouple and the methodology to address the limitation and drawbacks of the unsheathed fine gauge thermocouples can be used for future studies.

- Presentation of the methodology for determination of convective heat transfer coefficient and proposing a scanning algorithm to determine the optimum value for the h coefficient. This can be employed as the guideline for other researchers to determine the h coefficient for each particular study.
- Identification of the important process parameters that can affect the h coefficient and investigation the effect of each parameter on results.

In addition to the list of contributions reported above, the following publications have been accomplished relating to this study:

1. **Omid Aghababaei Tafreshi** , Suong Van Hoa, Farjad Shadmehri, Duc Minh Hoang, Daniel Rosca. October 2019. "Heat transfer analysis of automated fiber placement of thermoplastic composites using a hot gas torch", Published online, DOI: 10.1080/20550340.2019.1686820, Advanced Manufacturing: Polymer and Composites Science.
2. **Omid Aghababaei Tafreshi**, Suong Van Hoa, Duc Minh Hoang, Daneil Rosca, Farjad Shadmehri. 2019. "Heat Transfer by a Moving Heat Source in Automated Fiber Placement (AFP) Thermoplastic Composites Manufacturing", Proceedings of the 4th International Symposium on Automated Composites Manufacturing, Montreal, April 2019, published by Destech Publications.

7.3 Future Work

A vast opportunity for research exists in the automated fiber placement of thermoplastic composites using hot gas torch. Specially, in the context of making structures with free edges such as flat plates, flat panels and shells, where the warpage emerges during and after the process. As mentioned earlier, in testing and evaluation of composite structures made by AFP, due to the existing challenges in making a flat unidirectional composite plate to make a test coupon, it is necessary to rectify the issue of distortion. Therefore, the following recommendations for further research in this area can be offered:

- In thermal analysis model of the process, it was assumed that the temperature variation through the width direction can be ignored due to the even heat input over the tape width. However, in accurate modeling of the process, the temperature variation in the width direction can also be considered. Therefore, developing a three-dimensional thermal model of the process is recommended.
- The moving heat source problem was addressed in this thesis and it was assumed that there is no material deposition. However, in the actual process, the material deposition is part of the model and needs to be considered.
- The simulation presented in this thesis can be further generalized to consider the effect of compaction roller, its diameter and its geometry on the quality of the final composite part.
- From the thermal analysis of the process, along with the temperature distribution, it can be used to obtain the crystallization level and bonding quality of the composite parts.

REFERENCES

- [1] Hoa S.V. 2018. "Principles of the manufacturing of composite materials". second edition DEStech Publications, Inc.
- [2] Cai X. 2012. "Determination of process parameters for the manufacturing of thermoplastic composite cones using automated fiber placement", Master thesis at Concordia University.
- [3] Hoa S.V. 2017. "Analysis for Design of Fiber Reinforced Plastic Vessels", Routledge publication.
- [4] Boeing. (02/20). "787 Dreamliner program fact sheet", available: <http://www.boeing.com/commercial/787family/programfacts.html>
- [5] Jeyakodi GK. 2016. "Finite Element Simulation of the In - Situ AFP process for Thermoplastic Composites using Abaqus", Master thesis at Delft University of Technology.
- [6] Hoang MD. 2015. "Procedure for making flat thermoplastic composite plates by Automated Fiber Placement and their mechanical properties", Master thesis at Concordia University.
- [7] Elsherbini YM, Hoa S.V. 2017. "Experimental and numerical investigation of the effect of gaps on fatigue behavior of unidirectional carbon/epoxy automated fiber placement laminates", Journal of Composite Materials; 51:759–72.
- [8] Clancy GJ, Peeters D, Oliveri V, Jones D, O’Higgins R, Weaver PM. 2018. "Steering of carbon fiber/thermoplastic pre-preg tapes using laser-assisted tape placement", AIAA/ASCE/AHS/ASC Structures, Structural Dynamics and Materials Conference; p. 478.
- [9] Averous L, Moro L, Dole P, Fringant C. 2000. "Properties of thermoplastic blends: starch–polycaprolactone", Polymer ; 41:4157–67.
- [10] Drobny JG. 2014. "Handbook of thermoplastic elastomers". Elsevier.
- [11] Olabisi O, Adewale K. 2016. "Handbook of thermoplastics", CRC press.
- [12] Shadmehri F, Hoa S.V., Fortin-Simpson J, Ghayoor H. 2018. "Effect of in situ treatment on the quality of flat thermoplastic composite plates made by automated fiber placement (AFP)", Advanced Manufacturing: Polymer & Composites Science; 4:41–7.
- [13] Hoa S.V., Duc Hoang M, Simpson J. 2017. "Manufacturing procedure to make flat thermoplastic composite laminates by automated fibre placement and their mechanical properties", Journal of Thermoplastic Composite Materials;30:1693–712.
- [14] Seferis JC. 1986. "Polyetheretherketone (PEEK): Processing-structure and properties studies for a matrix in high performance composites". Polymer Composites; 7:158–69.
- [15] Talbott MF, Springer GS, Berglund LA. 1987. "The effects of crystallinity on the mechanical properties of PEEK polymer and graphite fiber reinforced PEEK", Journal of Composite Materials ; 21:1056–81.

- [16] Gurdal Z, Olmedo R. 1993. "In-plane response of laminates with spatially varying fiber orientations-variable stiffness concept", *AIAA Journal* ; 31:751–8.
- [17] Setoodeh S, Abdalla MM, Gürdal Z. 2006. "Design of variable–stiffness laminates using lamination parameters", *Composites Part B: Engineering* ; 37:301–9.
- [18] Omid Aghababaei Tafreshi , Suong Van Hoa, Farjad Shadmehri, Duc Minh Hoang, Daniel Rosca. 2019. "Heat transfer analysis of automated fiber placement of thermoplastic composites using a hot gas torch", Published online, DOI: 10.1080/20550340.2019.1686820, *Advanced Manufacturing: Polymer and Composites Science*.
- [19] Shadmehri F, Ioachim O, Pahud O, Brunel J, Landry A, Hoa S.V., 2015. "Laser-vision inspection system for automated fiber placement (AFP) process". 20th International Conference on Composite Materials, Copenhagen, Denmark ; p. 19–24.
- [20] Li X, Hallett SR, Wisnom MR. 2015. "Modelling the effect of gaps and overlaps in automated fibre placement (AFP)-manufactured laminates", *Science and Engineering of Composite Materials* ; 22:115–29.
- [21] Lan M, Cartié D, Davies P, Baley C. 2016. "Influence of embedded gap and overlap fiber placement defects on the microstructure and shear and compression properties of carbon–epoxy laminates", *Composites Part A: Applied Science and Manufacturing* ; 82:198–207.
- [22] Fayazbakhsh K, Nik MA, Pasini D, Lessard L. 2013. "Defect layer method to capture effect of gaps and overlaps in variable stiffness laminates made by automated fiber placement", *Composites Structures* ; 97:245–51.
- [23] Oromiehie E, Prusty BG, Compston P, Rajan G. 2018. "Characterization of process-induced defects in automated fiber placement manufacturing of composites using fiber Bragg grating sensors", *Structural Health Monitoring* ;17:108–17.
- [24] Zacchia TT, Shadmehri F, Fortin-Simpson J, Hoa S.V. 2018. "Design of Hard Compaction Rollers for Automated Fiber Placement on Complex Mandrel Geometries", *Journal of Mechanics Engineering and Automation*.
- [25] Kozaczuk K. 2016. "Automated fiber placement systems overview", *Prace Instytutu Lotnictwa*.
- [26] Gruber MB, Lockwood IZ, Dolan TL, Funck SB, Tierney JJ, Simacek P, 2012. "Thermoplastic in-situ placement requires better impregnated tapes and tows". *Proceedings of the SAMPE Conference*.
- [27] Kim BC, Hazra K, Weaver P, Potter K. 2011. "Limitations of fibre placement techniques for variable angle tow composites and their process-induced defects", 18th international conference on composite materials, Korea. p. 21–26.
- [28] Aized T, Shirinzadeh B. 2011. "Robotic fiber placement process analysis and optimization using response surface method", *International Journal of Advanced Manufacturing Technology* ;55:393–404.
- [29] Frketic J, Dickens T, Ramakrishnan S. 2017. "Automated manufacturing and processing of fiber-reinforced polymer (FRP) composites: An additive review of contemporary and modern techniques

for advanced materials manufacturing", *Additive Manufacturing* ; 14:69–86.

- [30] Omid Aghababaei Tafreshi, Suong Van Hoa, Duc Minh Hoang, Daneil Rosca, Farjad Shadmehri. 2019. "Heat Transfer by a Moving Heat Source in Automated Fiber Placement (AFP) Thermoplastic Composites Manufacturing", *Proceedings of the 4th International Symposium on Automated Composites Manufacturing*, Montreal, April 2019, published by Destech Publications.
- [31] Paul W, Binder K, Heermann DW, Kremer K. 1991. "Dynamics of polymer solutions and melts. Reptation predictions and scaling of relaxation times", *Journal of Chemical Physics* ; 95:7726–40.
- [32] Ghayoor Karimiani H. 2015. "Analysis of Residual Stresses in Thermoplastic Composites Manufactured by Automated Fiber Placemen", Master thesis at Concordia University.
- [33] Chapman TJ, Gillespie Jr JW, Pipes RB, Manson J.A, Seferis J.C. 1990. "Prediction of process-induced residual stresses in thermoplastic composites", *Journal of Composite Materials*; 24:616–43.
- [34] Sonmez FO, Hahn HT, Akbulut M. 2002. "Analysis of process-induced residual stresses in tape placement", *Journal of Thermoplastic Composite Materials*; 15:525–44.
- [35] Chinesta F, Leygue A, Bognet B, Ghnatios C, Poulhaon F, Bordeu F. 2014. "First steps towards an advanced simulation of composites manufacturing by automated tape placement", *International Journal of Material Forming*; 7:81–92.
- [36] Lamontia MA, Gruber MB, Tierney JJ, Gillespie Jr JW, Jensen BJ, Cano RJ. 2009. "Modeling the accudyne thermoplastic in situ ATP process", 30th International SAMPE Europe Conference, Paris.
- [37] Lamontia MA, Funck SB, Gruber MB, Cope RD, Waibel BJ, Gopez NM, 2003. "Manufacturing flat and cylindrical laminates and built up structure using automated thermoplastic tape laying, fiber placement, and filament winding", *SAMPE Conference* ; 39:30–43.
- [38] Khan MA. 2010. "Experimental and Simulative Description of the Thermoplastic Tape Placement Process with Online Consolidation" Ph.D. thesis in Technischen Universität Kaiserslautern.
- [39] Weiler T, Emonts M, Wollenburg L, Janssen H. 2018. "Transient thermal analysis of laser-assisted thermoplastic tape placement at high process speeds by use of analytical solutions", *Journal of Thermoplastic Composite Materials*; 31:311–38.
- [40] Lee M. 2004. "Heat transfer and consolidation modeling of composite fiber tow in fiber placement", Ph.D. thesis in Virginia Polytechnic Institute & State University.
- [41] Dai S-C, Ye L. 2002. "GF/PP tape winding with on-line consolidation", *Journal of Reinforced Plastics and Composites*; 21:71–90.
- [42] Tierney J, Gillespie Jr JW. 2003. "Modeling of heat transfer and void dynamics for the thermoplastic composite tow-placement process", *Journal of Composite Materials*; 37:1745–68.
- [43] Khan MA, Mitschang P, Schledjewski R. 2010. "Tracing the void content development and identification of its effecting parameters during in situ consolidation of thermoplastic tape material", *Polymers and Polymer Composites*; 18:1–15.
- [44] Beyeler EP, Guceri SI. 1988. "Thermal analysis of laser-assisted thermoplastic-matrix composite

- tape consolidation", *Journal of Heat Transfer*; 110:424–30.
- [45] Ghasemi Nejhah MN, Cope RD, Güçeri SI. 1991. "Thermal analysis of in-situ thermoplastic composite tape laying", *Journal of Thermoplastic Composite Materials*;4:20–45.
- [46] Grove SM. 1988. "Thermal modelling of tape laying with continuous carbon fibre-reinforced thermoplastic", *Composites (Butterworth & Co (publishers) Ltd.)*;19:367–75.
- [47] Mantell SC, Springer GS. 1992. "Manufacturing process models for thermoplastic composites", *Journal of Composite Materials*; 26:2348–77.
- [48] Sonmez FO, Hahn HT. 1997. "Modeling of heat transfer and crystallization in thermoplastic composite tape placement process", *Journal of Thermoplastic Composite Materials*; 10:198–240.
- [49] Sonmez FO, Akbulut M. 2007. "Process optimization of tape placement for thermoplastic composites", *Composites Part A: Applied Science and Manufacturing*; 38:2013–23.
- [50] Zhao Q, Hoa S.V., Gao ZJ. 2011. "Thermal stresses in rings of thermoplastic composites made by automated fiber placement process", *Science and Engineering of Composite Materials*;18:35–49
- [51] Li Z, Yang T, Du Y. 2015. "Dynamic finite element simulation and transient temperature field analysis in thermoplastic composite tape lay-up process", *Journal of Thermoplastic Composite Materials*; 28:558–73.
- [52] Han Z, Cao Z, Shao Z, Fu H. 2014. "Parametric study on heat transfer for tow placement process of thermoplastic composite", *Polymers and Polymer Composites*; 22:713–22.
- [53] Kollmannsberger A, Lichtinger R, Hohenester F, Ebel C, Drechsler K. 2018. "Numerical analysis of the temperature profile during the laser-assisted automated fiber placement of CFRP tapes with thermoplastic matrix", *Journal of Thermoplastic Composite Materials*; 31:1563–86.
- [54] James DL, Black WZ. 1996. "Thermal analysis of continuous filament-wound composites", *Journal of Thermoplastic Composite Materials*; 9:54–75.
- [55] Toso YMP, Ermanni P, Poulikakos D. 2004. "Thermal phenomena in fiber-reinforced thermoplastic tape winding process: computational simulations and experimental validations", *Journal of Composite Materials*;38:107–35.
- [56] Hassan N, Thompson JE, Batra RC, Hulcher AB, Song X, Loos AC. 2005. "A heat transfer analysis of the fiber placement composite manufacturing process", *Journal of Reinforced Plastics and Composites*;24:869–88.
- [57] August Z, Ostrander G, Michasiow J, Hauber D. 2014. "Recent developments in automated fiber placement of thermoplastic composites", *SAMPE Journal*;50:30–7.
- [58] Agarwal V, Guceri SI, McCullough RL, Schultz JM. 1992. "Thermal characterization of the laser-assisted consolidation process", *Journal of Thermoplastic Composite Materials* ; 5:115–35.
- [59] Shih P-J, Loos AC. 1999. "Heat transfer analysis of the thermoplastic filament winding process", *Journal of Reinforced Plastics and Composites* ; 18:1103–12.
- [60] Tumkor S, Turkmen N, Chassapis C, Manoochchri S. 2001. "Modeling of heat transfer in

- thermoplastic composite tape lay-up manufacturing", *International Communications in Heat and Mass Transfer* ; 28:49–58.
- [61] Stokes-Griffin CM, Compston P, Matuszyk TI, Cardew-Hall MJ. 2015. "Thermal modelling of the laser-assisted thermoplastic tape placement process", *Journal of Thermoplastic Composite Materials* ; 28:1445–62.
- [62] Stokes-Griffin CM, Compston P. 2015. "The effect of processing temperature and placement rate on the short beam strength of carbon fibre–PEEK manufactured using a laser tape placement process", *Composites Part A: Applied Science and Manufacturing* ; 78:274–83.
- [63] J.P.Holman. 1981. "Heat Transfer, fifth edition ", McGraw-Hill Book Company.
- [64] Bergman TL, Incropera FP, DeWitt DP, Lavine AS. 2011. "Fundamentals of heat and mass transfer", John Wiley & Son
- [65] Shin JG, Woo JH. 2003. "Analysis of heat transfer between the gas torch and the plate for the application of line heating", *Journal of Manufacturing Science and Engineering*; 125:794–800.
- [66] Mondo JA, Parfrey KA. 1995. "Performance of in-situ consolidated thermoplastic composite structure", *International SAMPE Technical Conference*, vol. 27, p. 361–70.
- [67] Zhao P, Shirinzadeh B, Shi Y, Cheuk S, Clark L. 2018. "Multi-pass layup process for thermoplastic composites using robotic fiber placement", *Robotics and Computer-Integrated Manufacturing* ; 49:277–84.
- [68] Cai X, Shadmehri F, Hojjati M, Chen J, Hoa S.V. 2012. "Determination of optimum process conditions for processing AS4/APC-2 thermoplastic composites by automated fiber placement", *International SAMPE Technical Conference*.
- [69] Hajiloo A, Xie W, Hoa S.V., Khan S. 2014. "Thermal control design for an automated fiber placement machine", *Science and Engineering of Composite Materials* ; 21:427–34.
- [70] Marsh G. 2011. "Automating aerospace composites production with fibre placement", *Reinforced Plastics* ; 55:32–7.
- [71] Shadmehri F, Cai X, Hojjati M, Chen J, Hoa S.V. 2011. "Determination of optimal process parameters for manufacturing thermoplastic composite rings by automated fiber placement", *26th Annual Technical Conference American Society of Composites*, vol. 2, p. 1309–18.
- [72] Ghasemi Nejhadd MN. 1993. "Issues related to processability during the manufacture of thermoplastic composites using on-line consolidation techniques", *Journal of Thermoplastic Composite Materials* ; 6:130–46.
- [73] Tewatia A, Hendrix J, Dong Z, Taghon M, Tse S, Chiu G. 2017. "Characterization of melt-blended graphene–poly (ether ether ketone) nanocomposite", *Materials Science and Engineering:B* ; 216:41–9.
- [74] Hwang Y, Kim M, Kim J. 2013. "Improvement of the mechanical properties and thermal conductivity of poly (ether-ether-ketone) with the addition of graphene oxide-carbon nanotube hybrid fillers", *Composites Part A: Applied Science and Manufacturing* ; 55:195–202.

- [75] CYTEC. "APC-2-PEEK Thermoplastic Polymer Technical Data". Available: <https://www.e-aircraftsupply.com>
- [76] Li CS, Vannabouathong C, Sprague S, Bhandari M. 2015. "The use of carbon-fiber-reinforced (CFR) PEEK material in orthopedic implants: a systematic review", *Clinical Medicine Insights: Arthritis and Musculoskeletal Disorders* ; 8:CMAMD-S20354.
- [77] Kersten RFMR, van Gaalen SM, de Gast A, Öner FC. 2015. "Polyetheretherketone (PEEK) cages in cervical applications: a systematic review", *The Spine Journal* ; 15:1446–60.
- [78] Schwitalla A, Müller W-D. 2013. "PEEK dental implants: a review of the literature", *Journal of Oral Implantology* ; 39:743–9.
- [79] Fu H, Liao B, Qi F, Sun B, Liu A, Ren D. 2008. "The application of PEEK in stainless steel fiber and carbon fiber reinforced composites", *Composites Part B: Engineering* ; 39:585–91.
- [80] Schwitalla AD, Spintig T, Kallage I, Müller W-D. 2015. "Flexural behavior of PEEK materials for dental application", *Dental Materials* ; 31:1377–84.
- [81] Cytec. 1999. "Thermoplastic composite material handbook".
- [82] OMEGA. "Temperature Measurement volume 2", Available: www.omega.co.uk.
- [83] AIRTECH. "Flashbreaker Data Sheet", Available: backend.airtech.lu.
- [84] Kim HJ, Kim SK, Lee W Il. 1996. "A study on heat transfer during thermoplastic composite tape lay-up process", *Experimental Thermal and Fluid Science* ; 13:408–18.
- [85] Kim HJ, Kim SK, Lee WI. 2004. "Flow and heat transfer analysis during tape layup process of APC-2 prepregs", *Journal of Thermoplastic Composite Materials* ; 17:5–12.
- [86] O'Donovan TS. 2005. "Fluid flow and heat transfer of an impinging air jet", Ph.D. thesis in Department of Mechanical and Manufacturing Engineering, University of Dublin.
- [87] Goldstein RJ, Franchett ME. 1988. "Heat transfer from a flat surface to an oblique impinging jet", *Journal of Heat Transfer* ; 110:84–90.
- [88] Zuckerman N, Lior N. 2005. "Impingement heat transfer: correlations and numerical modeling", *Journal of Heat Transfer* ; 127:544–52.
- [89] Rohsenow WM, Hartnett JP, Ganic EN, Richardson PD. 1986. "Handbook of heat transfer fundamentals", MCGRAW-HILL publications.
- [90] Martin H. 1977. "Heat and mass transfer between impinging gas jets and solid surfaces", *Advances in Heat Transfer*, vol. 13, Elsevier ; p. 1–60.
- [91] Incropera FP, Lavine AS, Bergman TL, DeWitt DP. 2007. "Fundamentals of heat and mass transfer", Wiley.
- [92] Foss JF, Kleis SJ. 1976. "Mean Flow Characteristics for the Oblique Impingement of an Axisymmetric Jet", *AIAA Journal* ; 14:705–6.

- [93] Viskanta R. 1993. "Heat transfer to impinging isothermal gas and flame jets", *Experimental Thermal and Fluid Science* ; 6:111–34.
- [94] Goldstein RJ, Behbahani AI, Heppelmann KK. 1986. "Streamwise distribution of the recovery factor and the local heat transfer coefficient to an impinging circular air jet", *International Journal of Heat and Mass Transfer* ; 29:1227–35.
- [95] Gori F, Bossi L. 2003. "Optimal slot height in the jet cooling of a circular cylinder", *Applied Thermal Engineering* ; 23:859–70.
- [96] Huber AM, Viskanta R. 1994. "Effect of jet-jet spacing on convective heat transfer to confined, impinging arrays of axisymmetric air jets", *International Journal of Heat and Mass Transfer* ; 37:2859–69.
- [97] San J-Y, Lai M-D. 2001. "Optimum jet-to-jet spacing of heat transfer for staggered arrays of impinging air jets", *International Journal of Heat and Mass Transfer* ; 44:3997–4007.
- [98] Goldstein RJ, Seol WS. 1991. "Heat transfer to a row of impinging circular air jets including the effect of entrainment", *International Journal of Heat and Mass Transfer* ; 34:2133–47.
- [99] Goldstein RJ, Behbahani AI. 1982. "Impingement of a circular jet with and without cross flow", *International Journal of Heat and Mass Transfer* ; 25:1377–82.
- [100] Lytle D, Webb BW. 1994. "Air jet impingement heat transfer at low nozzle-plate spacings", *International Journal of Heat and Mass Transfer* ; 37:1687–97.
- [101] Meola C, de Luca L, Carlomagno GM. 1996. "Influence of shear layer dynamics on impingement heat transfer", *Experimental Therm and Fluid Science* ; 13:29–37.
- [102] Mohanty AK, Tawfek AA. 1993. "Heat transfer due to a round jet impinging normal to a flat surface", *International Journal of Heat and Mass Transfer* ; 36:1639–47.
- [103] Tawfek AA. 1996. "Heat transfer and pressure distributions of an impinging jet on a flat surface", *Heat and Mass Transfer* ; 32:49–54.
- [104] Wen M-Y, Jang K-J. 2003. "An impingement cooling on a flat surface by using circular jet with longitudinal swirling strips", *International Journal of Heat and Mass Transfer* ; 46:4657–67.
- [105] Chan TL, Leung CW, Jambunathan K, Ashforth-Frost S, Zhou Y, Liu MH. 2002. "Heat transfer characteristics of a slot jet impinging on a semi-circular convex surface", *International Journal of Heat and Mass Transfer* ; 45:993–1006.
- [106] Florschuetz LW, Truman CR, Metzger DE. 1981. "Streamwise flow and heat transfer distributions for jet array impingement with crossflow", *ASME International Gas Turbine Conference and Products Show*, Texas, USA.
- [107] Sparrow EM, Lovell BJ. 1980. "Heat transfer characteristics of an obliquely impinging circular jet", *Journal of Heat Transfer*
- [108] Perry KP. 1954. "Heat transfer by convection from a hot gas jet to a plane surface", *Proceedings of the Institution of Mechanical Engineers* ; 168:775–84.

- [109] Singh D, Premachandran B, Kohli S. 2015. "Effect of nozzle shape on jet impingement heat transfer from a circular cylinder", *International Journal of Thermal Science* ; 96:45–69.
- [110] Gulati P, Katti V, Prabhu S V. 2009. "Influence of the shape of the nozzle on local heat transfer distribution between smooth flat surface and impinging air jet", *International Journal of Thermal and Science* ; 48:602–17.
- [111] Lee DH, Song J, Jo MC. 2003. "The effects of nozzle diameter on impinging jet heat transfer and fluid flow", *Journal of Heat Transfer* ; 126:554–7.
- [112] Garimella S V, Nenaydykh B. 1996. "Nozzle-geometry effects in liquid jet impingement heat transfer", *International Journal of Heat and Mass Transfer* ; 39:2915–23.
- [113] Womac DJ, Ramadhyani S, Incropera FP. 1993. "Correlating equations for impingement cooling of small heat sources with single circular liquid jets", *Journal of Heat Transfer*.
- [114] Stevens J, Webb BW. 1991. "Local heat transfer coefficients under an axisymmetric, single-phase liquid jet", *Journal of Heat Transfer*.

APPENDIX

Appendix A. Typical Polymer Properties for PEEK [75]

Property	Room Temperature	250 °F (121 °C)	250 °F (121 °C) wet
Tensile Strength, ksi (MPa)	14.5 (100)	8.5 (58)	8.5 (58)
Tensile Modulus, Msi (GPa)	0.52 (3.6)	0.49 (3.4)	0.49 (3.4)
Failure Strain, %	70	70	70
Flexural Strength, ksi (MPa) ¹	24.7(170)	14.5(100)	14.5(100)
Flexural Modulus, Msi (GPa)	0.59 (4.1)	0.58 (4.0)	0.58 (4.0)
Tg, °F(°C) *	289 (143)		
Density, g/cc	1.32		

Yield value at >5% strain

Appendix B. Mechanical Properties : High strength [>500 ksi] standard modulus [33 Msi]carbon fiber reinforced unidirectional tape APC-2/AS4 [75]

Mechanical Properties	Test Temperature					
	-67°F (-55°C)	75°F (24 °C)	180°F (82 °C)	180°F (82 °C) wet	250°F (121 °C)	250°F (121 °C) wet
0° Tensile Properties						
Strength, ksi (MPa)	300 (2070)	300 (2070)	295 (2030)	295 (2030)	290 (2000)	290 (2000)
Modulus, Msi (GPa)	20 (138)	20 (138)	20 (138)	20 (138)	20 (138)	20 (138)
Failure strain, %	1.45	1.45			1.35	
Poisson's ratio	0.30	0.30				
0° Compressive Properties						
Strength, ksi (MPa)	220 (1520)	197 (1360)	180 (1250)	180 (1250)	170 (1170)	170 (1170)
Modulus, Msi (GPa)	19 (131)	18 (124)	18 (124)	18 (124)	18 (124)	18 (124)
0° Flexural Properties						
Strength, ksi (MPa)	-	290 (2000)	270 (1860)	270 (1860)	257 (1770)	257 (1770)
Modulus, Msi (GPa)	-	18 (124)	18 (124)	18 (124)	18 (124)	18 (124)
90° Tensile Properties						
Strength, ksi (MPa)	14 (99)	13 (86)	-	12 (83)	-	-
Modulus, Msi (GPa)	1.5 (10.3)	1.5 (10.3)	-	1.4 (9.6)	-	-
Failure strain, %	0.94	0.88	-	0.86	-	-
In-plane Shear Properties						
Strength, ksi (MPa)	30 (207)	27 (186)	23 (159)	24 (166)	21 (145)	-
Modulus, Msi (GPa)	0.92 (6.3)	0.82 (5.7)	-	0.74 (5.1)	-	-
Open Hole Tension						
Strength, ksi (MPa)	-	56 (386)	-	-	-	-
Open Hole Compression						
Strength, ksi (MPa)	-	47 (324)	42 (290)	41 (283)	38 (262)	37 (255)

Appendix C. Thermophysical Properties of Nitrogen Gas [64]

T (K)	ρ (kg/m ³)	C_p (kJ/kg.K)	$\mu \cdot 10^7$ (N.s/m ²)	$\nu \cdot 10^6$ (m ² /s)	$k \cdot 10^3$ (W/m.K)	$\alpha \cdot 10^6$ (m ² /s)	Pr
100	3.4388	1.070	68.8	2.00	9.58	2.60	0.768
150	2.2594	1.050	100.6	4.45	13.9	5.86	0.759
200	1.6883	1.043	129.2	7.65	18.3	10.4	0.736
250	1.3488	1.042	154.9	11.48	22.2	15.8	0.727
300	1.1233	1.041	178.2	15.86	25.9	22.1	0.716
350	0.9625	1.042	200.0	20.78	29.3	29.2	0.711
400	0.8425	1.045	220.4	26.16	32.7	37.1	0.704
450	0.7485	1.050	239.6	32.01	35.8	45.6	0.703
500	0.6739	1.056	257.7	38.24	38.9	54.7	0.700
550	0.6124	1.065	274.7	44.86	41.7	63.9	0.702
600	0.5615	1.075	290.8	51.79	44.6	73.9	0.701
700	0.4812	1.098	321.0	66.71	49.9	94.4	0.706
800	0.4211	1.122	349.1	82.90	54.8	116	0.715
900	0.3743	1.146	375.3	100.3	59.7	139	0.721
1000	0.3368	1.167	399.9	118.7	64.7	165	0.721
1100	0.3062	1.187	423.2	138.2	70.0	193	0.718
1200	0.2807	1.204	445.3	158.6	75.8	224	0.707
1300	0.2591	1.219	466.2	179.9	81.0	256	0.701